Award Number: W81XWH-10-1-0923

TITLE: Lightweight Portable Plasma Medical Device – Plasma Engineering Research Laboratory

PRINCIPAL INVESTIGATOR: Dr. Magesh Thiyagarajan, Ph.D.

CONTRACTING ORGANIZATION: TEXAS A&M UNIVERSITY-CORPUS CHRISTI
CORPUS CHRISTI TX 78412-5503

REPORT DATE: December 2015

TYPE OF REPORT: Final Report

PREPARED FOR: U.S. Army Medical Research and Materiel Command
Fort Detrick, Maryland 21702-5012

DISTRIBUTION STATEMENT:

☑ Approved for public release; distribution unlimited

# REPORT DOCUMENTATION PAGE

*Form Approved*
*OMB No. 0704-0188*



| **1. REPORT DATE** *(DD-MM-YYYY)* | **2. REPORT TYPE** | **3. DATES COVERED** *(From - To)* |
|---|---|---|
| December 2015 | Final | 27 SEP 2010 – 26 SEP 2015 |

**4. TITLE AND SUBTITLE**
Lightweight Portable Plasma Medical Device
Plasma Engineering Research Laboratory

**5a. CONTRACT NUMBER**
W81XWH-10-1-0923

**5b. GRANT NUMBER**
#09211004 GRANT

**5c. PROGRAM ELEMENT NUMBER**

**6. AUTHOR(S)**
Dr. Magesh Thiyagarajan

email: magesh@tamucc.edu

**5d. PROJECT NUMBER**

**5e. TASK NUMBER**

**5f. WORK UNIT NUMBER**

**7. PERFORMING ORGANIZATION NAME(S) AND ADDRESS(ES)**
**TEXAS A&M UNIVERSITY-CORPUS CHRISTI**
**CORPUS CHRISTI TX 78412-5503**

**8. PERFORMING ORGANIZATION REPORT NUMBER**

**9. SPONSORING / MONITORING AGENCY NAME(S) AND ADDRESS(ES)**
U.S. Army Medical Research and Materiel Command
Fort Detrick, Maryland 21702-5012

**10. SPONSOR/MONITOR'S ACRONYM(S)**

**11. SPONSOR/MONITOR'S REPORT NUMBER(S)**

**12. DISTRIBUTION / AVAILABILITY STATEMENT**
Approved for public release; distribution unlimited

**13. SUPPLEMENTARY NOTES**

**14. ABSTRACT**
We have established a recognized plasma research program researching various interdisciplinary plasma research projects. We have conducted research on the development of DC RBD plasma system, 13.56 MHz RF DBD plasma system, laser induced breakdown plasma system, plasma shadowgraphy system and optical emission spectroscopy diagnostics, two color laser interferometry diagnostics. We have completed the re-design and optimization of the portable plasma jets. We have completed the testing and characterization and biological testing of the portable plasma jets and the optimization of the plasma jets were completed.

**15. SUBJECT TERMS**
Plasma, laser plasma, non-thermal plasma, medical applications

| **16. SECURITY CLASSIFICATION OF:** | | | **17. LIMITATION OF ABSTRACT** | **18. NUMBER OF PAGES** | **19a. NAME OF RESPONSIBLE PERSON** |
|---|---|---|---|---|---|
| **a. REPORT** | **b. ABSTRACT** | **c. THIS PAGE** | | | USAMRMC |
| U | U | U | UU | 156 | **19b. TELEPHONE NUMBER** *(include area code)* |

**Standard Form 298 (Rev. 8-98)**
**Prescribed by ANSI Std. Z39.18**

## Table of Contents


| | Page |
|---|---|
| **Introduction……..…….. .** | **4** |
| **Body…….. .** | **5** |
| **Key Research Accomplishments…….…….. .** | **148** |
| **Reportable Outcomes…… .** | **149** |
| **Conclusion…… .** | **154** |
| **References…… .** | **155** |

## INTRODUCTION

The project entitled - Lightweight Portable Plasma Medical Device – Plasma Engineering Research Laboratory has been completed and it made a significant advancement in the plasma engineering research area as well as met the proposed objectives and tasks. The project had two objectives, in which the objective 1 is to develop a plasma research facility and establish a range of experimental plasma systems and diagnostics. The tasks under objective 1 were completed. The project's second objective is to develop a prototype of a portable plasma source for biomedical applications such as sterilization, infection treatment and cancer treatment. We have developed a portable plasma source and tested on a range of bacteria and cancer cells and results were obtained. We have redesigned, reconstructed and optimized the portable non-thermal atmospheric pressure plasma jet that was developed earlier based on a dielectric barrier discharge configuration. The plasma and biological testing and characterization of the optimized plasma jet are completed. The PI has mentored over 25 undergraduate students and 2 graduate students to perform various research projects. Several of these students have presented their work at various conferences and symposiums and few of those presentations has received best paper awards. The PI has mentored a visiting scientist and 5 postdoctoral research associates. The PI and the research team have published over 10 journal articles and over 50 conference proceedings and over 50 symposiums and meetings. The PERL has received a great visibility in the university campus as well as in the nation and around the world.

# BODY

**Table 1. The Project Objectives and Tasks**

| Task | Proposed Milestones | Base Line Plan Date | Status |
|---|---|---|---|
| **Objective 1: Establish Plasma Engineering Research Lab** | | | |
| 1 | Setup a direct current - atmospheric - resistive barrier cold plasma system | 26 OCT 2011 | Completed |
| 2 | Setup a 13.56 MHz radio frequency dielectric barrier plasma system | 26 OCT 2011 | Completed |
| 3 | Setup a 900 MHz/2.45 GHz wave plasma system | 26 OCT 2011 | Completed |
| 4 | Setup a laser induced breakdown plasma experimental system | 26 OCT 2011 | Completed |
| 5 | Implement plasma shadowgraphy diagnostics Setup | 26 OCT 2011 | Completed |
| 6 | Implement a two color laser interferomtery diagnostics setup | 26 OCT 2011 | Completed |
| 7 | Implement a optical emission spectroscopy diagnostics setup | 26 OCT 2011 | Completed |
| **Objective 2: Develop Portable Plasma Source** | | | |
| 8 | Design phase: Design an optimized portable plasma source system | 26 OCT 2012 | Completed |
| 9 | Construction phase: Construct the portable plasma source based on the design analysis and utilizing the existing resources and knowledge gained from objective 1. | 26 OCT 2012 | Completed |
| 10 | Testing and characterization phase: Portable plasma source will be tested and characterized for its operating parameters and plasma parameters. | 26 OCT 2014 | Completed |
| 11 | Biological testing: In-vitro biological testing. | 26 OCT 2015 | Completed |

# I. OBJECTIVE 1: ESTABLISH PLASMA ENGINEERING RESEARCH LAB

## Setup a direct current - atmospheric - resistive barrier cold plasma system

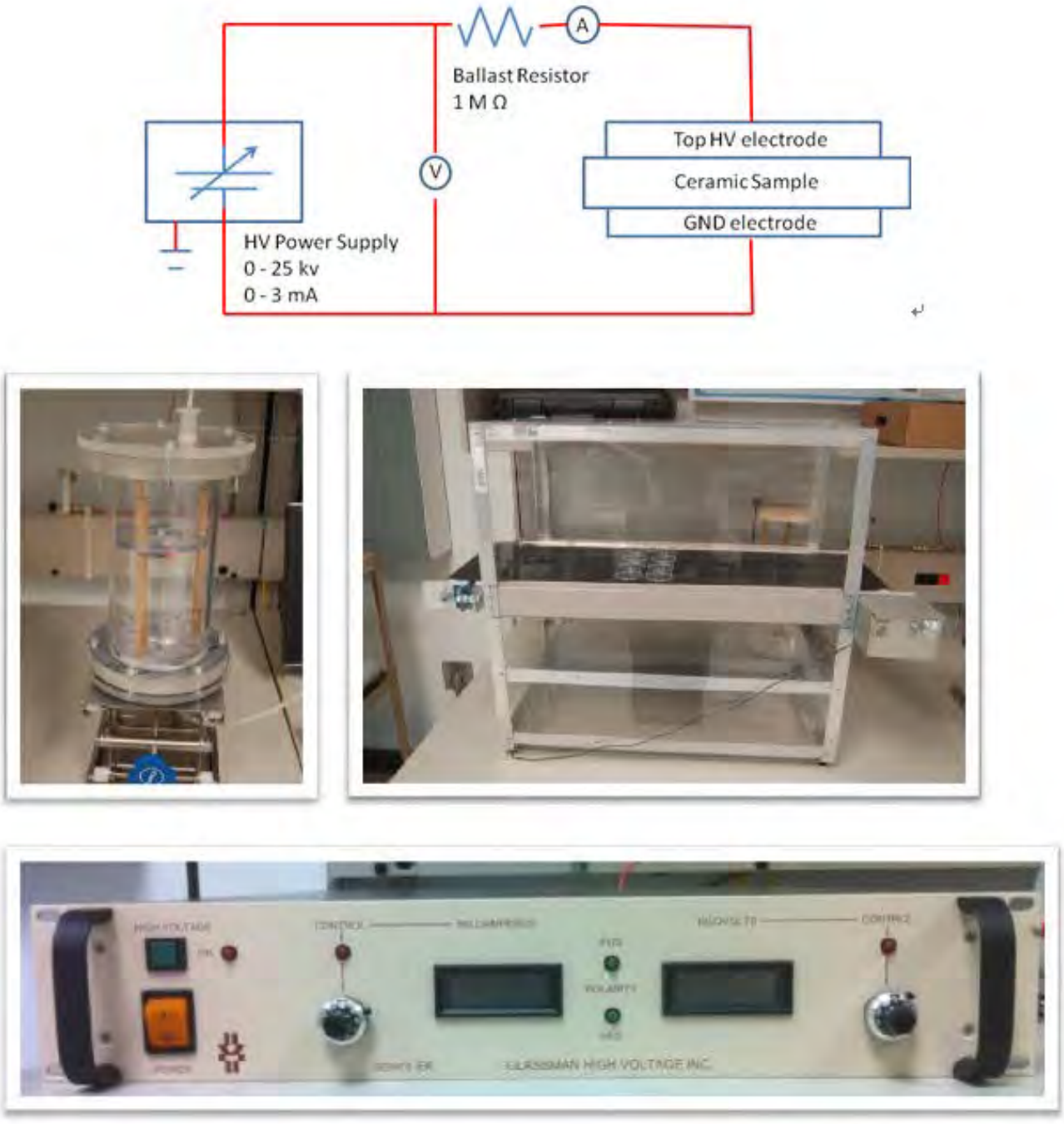


**Figure . DC atmospheric pressure resistive barrier discharge**

We have completed setting up the direct current atmospheric - resistive barrier cold plasma system. The DC power supply was acquired and atmospheric pressure plasma in air and helium has been experimented. Mechanical Engineering Undergraduate Students assisted in setting up the atmospheric Pressure resistive barrier discharge.

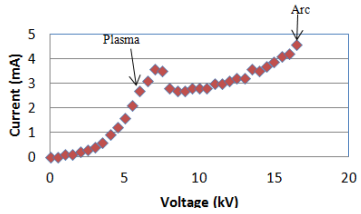


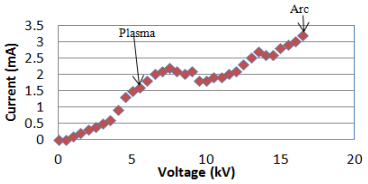


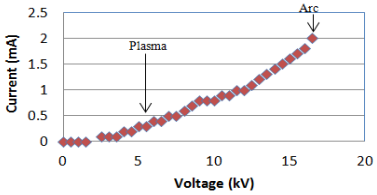


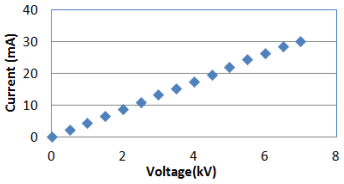


Fig.5– Moist Trial 1 of TAMUCC Stoneware

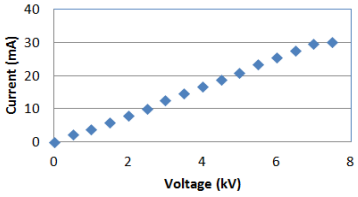


Fig. 6– Moist Trial 2 of TAMUCC Stoneware

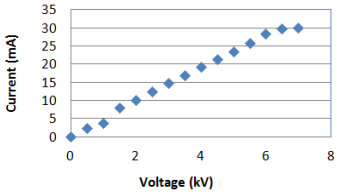


Fig. 7 – Moist Trial 3 of TAMUCC Stoneware

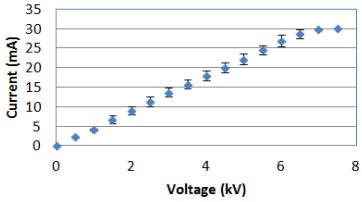


Fig8. – Moist Average of TAMUCC Stoneware

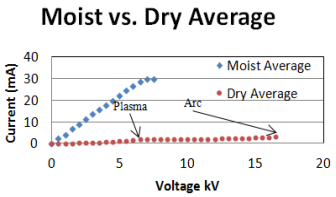


Fig.9 – Dry and Moist Average of TAMUCC Stoneware

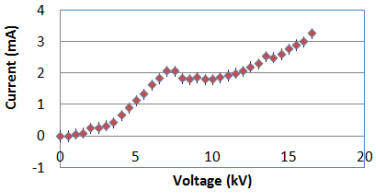


Fig.4– Average Dry Trial of TAMUCC Stoneware

**Figure . The V-I characteristics of the resistive barrier DC plasma characteristics**

The direct current resistive barrier discharge has been developed and tested for its voltage and current characteristics for different experimental conditions of the resistive barrier. The dryness and the moisture content of the resistive barrier has been varied and the VI characteristics and plasma parameters were diagnosed. The results are reported as technical report and presented in the key research accomplishments section.

## Setup a 13.56 MHz radio frequency dielectric barrier plasma system

**Figure . Setup a 13.56 MHz radio frequency dielectric barrier plasma system**

We have completed the setup of a RF system that generates atmospheric pressure plasma at a low temperature. Currently a Hispanic Minority Mechanical Engineering Undergraduate student assisted in setting up the experiment and collecting data. The data has been presented in a LSAMP conference and IEEE ICOPS conference.

Atmospheric pressure cold (non-thermal) plasmas have become increasingly prevalent within many research and industrial applications due to their range of reactive gas species produced that can be controlled and used in vast areas of application. In addition, the atmospheric plasma systems do not require expensive vacuum systems for their operation and generate a range of reactive ion species concentrations. This experimental research is being carried out to characterize and quantify the concentrations of the reactive ion species and other residual gases in order to theoretically extrapolate radial and axial distances.

A set of gas flow rates were tested at fixed RF powers range from 60 W to 180 W. Through proportionally increasing oxygen gas flow rate and applied RF power the amount of reactive ionized species are quantified and characterized. The experiment is also extended to various axial distances and the measured decay of reactive ion species which provides the required treatment distances based on the application treatment requirements.

The chemical characterization of the atmospheric pressure diffused plasma source was performed. The results confirm that the plasma source generates required amount of Nitrous Oxide gases that are the primary reaction agents to induce several healing mechanism in the human body.

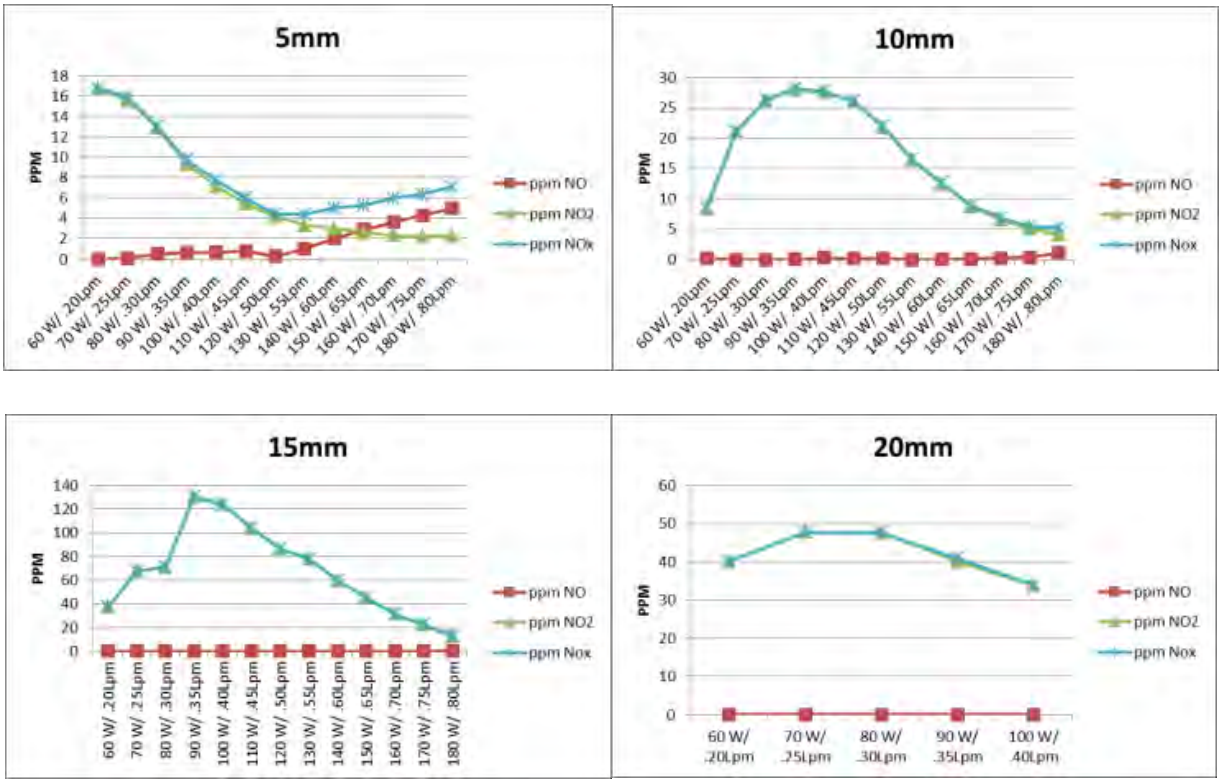


**Figure . ppm at varying distances of Surfx® – Atomflo™ AH-250C - Testo-350 Diagnostics, Acquisition Software and Plasma Data Comparison**

## Setup a laser induced breakdown plasma experimental system

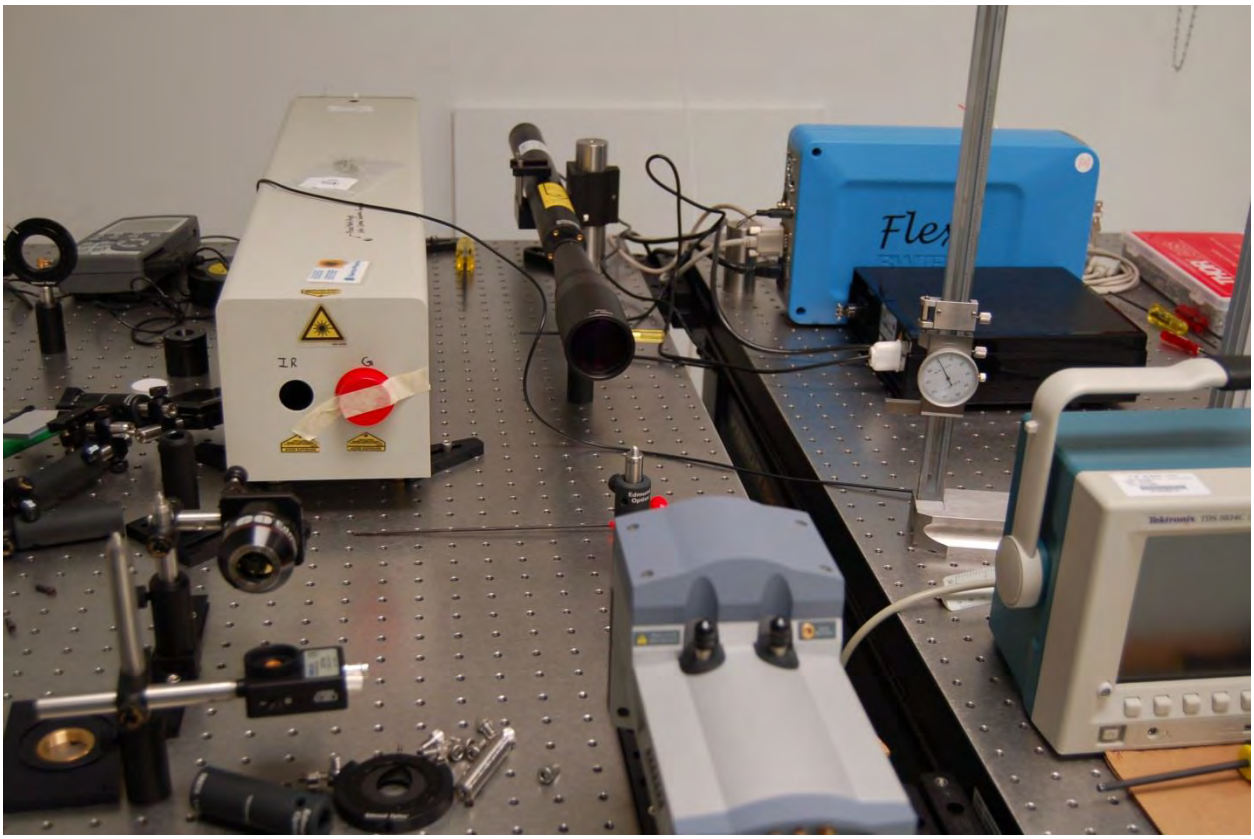

**Figure . Setup a laser induced breakdown plasma experimental system**

The picture of the experimental setup is shown in Fig. above. In this experiment, a pulsed Nd:YAG laser (Spectra-Physics, Indi 40), with a 1st harmonic at $\lambda = 1064$ nm, 1.165 eV per photon and a 2nd harmonic at $\lambda = 532$ nm, 2.33 eV per photon is used. The laser output is a circular beam of 1-cm cross section diameter with Gaussian distributed beam intensity and 1.0 mrad beam divergence. The full-width at half maximum (FWHM) of the laser pulse is $6 \pm 1$ ns, with a 1-ns rise/fall time and a maximum available laser output energy of 450 mJ at 1-20 Hz rep rate. The laser outputs both 1st and 2nd harmonic laser beams simultaneously and in order to study the infrared laser induced plasma the 532 nm 2nd harmonic crystal generator was detuned and a dichromatic mirror separates any minimal 532 nm laser output from the 1064 nm pump laser. The laser output beam energy is controlled using a variable attenuator and each laser pulse is sampled through an IR beam sampler and the laser output energy is measured using laser energy meter (Coherent, FieldMax II). In this experiment, all IR optical components are specially coated, with 98% transparency at 1064 nm. The IR beam is then reflected by a high damage threshold (20 J/cm2) IR coated kinematic mirror (TECHSPEC) in order to obtain a top-down configuration for the IR beam to enter the

plasma chamber. The 1-cm-diameter IR beam is then passed through a 1064 nm transmission coated 3-cm-diameter Zinc Selenide window. The laser beam was focused by using a high-power handling (500 MW/cm2) objective lens mounted inside the plasma chamber. The objective lens (Thorlabs, LMH-5X-1064) has an effective focal length of 40-mm, with a 10-mm entrance aperture and a 0.13 NA. Due to its short focal length, the objective lens is mounted inside the plasma chamber using an adjustable length holder, so that the laser-induced plasma will be positioned at the cylindrical chamber air and visible through side windows for diagnostics. The space between the entrance IR window and the objective lens is maintained at the same pressure as that of the chamber pressure in order to avoid differential pressures acting on the objective lens. Great care was taken to position the objective lens together with the plasma chamber precisely in the line of sight with the IR laser beam. In addition, using the laser energy meter, it is found that the laser beam experiences a 5% loss as it passes through the coated IR optics, including the attenuator, beam sampler, mirrors and windows. The laser energy available immediately after the objective lens corresponding to a 300 ± 5 mJ laser output was measured by the Coherent FieldMax II energy meter to be 285 ± 5 mJ, corresponding to the measured incident laser energy on the focal spot, in agreement with the analytical estimate. A high-speed (<2-ns rise time) visible photodetector (Thorlabs, DET10A/M) mounted with collection optics is used to detect and observe the laser breakdown visible spark. The photodetector is connected to a high speed 2.5 GS/S oscilloscope to monitor the laser induced plasma emission. The plasma chamber was made from stainless steel and flushed several times before finally filling with dry air (< 10 ppm water) to the desired pressure ranging from 2000 Torr to 100 mTorr. Optical view ports on both sides of the cell are made of 3-cm-diameter by 5-mm-thick sapphire windows. The view ports enabled observation of the interior at right angles to the cell axis which is coincident with the direction of the laser beam, as well as for diagnosing the plasma. The chamber pressure was measured precisely by a pressure gauge with a pressure controller–readout (MKS Instruments, 910-11 and PDR 900-11). The gas flow through the chamber was regulated by a needle valve in the gas line and another valve in the pumping line. For one set of experiments on determining the effects of removing micro dust particles of diameters ≥ 0.1 μm on the breakdown threshold of dry air, we have inserted a filter capsule in the incoming gas line and cleaned residual dust on window and lens surfaces by means of an aerosol jet. The filter houses a dual-pleated polytetrafluoroethylene (PTFE) filtering element with ≤ 0.1−μm pore size.

## Implement plasma shadowgraphy diagnostics Setup

We have completed the laser focused plasma and the shadowgraphy diagnostics together.

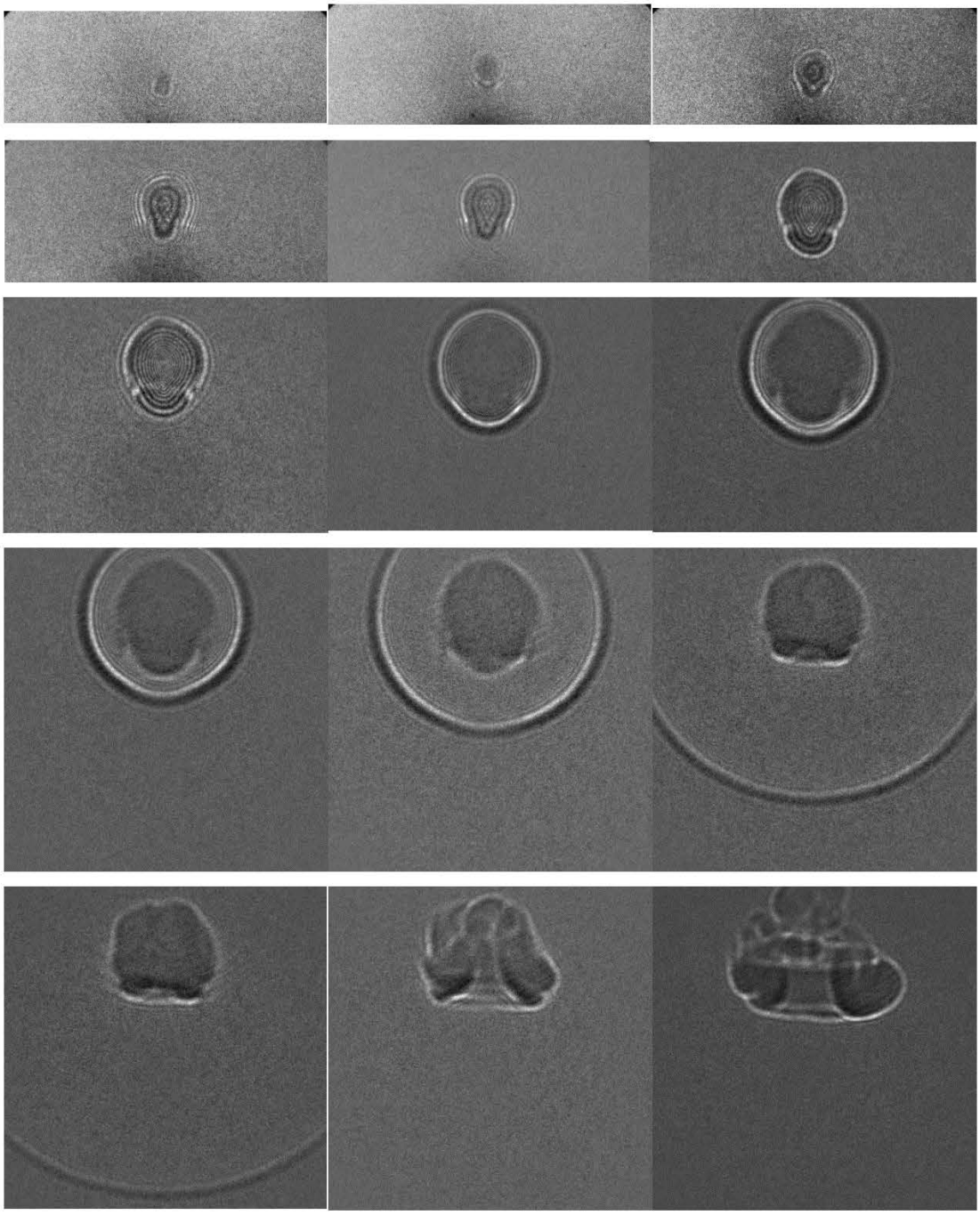

**Figure . Shadowgrams of the laser induced plasma in air**

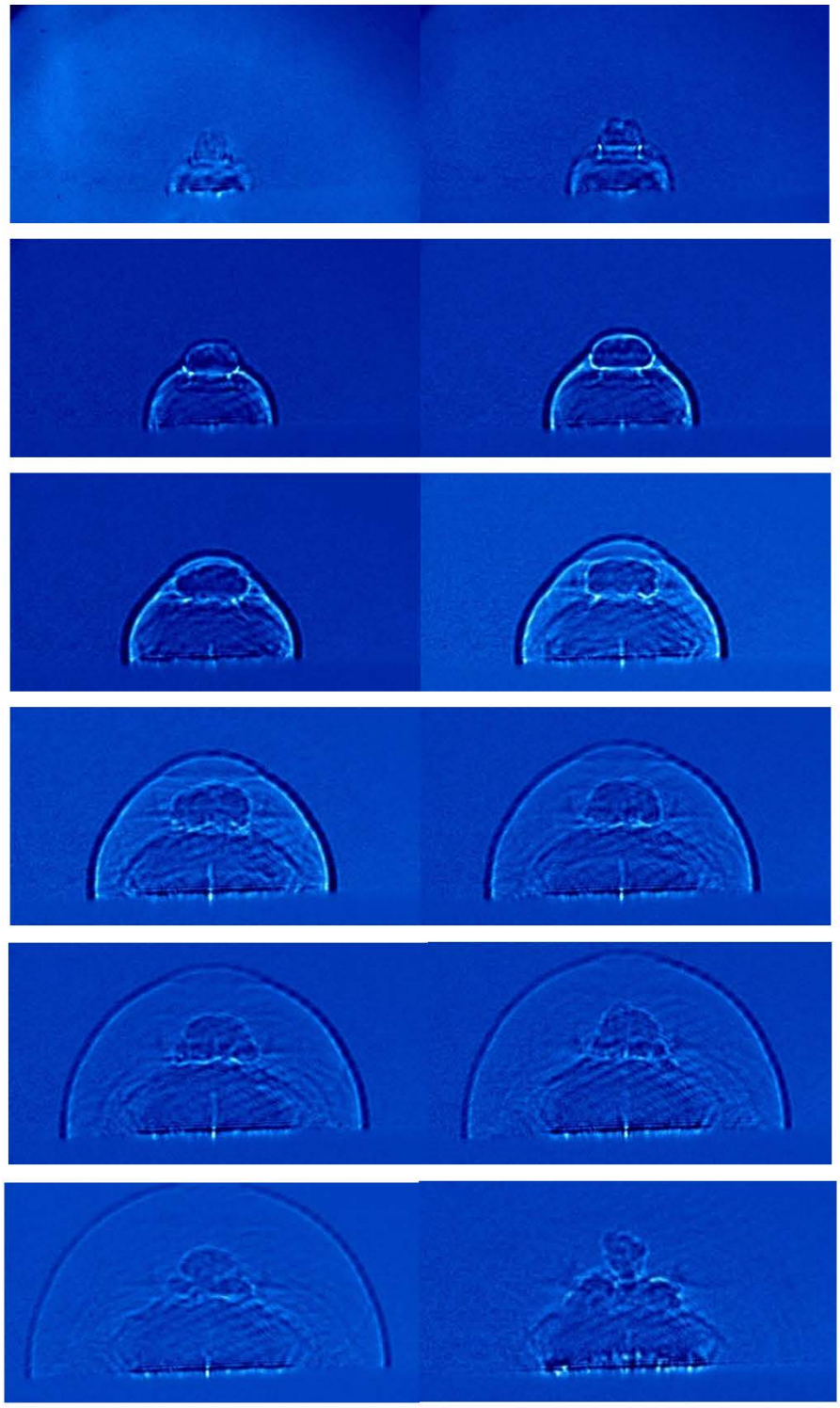

**Figure . Shadowgrams of the laser induced plasma at air target interface**

## Implement a two color laser interferometry diagnostics setup

High resolution two-color laser interferometry diagnostics were realized using two different wavelengths to measure the electron density ne of the laser induced plasma as well as the neutral gas density of the laser heated gas with spatial and temporal evolution. The interferometer works in the Mach–Zehnder configuration, in which the plasma is located in one of the arms of a two beam interferometer. The interferometer is configured to acquire an interference image of adjacent fringes of equal width when no plasma is formed. The changes in the optical index of the environment due to the presence of plasma and neutral gas profiles create a shift in the fringes that corresponds to the electron and neutral density profiles in the line of sight. These fringing patterns are captured by an intensified charged-coupled device ICCD ANDOR, DH 734of 1024x1024 active pixels and a 30 x 30 micro-$m^2$ resolution camera with a minimum gate width of 10 ns connected to a computer. The plasma is illuminated by two 1 mm diameter probe lasers, a He–Ne red laser emitting at lambda = 632.8 nm JDS Uniphase 1125P, and a high performance solid state green laser emitting at lambda G=532 nm Edmund Optics, NT56–484 operated independently at 5 mW power levels. The probe laser beam sizes are expanded by a factor of 20 using an optical beam expander Edmund Optics, NT55–579and a 20 mm aperture eliminates the edges of the expanded beam to improve the beam quality. The Gaussian wave front is split by a 50/50 beam splitter with one beam sent through the plasma chamber and the other used as a reference beam. Since the coherence length of the probe laser determined by the probe laser bandwidth of 0.05 nm is only 5.7 mm, both arms of the interferometer were adjusted to the same optical length of 61 cm within a few mm 5 mmoffset. A mismatch of the two wave fronts by one coherence length causes a drop of the fringe contrast by a factor of 1/e. The two view port windows on either side of the chamber are slightly tilted relative to the probe beam laser beam axis to avoid ghost images due to reflections. Optical interference filters with center wavelength at 5322 or 632.82 nm are used in front of the ICCD to suppress the plasma self-luminescence. Both the test and the reference beams are aligned to overlap within 200 m to assure the desired spatial resolution. The mirror for the reference beam is slightly tilted relative to the laser beam axis using a micropositioner. In this way a fringe pattern with the number of fringes proportional to the tilting angle is observed. A tilting of the mirror in the other plane rotates the fringe pattern. In the measurements, the null fringe pattern was arranged to show between eight and ten fringes over the 1.3 cm width field of view perpendicular to the observation axis.

By using a digital delay generator the gating trigger pulse of the ICCD is precisely synchronized with the firing pulse of the excimer UV laser. These two pulses are compared by means of a 1 GHz sample rate oscilloscope LeCroy, WaveRunner 6100A. The gate width of the ICCD is varied by using an electronic shutter controller with a typical gate width of 10 ns. Due to the high sensitivity of the ICCD, the milliwatt level cw powers of from the red and green lasers are sufficient to record images with a gate width of 10 ns.

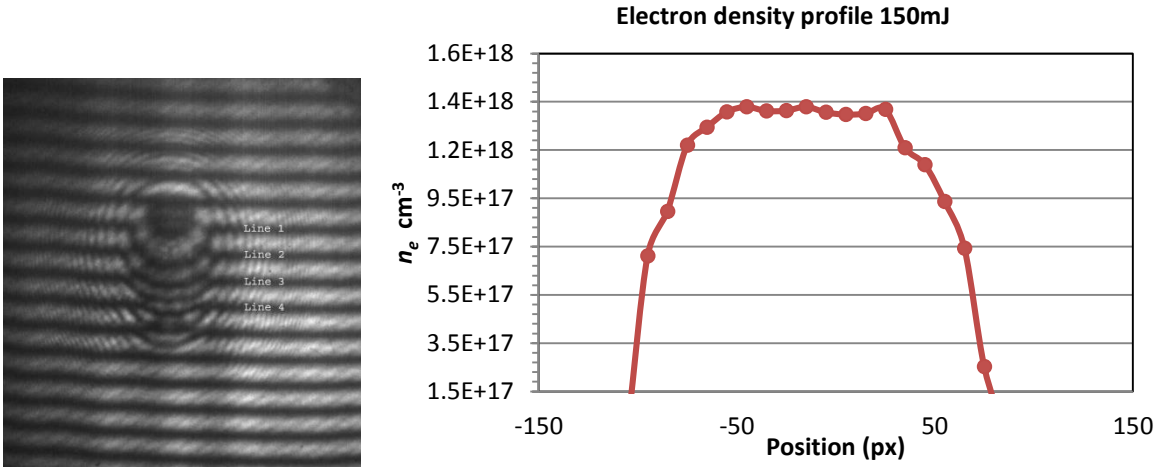


**Figure . Laser interferometry results**

Laser interferometry results recently obtained in an identical configuration indicate line-integrated electron density values ~$10^{18}$ cm$^{-3}$ at ~125 ns into the blast expansion. The density was calculated using [(Thiyagarajan and Scharer 2008), (Weber and Fulghum 1997; Zhang, Lu et al. 2009)]:

$$\Delta = (2\lambda n_c)^{-1} \int n_e dl$$

$$n_e = \frac{(2\lambda n_c)\Delta}{l}$$

Where, $\Delta$ is the ratio of the fringe shift to the fringe spacing, $\lambda$ is the wavelength of the probe laser, $n_c$ is the critical density, $n_e$ is the electron density which was assumed to be constant for this estimate, and the integral is over the path length. The image dimensions are 1.3cm x 1.3cm. This estimation is in agreement with the previously published work in this regime: including (Zhang, Lu et al. 2009).

## Implement optical emission spectroscopy diagnostics setup

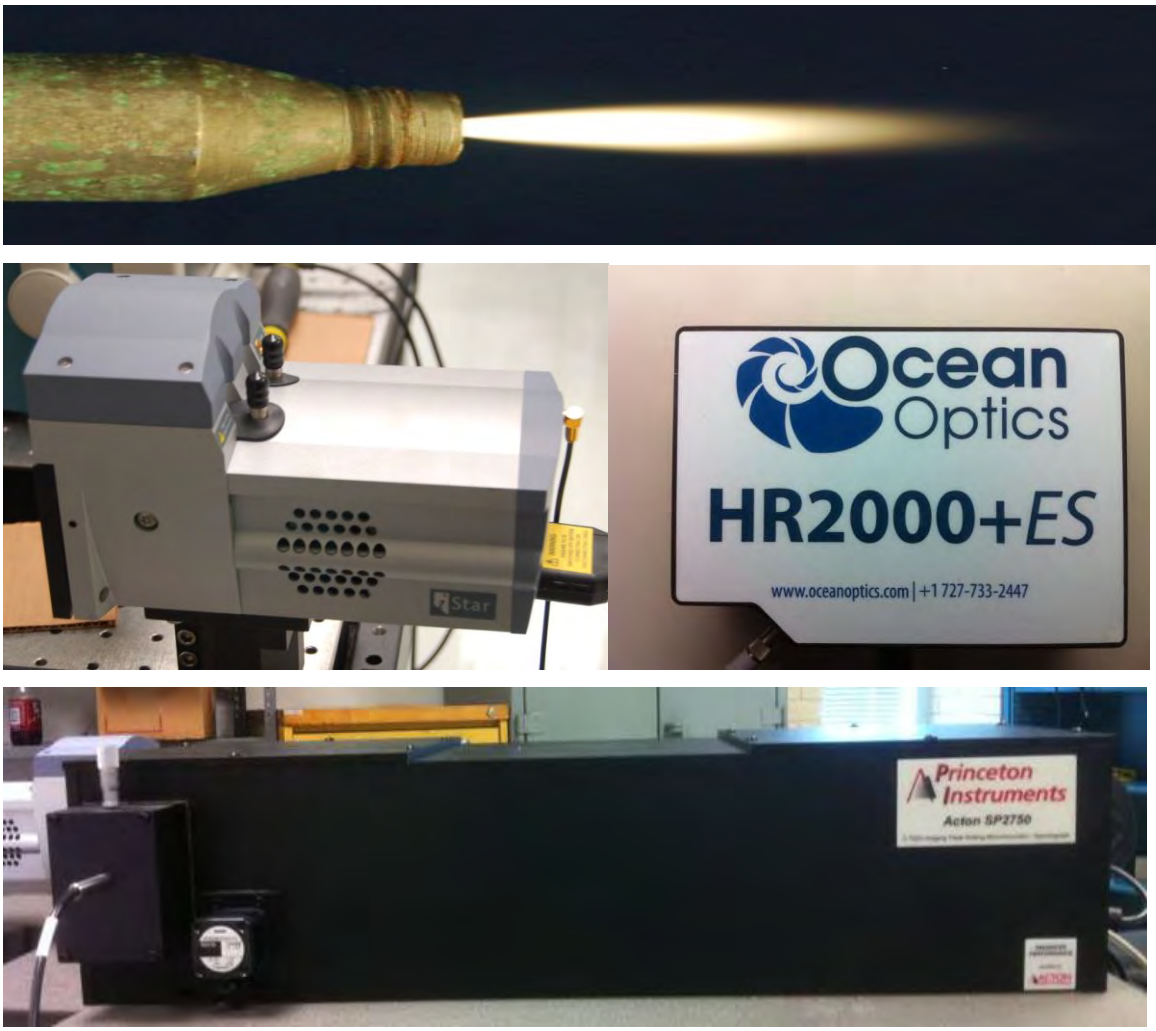


**Figure . Optical emission spectroscopy diagnostics setup**

The OES diagnostic setup is completed and used as shown in Fig.  to measure the rotational Trot and vibrational Tvib temperatures of the laser induced plasma. A high resolution narrow band 0.01 nm resolution monochromator Acton Research, model ARC-SP-2758 is used. The monochromator has a multiple grating option, which gives the flexibility of choosing the resolution and wavelength range. A holographic grating of 68_68 mm, 2400 grooves/mm, optimized for the entire visible wavelength range is used to acquire emission spectrum. The plasma emission is acquired by a collecting lens f 10 and sent to a fast gating Andor iStar ICCD ANDOR, DH 734 through a high-quality 200–800 nm fiber-optic bundle. The Andor iStar ICCD detector is integrated with an Acton SpectraPro 2750 spectrograph system. This system has a near-Lorentzian slit function with a

halfmaximum width of 0.2 nm when the grating density is set to 1200 lines/mm. The UV excimer laser is synchronized with the gated ICCD in such a way that the spectral emissions from the laser induced plasma are acquired at different plasma lifetimes ranging from 45 ns to 100 micros with a gating time of tg=45 ns for time windows t_100 ns and tg =100 ns for time windows t 100 ns. The spectral emission signal strength of the laser induced plasma spark is very weak due to small plasma dimension and short gating times of 45–100 ns. In order to obtain good signal strength and spectral profile, 2000 laser shots are used at each acquisition time and the laser is operated at 1 Hz to maintain the same laser energy output.

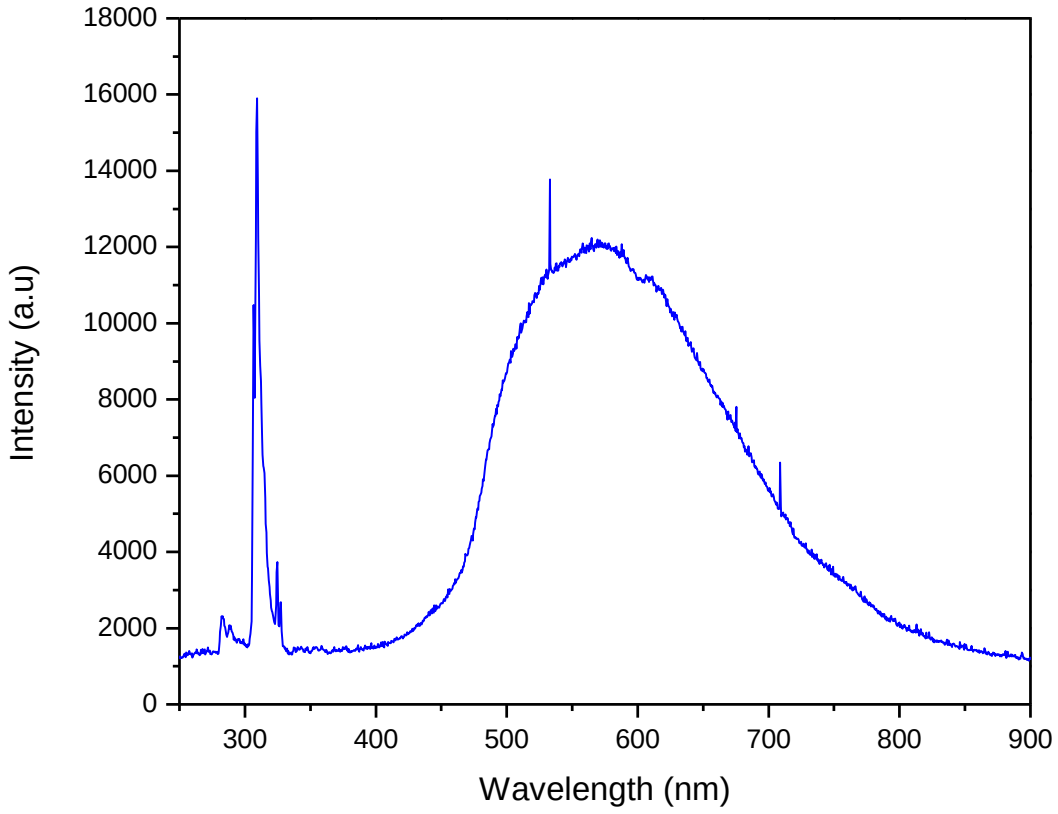


**Figure . Optical emission spectrum of air plasma**

## II. OBJECTIVE 2: DEVELOP PORTABLE PLASMA SOURCE

Atmospheric pressure non-thermal resistive barrier plasma (RBP) jet was designed, constructed and characterized for plasma surface treatment procedures applied in biomedical applications. The RBP source can operate in both DC (battery) as well as in standard 60/50 Hz low frequency AC excitation, and to function effectively in both direct and indirect plasma exposure configurations depending on the type of treatment targets and applications. The design and construction aspects of the RBP source are presented including the electrode configuration, electrical, cooling and gas flow aspects. The RBP jet is tested and its characteristics such as the propagation velocity of the plasma jet, electrical properties, plasma gas temperature and nitric oxides concentration are characterized using optical laser plasma shadowgraphy, voltage-current characterization, optical emission spectroscopy and gas analyzer diagnostic measurements respectively.

Using a laser shadowgraphy diagnostic we have measured the average propagation velocity of the plasma jet to be 150 - 200 m/s at 1 cm from the probe end. Discharge power is calculated from voltage-current characterization and plasma power is 26.33 W. An optical emission spectroscopy was applied and the gas temperature which is equivalent to the nitrogen rotational (Trot) temperatures was measured. After approximately 2 cm from the tip, along the axis the plasma emission drops and the high-temperature ceramic fiber-insulated-wire thermocouple probe was used to measure the temperatures of the gas flows along the downstream jet. The addition of a small portable external cooling unit has brought the temperatures of reactive oxygen species and other gases close to room temperature at the tip of the handheld plasma source unit. The concentrations of the reactive oxygen species at different spatial distances from the tip of the plasma jet were measured, at 5 cm distance from the electrode the nitric oxides level was measured to be in the rage of 500-660 ppm and drops to ~100 ppm at 60 cm.

The ppm values of nitric oxides after the cooling unit are observed to be of the same order of magnitude as compared to plasma jet. The portable RBP source was tested to be very effective for decontamination and disinfection of a wide range of foodborne and opportunistic nosocomial pathogens such as Escherichia coli, Staphylococcus aureus, Pseudomonas aeruginosa and Bacillus cereus and the preliminary results are presented. The effects of indirect exposure of the portable RBP source on monocytic leukemia cancer cells (THP-1) were also tested and the results

demonstrate that a preference for apoptosis in plasma treated THP-1 cells under particular plasma parameters and dosage levels. The tasks 8 and 9 under the objective 2 are completed as per the proposed milestones and the tasks 10 and 11 are in progress.

**Design and Construct the portable plasma source based on the design analysis and knowledge gained from objective 1.**

The schematic block diagram of the portable resistive barrier plasma (RBP) source is shown in below. The RBP jet was designed and constructed for biomedical applications. The RBP jet was based on the principles of large volume non-thermal resistive barrier discharge (RBD) researched in the past by the PI Thiyagarajan et. al. The instrument was designed to be a light-weight portable handheld plasma source which is capable of operating in both direct and indirect plasma exposure modes. Direct exposure of plasma involves exposure of plasma directly on to a target treatment surface whereas the indirect plasma exposure involves exposure of only the ROS generated by the plasma instead of the plasma itself, thus eliminating the effect of any possible UV radiation produced by plasma in the case of direct plasma exposure.

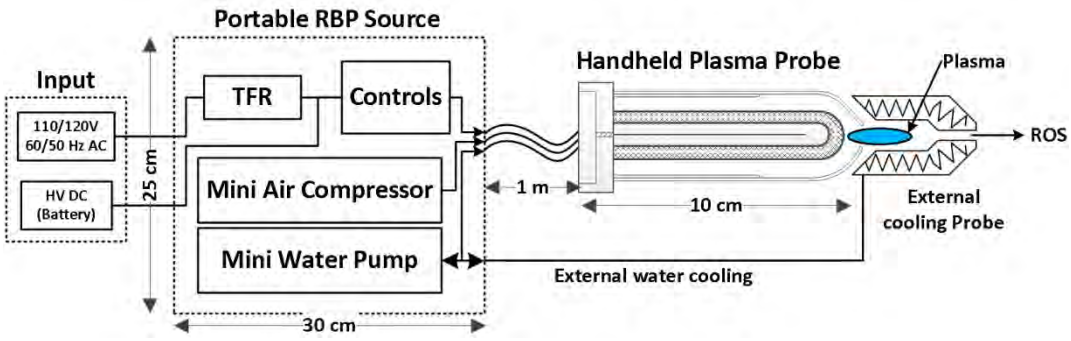


**Figure . Design Schematic of the portable plasma source design**

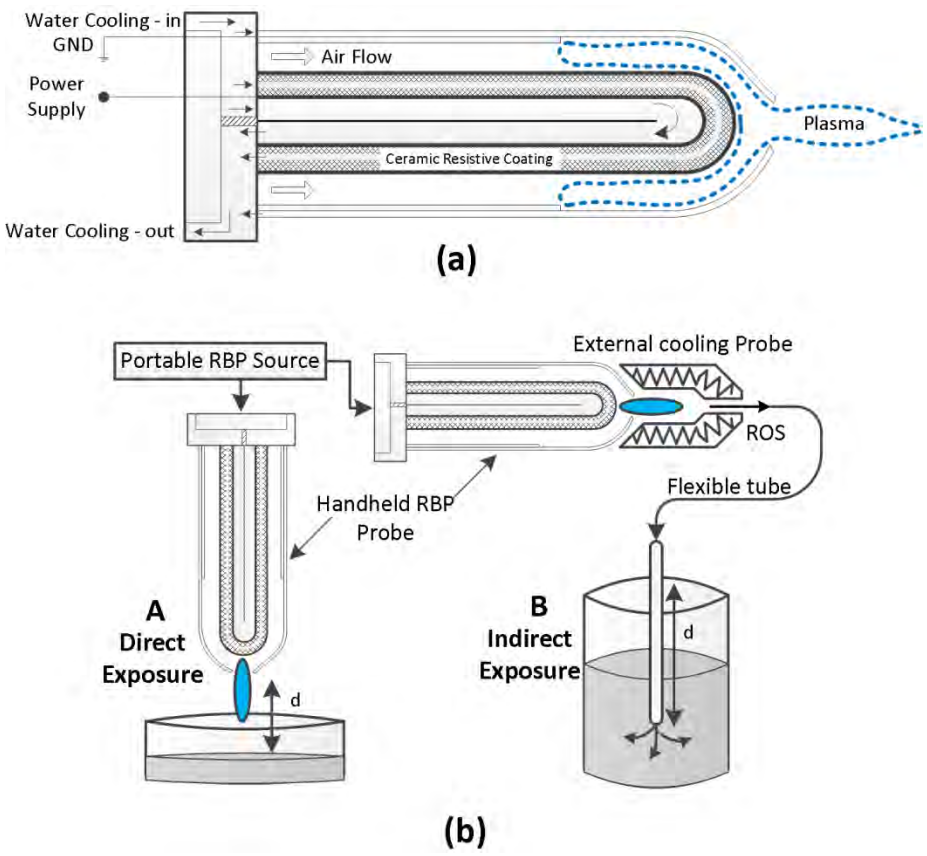


**Figure . Direct and Indirect treatment methods**

Since, the plasma instrument is principally a resistive barrier plasma source, it is capable of operating at both DC and low frequency AC, such as the standard operating voltages 120 V/60 Hz and 230 V/50 Hz which is stepped-up using a 6 kV, 30 mA (max) portable lightweight transformer housed in the power supply unit. The portable plasma source is primarily made up of two units namely the power supply control unit and the handheld plasma probe where the plasma jet is being generated. The handheld plasma probe unit is lightweight and maintained at room temperature through a cooling circuit and it is connected to the power supply unit through a flexible chord to facilitate the remote workability for medical practitioners and biomedical applications. The power supply unit was constructed in a portable form such that it can be easily carried over by operators, when needed. The power supply unit contains a mini 12 V DC water pump (Geo-Inline) for cooling the electrodes in the handheld plasma probe unit as well as the optional external cooling unit. The power supply unit also contains a mini 12 V DC air compressor weighing less than 3 lbs. to supply the forced air as an operating gas to the handheld plasma probe unit. The power supply unit also

houses transistor-transistor logic (TTL) and relay controls to select between AC and DC, and power levels and flow controls. The entire RBP source is constructed to fit within 12 × 10 × 10 inch3 portable metallic case and the entire power supply and RBS plasma source weighs ~20 lbs. The schematic of the handheld plasma probe unit is shown, which consists of central deionized water cooled cylindrical electrode surrounded by deionized water cooled high density alumina ceramic resistive coating. The central electrode which is approximately 1 cm diameter and 10 cm long is surrounded by a double layer hollow ground electrode separated by an electrode gap space of 2 mm. The plasma source uses atmospheric pressure air as the operating gas, in which the air forced through the resistive barrier plasma source electrode gap space using a mini-compressor such that the plasma and ROS including nitric oxides at the tip of the handheld plasma source tip are controlled and maintained based on the plasma power and flow-rate. Plasma streamers are formed between the high-voltage resistive electrode and the ground electrode. A fraction of the forced air passing through the RBP source gets ionized and exits through a 2 mm pinhole type opening at the tip of the plasma source generating a stable plasma jet and continuous flow of ROS including nitric oxides. The plasma streamers formed in the cylindrical hollow electrode configuration are dynamic with respect to its location between the electrodes, which also assists in preventing localized heating and arc formation. The ceramic electrodes are water cooled through a mini-water pump.

For the indirect exposure method the concentrations of the nitric oxides are preserved by reducing the plasma temperature rapidly through a separate external small efficient cooling unit. For applications that require high temperature plasma, the additional cooling unit can be easily separated from the hand held plasma jet. The temperatures of selected ROS flow from the cooling unit tip were measured to be at room temperature which is ideal for treating heat sensitive materials and targets in the biomedical applications and medicine such as human skin treatment. The external cooling units are scalable and additional units can be added or removed in order to vary the exit temperature of selected ROS.

**10. Testing and characterization phase: Portable plasma source will be tested and characterized for its operating parameters and plasma parameters.**

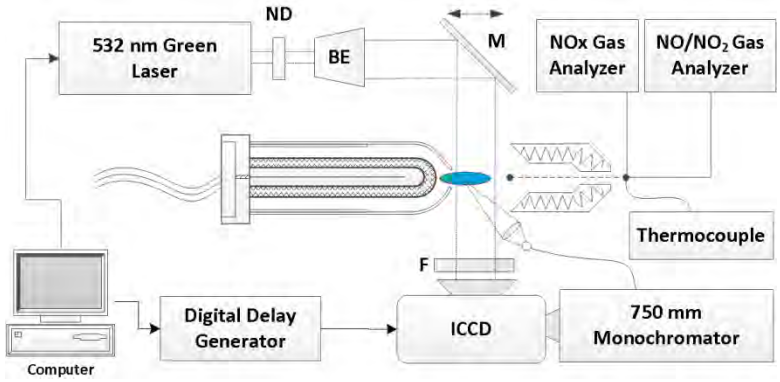


**Figure . Schematic of Testing and characterization of portable plasma system**

The characteristics of the resistive barrier plasma source such as the propagation velocity of the plasma jet, electrical characterization of the plasma jet, gas temperature and concentration of ROS including nitric oxides are characterized using diagnostics techniques namely optical laser plasma shadowgraphy, voltage current characterization, optical emission spectroscopy and gas analyzer techniques.

A high resolution 532 nm laser shadowgraphy diagnosticwas setup as illustrated, to measure the propagation velocity of the plasma jet. A computer-controlled 532 nm continuous-wave (CW) diode-pumped solid state probe laser outputs a 1 mm beam diameter TEM00 laser beam with 0 – 10 mW adjustable power output that was expanded to 20 mm beam diameter using an anti-reflective (AR) coated 20X Galilean laser beam expander (Thorlabs, BE20M) with collimation adjustment. The expanded 532 nm laser beam axis was aligned to pass through the plasma jet and captured using an intensified charge coupled device (ICCD; Andor, iStar 734). The ICCD was computer controlled and capable of capturing high-resolution 1024 × 1024 pixel (13.6 x 13.6 mm) images with a minimum gating width of 2 ns and a maximum gain of 104. It was synchronized with a digital delay generator and shutter control. The delay timings were monitored and measured using a high speed digital oscilloscope. Optical interference filters with center wavelength at 532 ± 2 nm was used in front of the ICCD to suppress the plasma jet self-luminescence. The shadow of the laser induced plasma falls onto the ICCD sensor with a 1:1 ratio (1 pixel = 13.2 μm). The voltage applied to the high-voltage electrode is measured using a high voltage probe (Tektronix P6015A) and the discharge current is measured using a current probe (Tektronix TCP202). The

voltage–current waveforms are recorded using a 2 GHz digital oscilloscope (Tektronix TDS3034C). The optical emission spectroscopy diagnostic setup was used as shown, to measure the plasma gas temperature rotational (Trot) of the nitrogen in the plasma jet. A high resolution narrow band (0.01 nm resolution) monochromator (Acton Research, Model: SP-2750) was used. The monochromator has a multiple grating option, which gives the flexibility of choosing the resolution and wavelength range. A holographic grating of 68 x 68 mm, 2400 G/mm, optimized for the entire visible wavelength range was used to acquire emission spectrum. The plasma emission was acquired by a collecting lens (f /10) and sent to a fast gating Andor iStar ICCD (ANDOR, DH 734) through a high-quality (200-800 nm) fiber-optic bundle. The Andor iStar ICCD detector was integrated with an Acton SpectraPro 2750 spectrograph system. This system has a near-Lorentzian slit function with a half-maximum width of 0.2 nm when the grating density was set to 1200 lines/mm. A high-temperature ceramic fiber-insulated-wire thermocouple probe capable of measuring temperatures up to 1400 °C was used to measure the temperature of the downstream jet when plasma emission ends after approximately 2.5 cm.

The parts per million (ppm) concentration of the ROS including nitric oxides at different spatial distances from the tip of the plasma jet was measured using two gas sensors namely NOXCANg and Testo 350 M/XL gas analyzer as shown. The NOXCANg is a versatile and highly integrable nitric oxides measurement diagnostics instrument which uses ceramic NOx sensor to withstand high temperatures that was mounted in the probe tip and communicates the measured NOx parameters from 0 to 5000 ppm to the Kvaser Leaf Light HS data bus and logs the data in the computer via its controller area network (CAN) bus port with a 150 ms response /refreshing time. The NOxCANg sensor was externally powered at 18V DC using Agilent E3631A Triple Output DC Power Supply. A data acquisition tool communicates with the NOxCANg sensor module through Kvaser Leaf Light HS data bus and logs the NOx concentrations in ppm.

The non-thermal atmospheric pressure resistive barrier plasma (RBP) source was designed and constructed for surface treatment and biomedical applications. The RBP source was tested for its propagation velocity of the plasma jet, electrical diagnostics, plasma gas temperature and selected ROS concentrations such as nitric oxides that are primary characteristics needed for biomedical applications.

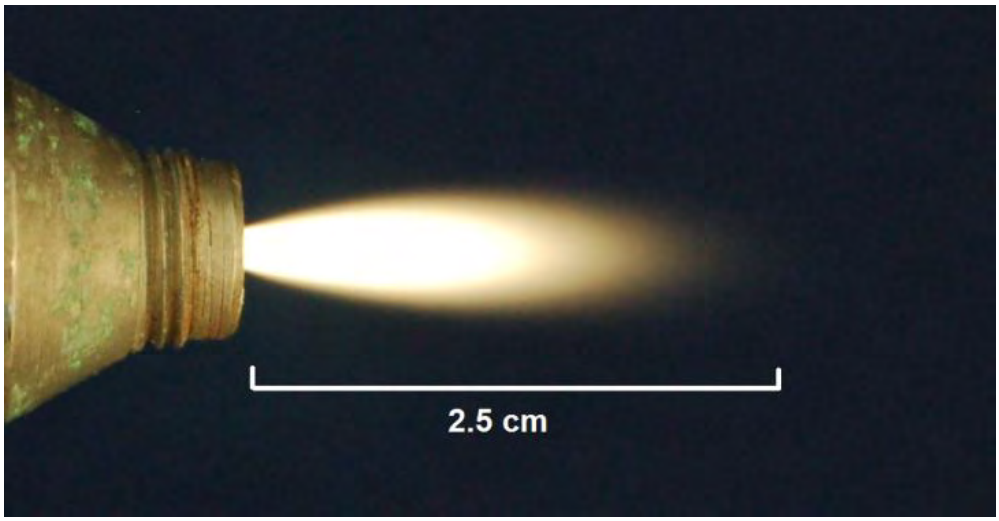


**Photograph of the RBP jet.**

A photograph of the portable RBP jet is shown. The visible plasma jet spans approximately 2.5 cm from the exit tip and decays as it recombines and diffuses into the surrounding atmosphere.

The propagation velocity of the plasma jet is an important parameter in determining the treatment distances of surfaces to be treated in biomedical applications. We have developed a 532 nm laser shadowgraphy diagnostic technique to measure the propagation velocity of the portable resistive barrier plasma jet. The laser shadowgraphy technique also provided the flow dynamics of the plasma jet and neutral gases at elevated temperatures. In the laser plasma shadowgraphy technique, a synchronized CW 532 nm probe laser beam was expanded and sent through the test section where the plasma jet is located and its image falls directly onto the ICCD on the image plane. In a plasma, the refractive index is primarily a function of the electron density, which is the main plasma parameter determined by refractive-index measurements. Typical plasma diagnostics based on refractive effects include interferometry, Schlieren imaging, and shadowgraphy measurements. While the first technique gives a direct measure of the refractive index $\mu$, the Schlieren image responds to the first spatial derivative of the index of refraction. The shadowgram however responds to the second spatial derivative or Laplacian. A shadowgraph measures lateral displacement of the light rays after passing through a medium such as plasma. An electromagnetic wave exerts a force on the charged constituents of the medium through which it propagates. This force accelerates the charge which, in turn, modifies the time-varying electromagnetic field. A solution of electromagnetic-wave propagation in plasma can be obtained by solving the wave equation for a plane wave in the small amplitude approximation [58]. The refractive index of high-frequency electromagnetic wave propagation in unmagnetized plasma is:

$$\mu_e = \sqrt{1 - \frac{\omega_p^2}{\omega^2}} = \sqrt{1 - \frac{n_e}{n_c}} \quad (1)$$

where $\omega = 2\pi c/\lambda$ the frequency of the electromagnetic wave, $\omega_p = (n_e e^2/\varepsilon_0 m_e)^{1/2}$ is the electron plasma frequency, and $n_c = m_e \epsilon_0 \omega^2 e^{-2}$ is the cutoff electron density for which electromagnetic wave propagation is possible. If the refractive index in the test section $\mu$ is uniform, the screen will be essentially uniformly illuminated. If, however, the gradient of $\mu$ varies in space, as one may expect for high-temperature plasmas, i.e., when there is a significant second derivative of the refractive index, there will be variations in the illumination at the imaging screen. Regions where the second derivative of the refractive index is negative that will act like a converging lens.

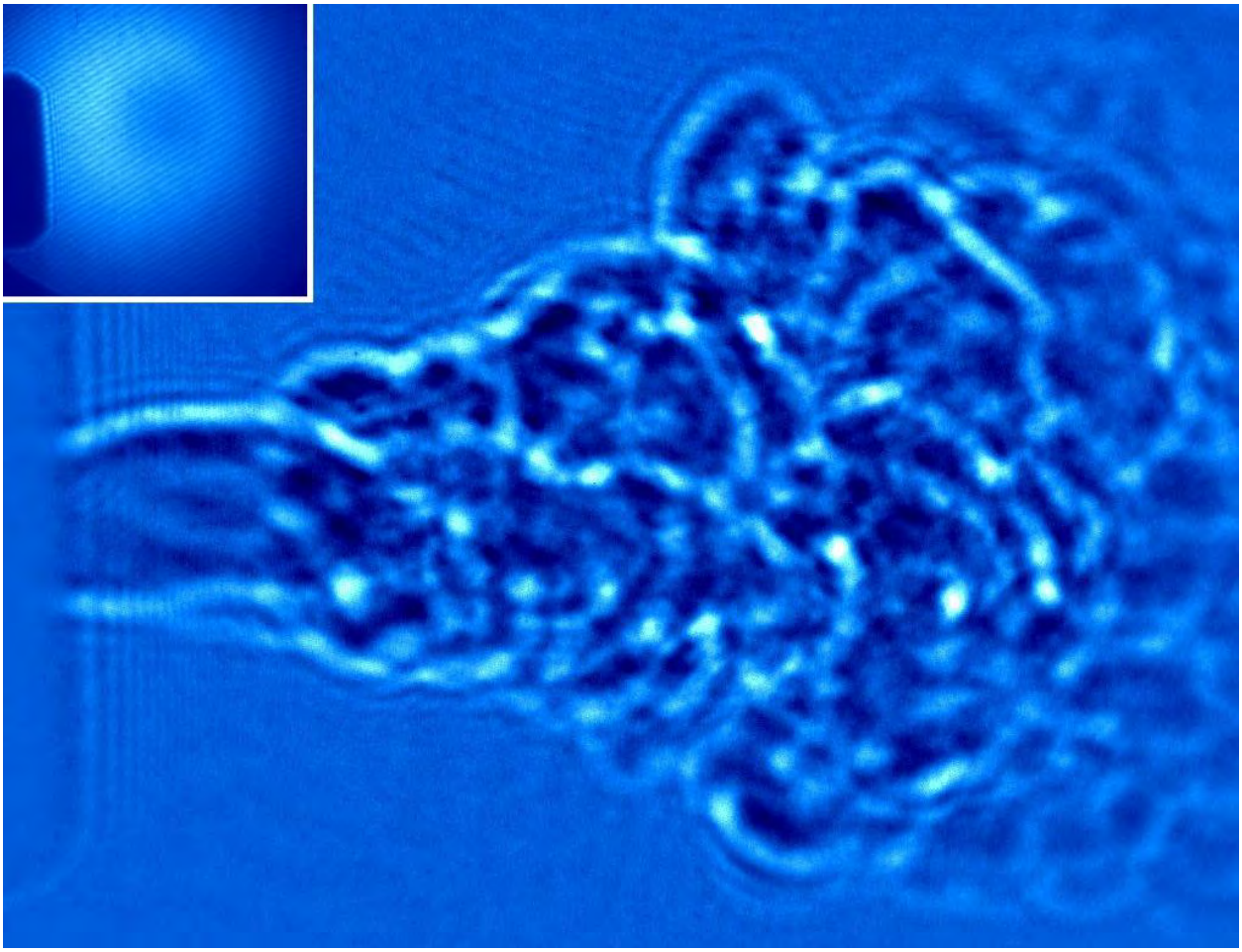

**Laser shadowgram of the plasma jet. Image size-1.25 x 1.75 cm. Sub-figure (top-left): laser shadowgram of gas flow-only and with power off (no plasma).**

A laser shadowgram of the plasma jet obtained is shown, by passing an expanded 532 nm probe laser beam through the plasma jet and capturing the transmitted laser beam on an image pane using a fast gated ICCD. Several shadowgrams were obtained at 100 ns gating time with a ICCD triggering delay time of 125 $\mu$s, as

indicated with an arrow in Figure. The same triggering signal is used to capture the voltage-current signals without the signal delay. By tracking the plasma eddies in the shadowgrams, we have measured the average propagation velocity of the plasma jet to be 150 - 200 m/s at 1 cm from the probe end. The laser shadowgraphy technique is based on the presence of significant second derivative of the refractive index, which can be caused by the presence of plasma as well as the neutral gas at elevated temperatures. Unlike Schlieren diagnostics that is based on the first derivative of the refractive index changes, the flow dynamics of the gas at near room temperatures are generally not captured through the laser shadowgraphy technique since it does not create enough second derivative refractive index changes in the laser beam path. Therefore the shadowgrams obtained through our laser shadowgraphy diagnostics can be caused by both the plasma jet and the heated neutral gas. It is further verified through turning on only the gas flow at room temperature and keeping the high-voltage off (plasma off), resulted in no observable shadowgrams in the ICCD, as shown in the sub-figure of Fig. However, when we used a separate source of gas that is heated up to few hundred degrees C resulted in weak shadowgrams.

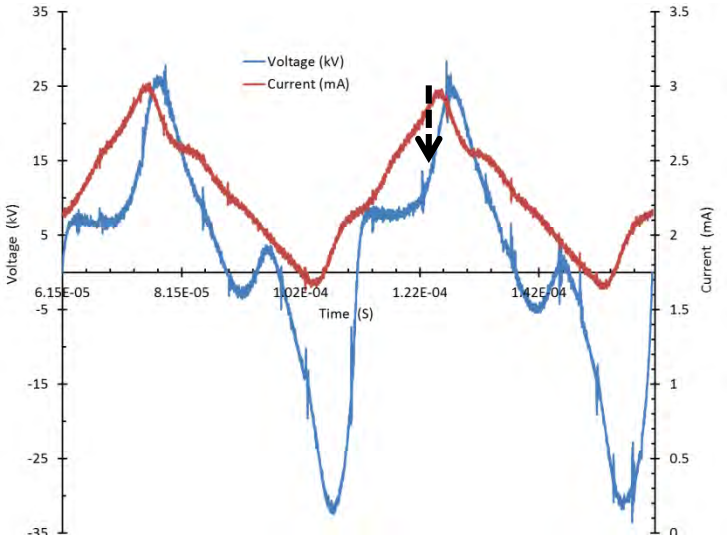


**Fig 14. Voltage-Current waveform of the RB plasma jet in air. Discharge power is 26.33 W.**

In the RBP jet, the discharge is initiated by applying a sufficient voltage between the electrodes by which the air between the electrodes breakdowns and results in a plasma jet sustained by applied voltage. Above Figure, shows the voltage-current waveform of the RBP jet. Both voltage and current waveforms exhibit pulses of few microseconds long. The positive and negative half periods of the applied voltage are unsymmetrical due to the existence of only one resistance between the electrodes. The maximum voltage and current values are approximately 25 kV and 3 mA on the positive half period of the applied voltage, correspondingly. Using the voltage–current waveforms, the average power dissipated in the discharge is calculated by integrating the product of the discharge voltage and current over one cycle; according to the following equation ($T$ = period of the discharge).

$$W = \frac{1}{T}\int_{t}^{t+T} I(t)V(t)dt \quad (2)$$

and the measured plasma power is 26.33 W.

Optical emission spectroscopy can be used to determine the plasma temperatures of the RBP jet with some assumptions. To determine the plasma rotational gas temperatures, local thermodynamic equilibrium (LTE) must be assumed. The local thermodynamic equilibrium is valid in the central region of the plasma jet but not at the larger outer radii. The ROS produced in the plasma are long lived active species that can propagate far beyond the plasma jet and in to the surrounding environment preferentially following the plasma jet direction. These long lived active species are important for biomedical applications and we have measured the $NO_x$ concentration of ~900 ppm at 10 cm away from the plasma source exit nozzle. In this section the plasma temperature measurements using optical emission spectroscopy and the downstream neutral gas temperature measurements using thermocouple are presented.

The nitrogen rotational ($T_{rot}$) temperature which is equivalent to plasma gas temperature was measured using the $N_2$ C-B (2+) ($N_2$ second positive band system) rotational transitions in the range 364-383 nm, by matching them with a code simulated results from SPECAIR. This spectral range corresponds the $\Delta\ v$ = -2 vibrational sequence of $N_2$ C-B (2+) band system and the best-fit SPECAIR spectrum can yield rotational temperatures ($T_{rot}$). SPECAIR is computer simulation software developed by Laux *et. al.* on the basis of the NonEQuilibrium Air Radiation code (NEQAIR) by Park. SPECAIR performs the OES by determining the populations of the states of the radiative transitions using user-specified electronic, vibrational and rotational temperatures. The modeled transition rates are calculated based on tabulated data for the transitions. From the calculated transition probabilities and populations of radiating species, the line-by-line optical emission intensity was computed for the wavelengths of the transitions. The experimental spectra measured at different distances ranging from 0.2 cm to 2 cm and SPECAIR code matched spectrum are shown.

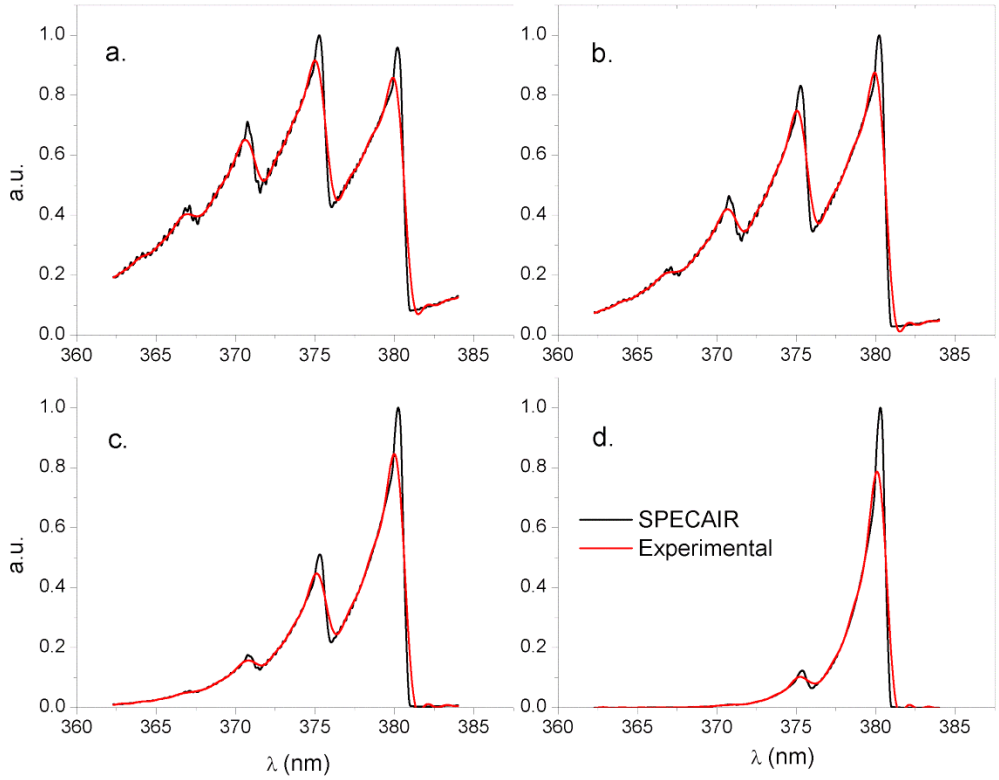


**Experimental and SPECAIR code simulated matching of emission spectra of RBP jet at different distances from exit. a. 0.2 cm – 3000 ○C, b. 0.8 cm – 2000 ○C, c. 1.5 cm – 1500 ○C, d. 2 cm – 1000 ○C.**

The temperatures measured from the SPECAIR code matched spectrum resulted at temperatures as high as 3000 °C at 0.2 cm from the exit and decays to 2000 °C at 0.8 cm and continues to decay to 1500 °C at 1.5 cm and to 1000 °C at 2 cm. After approximately 2 cm from the exit nozzle tip along the axis, the plasma emission drops and therefore a high-temperature ceramic fiber-insulated-wire thermocouple probe was used to measure the temperatures of the neutral gas propagating in to the surrounding environment (downstream jet). The axial temperature decay of the plasma jet from the plasma source tip before entering the cooling unit or without the cooling unit is shown., in which the data in solid circles (red) represent the optical emission spectroscopy results and the data in solid squares (black) represent the results from thermocouple measurements.

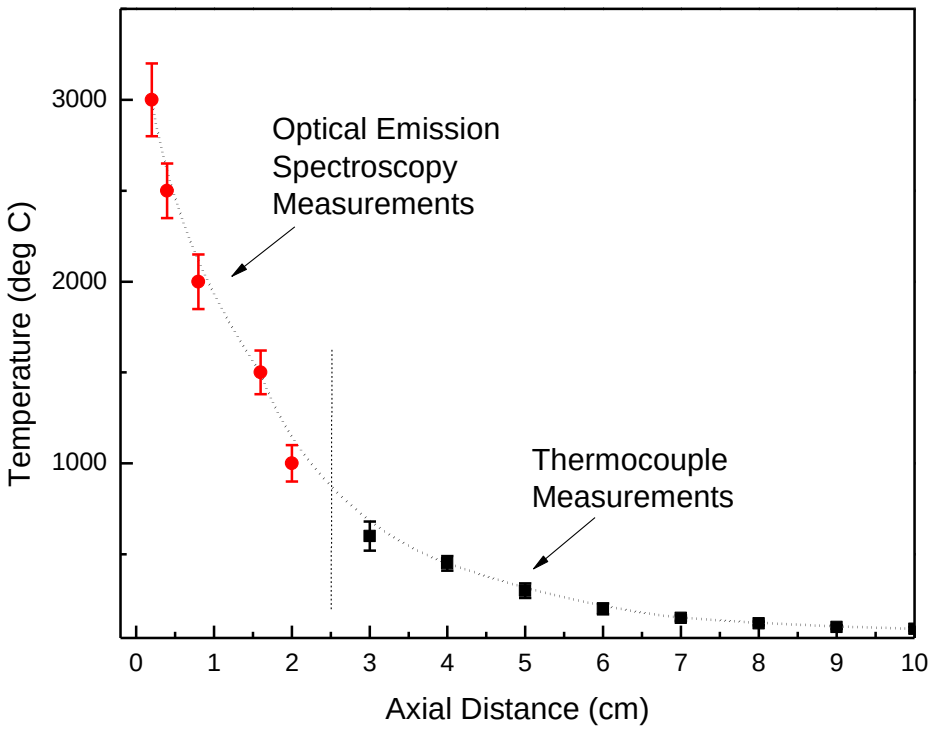


**The axial temperature decay of the plasma jet from the RBP source tip before entering the cooling unit.**

The plasma temperature at the nozzle exit of the plasma source reaches around 3000 °C and the temperature drops rapidly to less than 100 °C at approximately 8 cm from the tip. The high gas temperature obtained from $N_2$ rotational temperature is due to excitation of $N_2$ to high rotational/vibrational levels and the excited $N_2$ species are generated in the plasma jet. However, plasma gas temperature drops rapidly towards the end of visible plasma jet. The temperature of the plasma plume at the exit reaches >2500 °C which is sufficient to generate nitric oxides. When the external cooling units were added the gas temperatures were brought close to room temperature at the tip of the handheld plasma source unit.

The concentration of the ROS produced by the plasma jet with and without the cooling unit are measured. The majority of the ions recombine before it exits through the cooling unit and at this stage several gas species and other parameters were monitored, including $O_2$, $O_3$, CO, $CO_{low}$, $NO/NO_2$, $NO_{low}$, $NO_X$, $CO_{2(Infrared)}$, $SO_2$, HC, $H_2S$, temperature, pressure, flow, velocity, efficiency, mass, etc. Based on the results we observed that nitric oxides are the predominant long lives species produced by the RBP source and some trace $O_3$. The nitric oxide formation is a reversible plasma chemical reaction and it can be expressed as

$$N_2 + O_2 \Leftrightarrow 2NO - \Delta E \quad (3)$$

The nitric oxides from the tip of the hand held plasma jet are measured using gas analyzers. The nitric oxide contains the active oxidation potential and reacting with oxygen in the environment as it exits the plasma source induces the formation of nitrogen dioxide at a smaller concentration. The decaying concentration of the nitric oxides from the plasma jet can be used as reference for the treatment distance between the target surface and the plasma source tip. The background $NO_x$ concentration are measured using $NO_x$CANg module at various timings and at standard laboratory conditions well before the plasma source was operated and it was measured to be less than 0.5 ppm. The measurements are carried out at 20 data sets separated by 1 min with 1 second acquisition time at distances 5, 10, 20, 30, 60 and 100 cm from the tip. For consistency in the concentration measurements, three other sampling timings such as 10, 30 and 60 second are tested in addition to 1 second acquisition time. The $NO_X$ concentrations of the plasma jet in ppm without the cooling unit are measured at various axial distances (in cm) from the tip and shown.

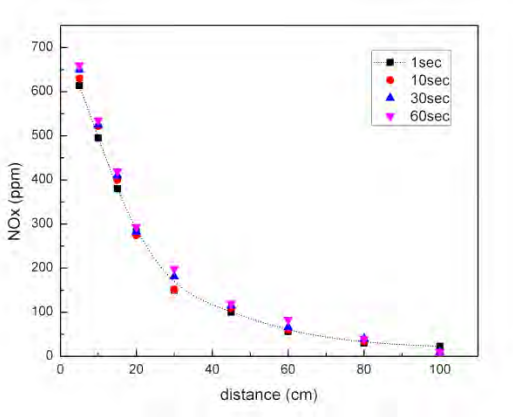


**The NOX concentrations of the plasma jet from the RBP source in ppm without the cooling unit at various axial distances from the tip.**

The results indicate the consistency of the plasma output characteristics and $NO_x$ concentration levels for varied time averaged integration times and data sampling frequencies. The $NO_x$ concentration peaks right at the electrode tip as expected and at 5 cm from the electrode, $NO_x$ concentration was measured to be in

the rage of 500-660 ppm at different exposure times. The concentration drops to half of its initial value at ~20cm and it continue to drop to ~100 ppm at 60 cm and at 100 cm distance from the tip the concentration was very low (<10 ppm). The $NO_x$ concentrations in ppm with the cooling unit added and measured at various axial distances (in cm) from the out tip of the cooling unit is shown in Figure below.

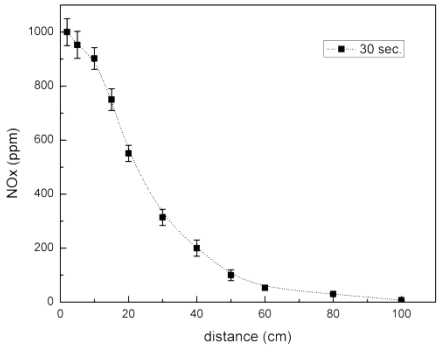


**The $NO_x$ concentrations in ppm with the cooling unit added to the RBP tip at various axial distances (in cm) from the out tip of the cooling unit.**

Based on the measurements it was observed that the $NO_x$ concentration after the cooling unit was slightly higher (~950 ppm) compared to that of plasma jet (~615 ppm), this was due to the fact that plasma jet diffuses out after it exits from the handheld electrode whereas the probe diameter after the cooling unit is very small like a pinhole arrangement with 1 cm diameter opening leading to increased concentration.

$NO_x$ is composed of two components such as the mono-nitrogen oxides or nitric oxides (NO) and nitrogen dioxide ($NO_2$). In order to measure the individual concentration levels of NO and $NO_2$ a different diagnostic tool was realized using a gas analyzer (Testo 350 M/XL) capable of identifying and characterizing over several molecular gases including NO and $NO_2$. The Fig. below shows the concentrations of NO and $NO_2$ for the plasma jet without the cooling unit.

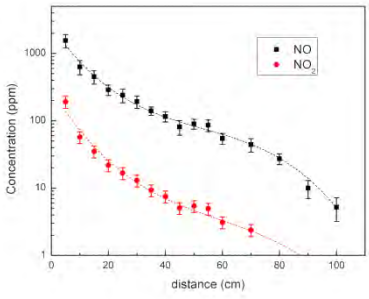


The concentrations of NO and $NO_2$ for the RBP jet without the external cooling unit.

The Fig. below shows the concentrations of NO and $NO_2$ from the probe with external cooling unit.

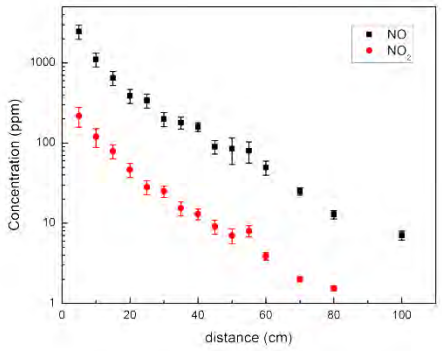


The concentrations of NO and $NO_2$ from the RBP probe with external cooling unit.

The concentration of $NO_2$ was much lesser compared to that of NO by an order of magnitude or higher. The ppm concentration of NO is at the preferred level for a wide range of standard biomedical treatment applications. The ppm concentration of $NO_2$ is below the OSHA safety standards. The formation of different active species produced in non-thermal air discharges involves complex plasma chemistries. At relatively high gas temperatures various nitrogen oxides ($NO_x$) are produced through $N_2$ and $O_2$ reactions [62, 63]. The production of $NO_x$ species is mainly dependent on the oxygen ($O_2$) concentration in air plasmas. It has been shown that in air plasmas, a threshold value of 5% $O_2$ concentration is necessary for $NO_x$ formation [62] mechanisms.

$$N_2 \rightarrow 2N \qquad \Delta G^\circ = +911.1 \text{ kJ}.mol^{-1} \quad (4)$$

$$N + O_2 \rightarrow NO_2 \qquad \Delta G^\circ = -404.3 \text{ kJ}.mol^{-1} \quad (5)$$

$$N + O_2 \rightarrow NO + O \qquad \Delta G^\circ = -137.3 \text{ kJ}.mol^{-1} \quad (6)$$

Based on the reactions 5 and 6, the $NO_2$ production (reaction 5) is more favorable than the NO production (reaction 6) in such plasma conditions.

$$NO_2 \rightarrow N + O_2 \qquad \Delta G^\circ = +404.3 \text{ kJ}.mol^{-1} \quad (7)$$

$$NO_2 \rightarrow NO + O \qquad \Delta G^\circ = +267.0 \text{ kJ}.mol^{-1} \quad (8)$$

Furthermore, $NO_2$ decomposes into $N + O_2$ (reaction 7) and $NO + O$ (reaction 8), in which the reaction 8 is more favorable than the reaction 7. Therefore it results in a higher NO concentration along the plasma jet compared to $NO_2$ as shown in above two Figures.

## 11. Biological testing: In-vitro biological testing.

The effective sterilization of foodborne and opportunistic nosocomial pathogens is a major problem in food industry, biomedical and hospital applications, respectively. The resistive barrier plasma (RBP) jet was tested over a wide range of microbes for its decontamination and disinfection efficacy and we have found that the RBP source is very efficient in decontaminating wide range of infection and contamination causing bacteria. The direct and indirect exposure of the RBP jet (with the cooling unit) as a non-thermal sterilization method was tested on regrowth potential of post-partial-plasma-exposure of foodborne and nosocomial pathogens. Similarly the RBP jet was also tested on plasma efficiency at different bacterial concentrations for its effects on growth for pre and post plasma treated bacteria. In these tests, the ROS produced by the RBP source was applied to Escherichia coli ATCC 11775, Bacillus cereus ATCC 14579, Staphylococcus aureus ATCC 25923 and Pseudomonas aeruginosa ATCC 27853. An average of 30 CFU per 71 mm2 was inoculated with the corresponding bacterium on a dry surface-agar plate, followed by the following exposure times 0, 30, 60,120 and 180 seconds of plasma. 20 µl of E. coli 107 CFU/ml and P. aeruginosa 108 CFU/ml were treated with plasma for 0, 120, 240 and 360 seconds. The colonies that survived the plasma treatment and control colonies were transferred to tryptic soy broth (TSB) and their growth was observed for 24 hrs. Results have showed 100% and 96% of inactivation after 180s of treatment for E. coli and S. aureus respectively. A 100% of inactivation was observed for B. cereus and P. aeruginosa after 60s. E. coli and P. aeruginosa showed a log reduction of 3.4 and 3.9 orders respectively after 360s. The 24 hours re-growth results of direct exposure of plasma for 30, 60 and 120 seconds on Escherichia coli (ATCC 11775), Neisseria meningitidis (ATCC 700532) and Staphylococcus aureus MRSA (ATCC 259231) are shown in Fig. below.

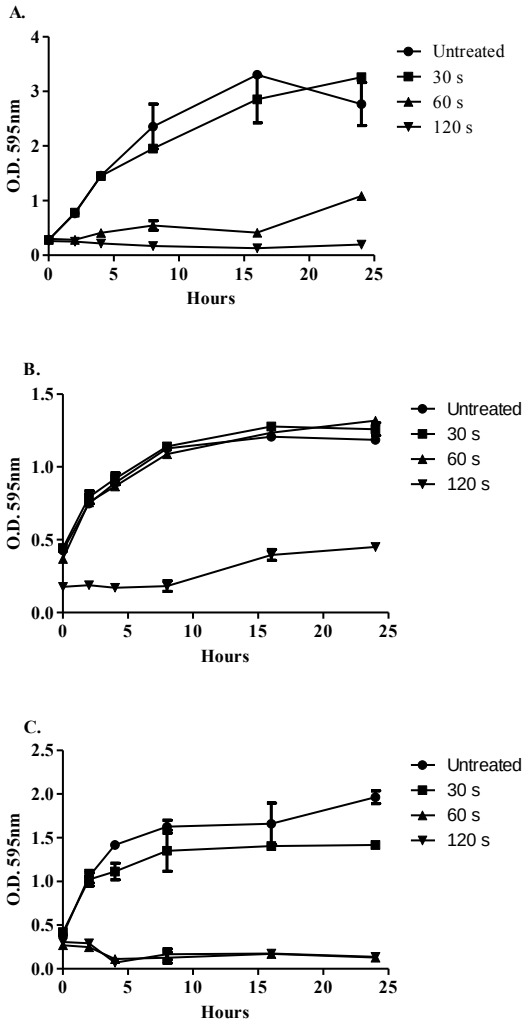


Density measurements over a 24 hour period of bacteria without direct plasma treatment (closed circles ●) or with direct treatment of plasma for 30 seconds (closed square ■), 60 seconds (closed up-pointing triangle ▲), or 120 seconds (down-pointing triangle▼). A.) *Escherichia coli* (ATCC 11775). B.) *Neisseria meningitidis* (ATCC 700532). C.) *Staphylococcus aureus* (ATCC 259231).

The 24 hours re-growth results of indirect exposure of plasma 120 seconds on Escherichia coli (ATCC 11775), Neisseria meningitidis (ATCC 700532) and Staphylococcus aureus MRSA (ATCC 259231) are shown in Fig. below.

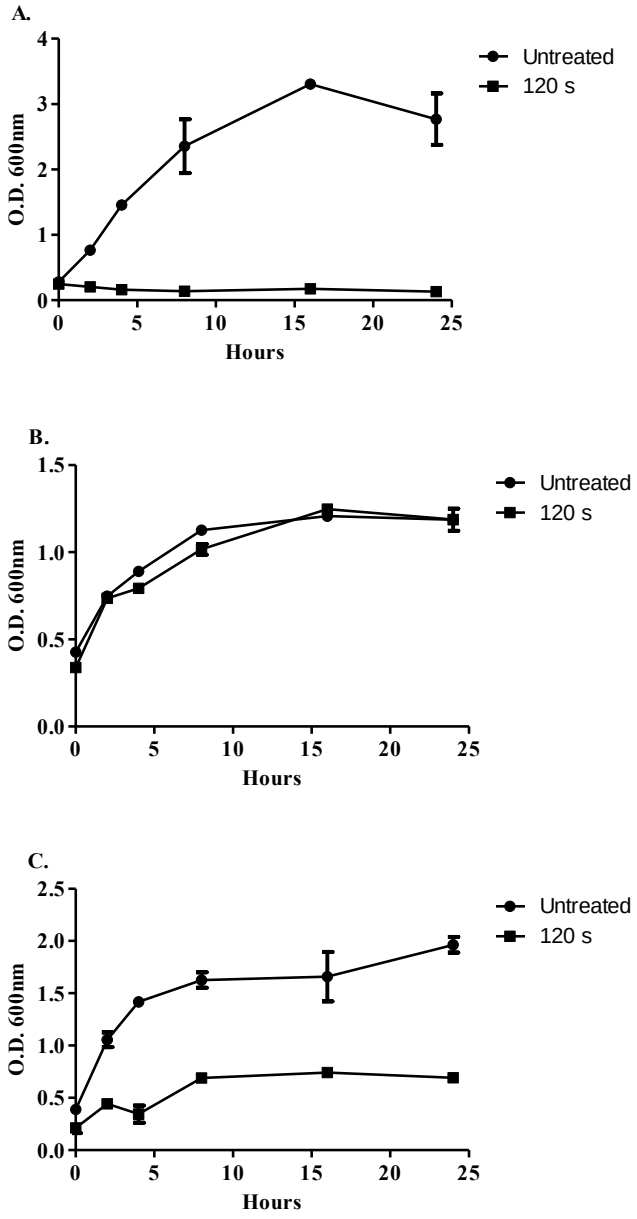


Density measurements over a 24 hour period of bacteria without indirect plasma treatment (closed circles ●) or with indirect treatment of plasma for 120 seconds (closed square ■). A.) *Escherichia coli* (ATCC 11775). B.) *Neisseria meningitidis* (ATCC 700532). C.) *Staphylococcus aureus* (ATCC 259231).

The growths of survived colonies were monitored and subjected to further treatment. The results indicate that the post treatment growth rates are similar to the pre-treatment growth rates. Therefore

non-equilibrium plasma is effective in sterilizing bacteria at different concentrations with potential applications in the food industry and the medical field.

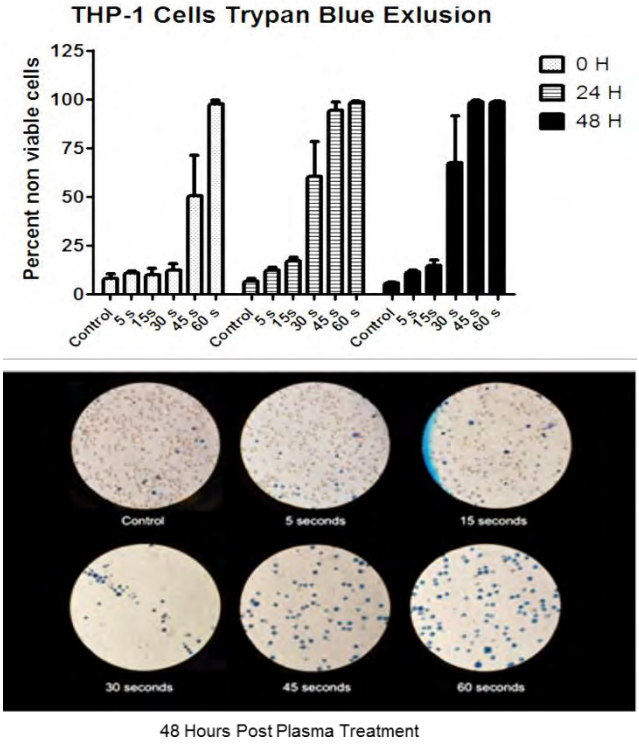


**Viability of THP-1 cells after RBP treatment. (A) THP-1 cells 0 hours, 24h and 48h post plasma treatment of 0 seconds, 5s, 15s, 30s, 45s and 60s. Non viable cells are presented as the percent of treated cells that absorbed trypan blue dye as compared to control cells not treated by RBP. (B) Photograph of cells stained with typan blue dye 48h post plasma treatment.**

The possibility of using the RBP jet for treating cancer cells was also tested, since the need for new and effective mechanisms to induce programmed cellular death (apoptosis) in cancerous cells is of great importance in cancer research. Application of direct as well as indirect exposure of plasma for cancer research is still in the exploratory stage and there remain several unanswered questions. We have tested the effects of indirect exposure of non-thermal air plasma on monocytic leukemia cancer cells (THP-1) and deciphering the mechanisms that modulate cellular induction of apoptosis. The phenotypes of interest were cells demonstrating death morphologies of apoptosis or necrosis. This is important since cells undergoing necrosis can initiate an inflamed immune response that can be detrimental to a treated individual. The type of morphological cell death that

occurred in THP-1 for various plasma treatment dosages (plasma power, flow and distance) was tested and the results are shown in Fig. above.

The results demonstrate that a preference for apoptosis in plasma treated THP-1 cells under particular plasma parameters and dosage levels. The THP-1 cells were identified as apoptotic utilizing a fluorescent dye conjugated with annexin V followed by identification of the cells through fluorescent microscopy and flow-cytometry diagnostics as shown in Fig. below.

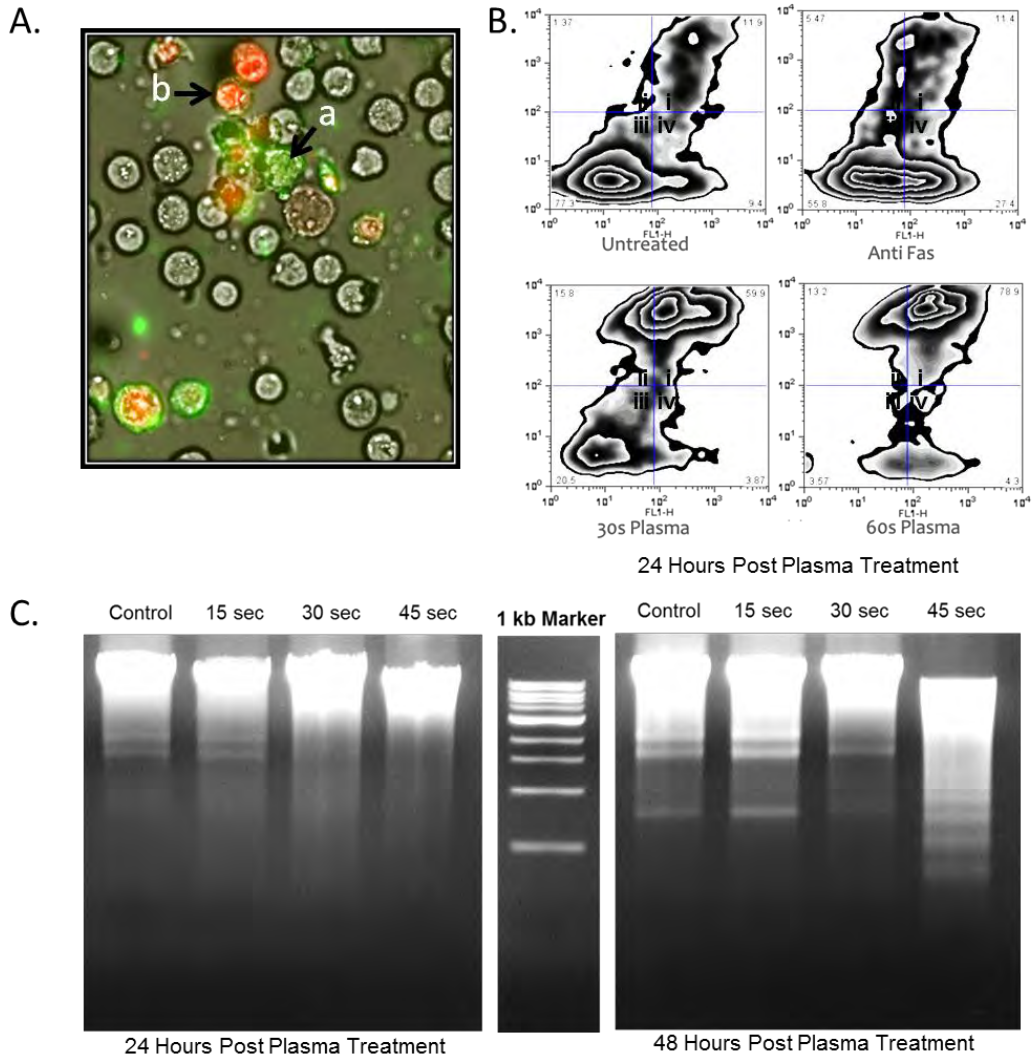


**Induction of apoptosis in THP-1 cells after RBP treatment. (A) Fluorescence microscopy of THP-1 cells stained with Annexin V FITC and propidium iodide. Cells undergoing apoptosis stain with Annexin V and appear green (a), while cells without intact membrane due to necrosis appear red (b). (B) Flow cytometry detection of Annexin V and propidium iodide**

**staining 24h post RBP treatment of 30s and 60s. Controls are untreated cells and anti-fas treated cells. Presented are the detection of stains from 10,000 events in which quadrants indicated (Q-I) propidium iodide stain, (Q-II) background, (Q-III) unstained, (Q-IV) annexin V. (C) DNA fragmentation assay of DAN from THP-1 cells 24h and 48h post RBP treatment of 0s, 15s, 30s and 45s. A 1kb ladder was used as a comparative indicator of the separation of DNA.**

Further, DNA fragmentation assays, for late detection of apoptosis, correlated with are fluorescence data demonstrating patterns of apoptotic events. However, the data also revealed that higher plasma dosages presented with undesired necrotic morphologies in the THP-1 cells. The presented variabilities in the death morphologies by plasma treated THP-1 cells signify the need for further investigation on the cellular mechanisms induced by the indirect plasma exposure. Along with taking into account other death processes such as autophagy, a catabolic process involving the degradation of a cell's own components through the lysosomal machinery. The results obtained from this research indicate great potential for the use of our non-thermal resistive barrier based indirect plasma treatment method as an inexpensive and less invasive method for treating leukemia and other cancerous lesions.

**Testing and characterization phase: Portable plasma source will be tested and characterized for its operating parameters and plasma parameters, and Biological testing: In-vitro biological testing.**

Atmospheric pressure non-thermal plasma sources operating over a range of power levels has been used for industrial and materials processing applications,[1-4] and increasingly applied in biomedical applications.[2, 3, 5, 6] Several atmospheric pressure plasma sources have been developed recently, including the plasma pencil that produces stable plasma at room temperatures applied for bacterial inactivation,[7] non-destructive sub-mm radio frequency plasma needle applied for surface treatment of biomaterials,[8] one atmosphere uniform glow discharge plasma,[9] dielectric barrier discharge based atmospheric pressure plasma jet,[10] resistive barrier plasma discharge,[11-13] and microwave powered atmospheric pressure plasma jets.[14] In

general, the majority of the plasma sources operate with a flow of noble gasses like helium, argon and/or their mixtures with other gases such as air, nitrogen, oxygen and water vapor.[14] Depending on the specific application requirements, a plasma source has to be developed and the characteristics of the plasma need to be diagnosed. In this work, we have constructed an atmospheric pressure plasma pencil in our laboratory based on kHz driven dielectric barrier discharge suitable for biomedical applications.

In this work, we describe the characteristics of an atmospheric pressure plasma pencil in helium and helium/oxygen mixture propagating in to open air. The plasma pencil is capable of working in different gas mixtures, e.g. argon, helium and their mixture with oxygen and water vapors. The different modes of operation and its low gas temperatures along with its efficient production of active species will potentially allow for a wide range of applications. The electrical characterization was performed based on voltage-current characterization of the plasma pencil operated in helium and $He/O_2$ gas mixtures. The plasma power was estimated from voltage-current waveforms and the input power was kept constant while varying the applied voltage. Subsequently, optical emission spectroscopy was utilized for investigation of reactive species in plasma and determination of OH radical rotational temperature.

The size and preciseness of the plasma pencil would allow it for a range of biomedical applications that involves localized treatments. One such area of interest is pediatric otorhinolaryngology, specifically the treatment of middle ear and paranasal infections in infants and children. *Streptococcus pneumoniae* (the pneumococcus) is one the primary bacteria that causes such infections in the different locations of the respiratory tract of humans, including acute otitis media (middle ear infection), sinusitis (paranasal infection), bronchitis and pneumonia (lung infections).[16] Of the infections caused by the pneumococcus, otitis media (OM) is one of the

highest prevalent pediatric diseases worldwide.[17] OM is the most frequently diagnosed illnesses in children under 15 years of age and is the primary reason for frequent physician visits.[18] Traditional treatment of pneumococcal infections in the middle ear and sinuses has consisted of a series of antibiotics; in fact, OM infections are considered the major reason for antibiotic use in children in developed countries.[19] Due to the rise in acquired bacterial resistance to antibiotics, there is a pressing need for alternative treatments to both reduce the antibiotic use in children and to combat bacterial infections from already resistant bacteria. To identify the usefulness of the plasma pencil for biomedical applications, we assessed plasma pencil treatment on pneumococcal cultures grown on solid blood agar plates and within liquid media.

## EXPERIMENTAL SET UP

### Plasma pencil and diagnostics

In this investigation an atmospheric pressure plasma pencil has been developed. The plasma was generated in a quartz capillary with inside and outside diameters of 1.3 and 3.0 mm, respectively. A Figure shows a schematic of our atmospheric pressure plasma pencil system and diagnostics. The plasma pencil consists of two electrodes, separated by air gap and a dielectric quartz capillary tube. The high voltage electrode is a 0.5 mm diameter tungsten rod placed inside the quartz capillary connected to a 25 kV, 60 kHz in-house constructed high voltage power supply. The electrical circuit of the power supply has been purchased from Piezomechanik GmbH, Germany. The ground electrode is a copper ring of 10 mm long placed around the capillary tube and axially positioned at 40 mm away from the high voltage electrode tip. The gas flow was monitored by a two channel power supply/readout (model: MKSPR400) and controlled by two mass flow meters (Model: MKS 1179A).

Plasma is generated inside the quartz capillary and in between the electrodes excited by a 60 kHz sinusoidal wave voltage. The applied voltage was varied from 8 $kV_{pk-pk}$ to 16 $kV_{pk-pk}$. The applied voltage waveforms were monitored using a high voltage probe (Tektronix P6015A) and the current waveforms were monitored by a current probe (Tektronix TCP202). The current and voltage signals were recorded using a digital oscilloscope (Tektronix TDS 3034C). High purity helium (99.99%) was purchased from MATHESON, TX for generating plasma at flow rates ranging from 1 slm to 7 slm (slm: standard liters per minute). A very low concentration of the water vapor present in the helium cylinder at a range of 0.5 ppm. In our experiments, admixtures of oxygen at varied percentages from 0.1 to 1% of the primary He operating gas were employed by changing of the gas flow rates. Two types of optical diagnostics were used for characterization of the plasma pencil. The time and space resolved spectroscopy measurements of the plasma emission was carried out using a broadband spectrometer (Ocean Optics HR2000+ES) in the range of 200-900 nm with 0.83 nm resolution. The emission of OH radicals in the range of 300-350 nm (transition $A^2\Sigma^+(v=0) \rightarrow X^2\Pi(v=0)$) was recorded with 500 $\mu$s integration time using a 0.08 nm resolution spectrometer system made up of a monochromator (Princeton Instruments Acton SP2750) and a CCD (ACTON IStar). The plasma emissions were collected in a direction perpendicular to the plasma pencil axis and at 1 mm increments in axial direction using a collimating lens. The plasma emission was transmitted to the spectrometer via optical fiber. The spectrometer was equipped with double grating turrets, one with 1200 grooves $mm^{-1}$ grating and the other 2400 grooves $mm^{-1}$ grating. The grating with 2400 $g.mm^{-1}$ and holographic blaze is selected to record OH (A-X) band at 306-312 nm for determination of the gas temperature using Boltzmann plot of the rotational population of the OH radicals. The second grating of 1200 g.mm-

[1] and blaze wavelength of 500 nm, is selected to record $H_\alpha$ (656.4 nm) and Ar 435 nm for plasma electron density measurements using Stark broadening method.

**Bacterial sample preparation and plasma treatment procedure**

*S. pneumoniae* strain TIGR4 was grown in Todd-Hewitt broth with 0.3% yeast extract and cells were collected during logarithmic growth $OD_{620nm} = 0.5$ for solid surface cultures and $OD_{620nm} = 0.4$ for liquid media cultures. The bacterial concentration for $OD_{620} = 0.5$ was $10^7 – 10^8$ CFU $ml^{-1}$ (CFU = colony forming units) and for $OD_{620} = 0.4$ was $10^6$-$10^7$ CFU $ml^{-1}$. For treatments of solid surfaces, 100µl ($4 \times 10^6$ CFU) of bacterial samples were inoculated onto the center of a 50 mm diameter Petri dish (plate). A disposable 35 mm wide Drigalski spatula was placed with one end at the inner edge of the Petri dish and the other end over the inoculated sample. The plate was rotated at least 10 times to allow for spread of bacterial sample over the entire agar surface, allowing a pneumococcal density of approximately $2.04 \times 10^3$ CFU $mm^{-2}$ on the blood agar plate. All treated samples were insulated from ground. For treatment of bacteria on the agar surface, the plasma pencil was fixed at distance of 10 mm between the plasma-pencil nozzle and agar surface. The cultures were exposed to 60s and 120s of either He or He/0.5% $O_2$. After treatment with plasma, the cultures were grown overnight at 37°C in 5% $CO_2$. The treated area was assessed in comparison to the untreated surrounding agar surface for zones of inactivation. The areas of the zones of inactivation were measured to quantify the amount of pneumococcal inactivation.

For treatment of the pneumococcus in liquid cultures, the bacteria suspension was prepared as described above to $OD_{620} = 0.4$. From the prepared bacterial suspension, 200 µl was transferred to a 96 well micro-well plate. The plasma pencil was fixed at distance of 3 mm between the plasma-pencil nozzle and the liquid media surface. The pneumococcal suspensions were exposed to 60s,

120s, and 300s of either He or He/0.5% $O_2$. After treatment, serial dilutions were performed and 10 µl of sample was placed onto a blood agar plate to grow overnight at 37 °C in 5% $CO_2$. After overnight growth, the efficacy of the inactivation was determined by taking CFU counts of the untreated and treated samples.

**Electrical characterization**

The electrical characterization experiments were performed on the atmospheric pressure plasma pencil with helium and oxygen admixtures. Initially, the helium gas was injected into the quartz capillary at a flow rate of 1 slm and the breakdown discharge occurred between the two electrodes and inside the quartz capillary occurred at a minimum input voltage of 7 $kV_{pk-pk}$. However, the discharge was unstable inside the quartz capillary at this minimum input voltage of 7 $kV_{pk-pk}$ and therefore plasma did not exit from the capillary in to surrounding air resulting an absence of a prominent afterglow region. By increasing the input voltage to 8 $kV_{pk-pk}$, the plasma pencil successfully produced an afterglow plasma in to the open air and a long plasma plume length was formed. In order to diagnose the electrical properties of the plasma pencil, the voltage and current waveforms were measured during the discharges at 8, 9, 10, 11 and 12 $kV_{pk-pk}$ and the effects of gas flow rates and oxygen admixture percentages in the plasma discharge were investigated. We demonstrated the voltage and current waveforms for the plasma pencil for pure helium and helium-oxygen mixture (0.5% $O_2$ in the discharge) at a total gas flow rate of 4 slm.

The plasma pencil generates a very uniform discharge in pure helium gas and only small current peaks exist on the current waveform during each half period of the applied voltage. The maximum current is 10.2 mA. A clear change in the voltage-current waveform was observed when oxygen was added to the plasma pencil. Addition of the oxygen to the plasma pencil results in a small

increase of the current peak intensity to 10.8 mA. The results indicate that the voltage slightly decreases with increase of the current peaks.

Using the voltage-current waveforms, the average power (W) of the discharge was calculated according to the following equation, where T is the period of the discharge:[20, 21]

$$W = \frac{1}{T}\int_{T}^{T+t} I(t)V(t)\,dt. \quad (1)$$

power dissipated in the discharge is presented as a function of the applied voltage for different operating gas flow rates used. The minimum power of the plasma pencil is observed to be about 8.8 W for pure Helium plasma at an applied voltage (peak-to-peak) of 8 $kV_{pk-pk}$ and a gas flow rate of 1 slm. The applied voltage was increased up to 12 $kV_{pk-pk}$, which is the breakdown point of the quartz capillary, resulting in an increase of power up to 20.4 W for discharge in pure helium at a gas flow rate of 4 slm. The plasma power as a function of oxygen percentage in the plasma pencil is presented. Basically, the power dissipation in pure helium discharge is higher, which is explained by broader current peaks. It is necessary to mention that the addition of oxygen to gas flow results in a decrease of the input power from 20.4 W (in case of pure helium) to 17.8 W and 15.8 W for discharges containing 0.1% and 1% of oxygen, respectively. The decrease in plasma power with addition of oxygen is due to contraction of the current peaks at higher amounts of oxygen in gas mixture that results in decrease of the integral determining power dissipation in the discharge.

**Visualization of the plasma pencil in helium and helium/oxygen admixtures**

The plasma pencil can be successfully launched in pure helium discharge with application of voltage at values higher than 6 $kV_{pk-pk}$. Addition of oxygen admixture to the feed gases required higher threshold voltages of up to 10 $kV_{pk-pk}$, especially at a higher concentration of oxygen (1%

oxygen). The plasma pencil generated from a complete breakdown of entire inter-electrode gap (active zone) with formation of a long bright afterglow propagating in to open air and its plume length depends on the composition of the feed gas, applied voltage and flow rates of the operating gas. We demonstrated a displays color photographs of the plasma pencil (without Teflon cover) generated at 12 $kV_{pk-pk}$ and in pure helium for different flow rates in the range of 1-7 slm and FIG 4.b displays the images of the plasma pencil in $He/O_2$ gas mixture from 0-1% of Oxygen in discharge.

In addition, we observed that the plasma pencil's plume length is greatly depends on the gas flow rate and it shows very small noticeable dependence with changes in applied voltage. Next, the plasma plume length has been measured using the plasma pencil images. We demonstrated the plasma plume lengths as a function of helium gas flow rates and oxygen percentages in the discharge, respectively. As can be seen for discharges in pure helium the plume length at lowest flow rate of 1 slm is about 10 mm and sharply increases to the maximum value of 27 mm at a flow rate of 7 slm. Increase of the gas flow rates to a value higher than 7 slm, results in a decrease in the plasma pencil plume length due to change of the gas dynamic from laminar to turbulent flow. the addition of the oxygen to the plasma pencil results in a sharp decrease of the pencil's plume length. Plasma pencil's plume length in pure helium discharge at 5 slm is 18 mm, while the plume length decreases with addition of oxygen to 15 mm and 10 mm, at discharges contain 0.1% and 1% of oxygen, respectively. The reason for decrease of the plume length is that oxygen is an electronegative molecular gas, therefore, the addition of the oxygen to the plasma pencil results to electron attachment reactions with oxygen molecules and therefore, the electron density in the discharge and consequently the helium metastable concentrations in the discharge decreases which results in a decrease of the plasma pencil's plume length.

**Optical emission spectroscopy and plasma pencil species identification**

Optical emission spectroscopy is considered to be a suitable tool in characterizing the plasma properties in terms of the identification of the reactive plasma species, plasma gas temperature evaluation and the relative emission intensities of the various species in different conditions.[22-26] In the non-thermal plasma pencil at atmospheric pressure, the mean electron energy is significantly higher than the energy of neutral plasma species.[27] The reaction between high energy electrons with helium, water vapor, nitrogen and oxygen at atmospheric pressure will induce the molecules to be dissociated, excited and ionized for production of different radicals and active species. In this section, the optical emission spectroscopy was used to study the plasma pencil in He and $He/O_2$ gas mixture and the reactive plasma species were identified. The axial and space resolved emission spectra in the range of 200-900 nm were recorded and analyzed. Axial emission spectrum of the plasma pencil allowed determination of the main reactive plasma species produced in the plasma pencil. the results of spectroscopic measurements with 0.83 nm resolution of the plasma discharge in He and $He/O_2$ mixtures (0.5%) are presented. The emission spectra were recorded in the middle of the active zone region (the region between the HV and ground electrode) of the plasma pencil. The emission spectra were recorded at 5 mm from the edge of the capillary (afterglow region). The emission spectra are mainly composed of the spectral line of the He atoms. The most intensive emission lines correspond to He I transition $3p^3P^0 \rightarrow 2s^3S$ at 388.8 nm, He I transition $3p^1P^0 \rightarrow 2s^1S$ at 501.6 nm, He I transition $3d^3D \rightarrow 2p^3P^0$ at 587.6 nm, He I transition $3d^1D \rightarrow 2p^1P^0$ at 667.8 nm, He I transition $3s^3S^1 \rightarrow 2p^3P^0$ at 706.5 nm, and He I transition $3s^1S^0 \rightarrow 2p^1P^0$ at 728.1 nm. In addition to He lines, the other identified reactive plasma species include intensive emission lines belonging to OH transition $A^2\Sigma^+ \rightarrow X^2\Pi, \quad \Delta v = 0$, at 308 nm,

and OH transition $A^2\Sigma^+ \rightarrow X^2\Pi, \quad \Delta v = 1$, at 287 nm, the spectral band of the $N_2$ transition $C^3\prod_u - B^3\prod_g, \quad \Delta v = 0$, at 337.1 nm, $H_\alpha$ transition 2p-3d at 656.3 nm, O I transition $3p^5P \rightarrow 3s^5S^0$ at 777.41 nm and O I transition $3p^3P \rightarrow 3s^3S^0$ at 844.6 nm. The OH radicals in the active zone region of the plasma are formed from water vapor present in the helium gas cylinder.[28] Another investigation by Sarani et al. [15] has been shown that the OH radicals concentration can be precisely controlled by using bubbling system and controlling the water vapor content in the feed stream. The corresponding emission lines are identified based on the NIST atomic spectra database[29] and Lofthus et. al.[30]

In order to investigate the effect of $O_2$ on the emission intensities of the reactive plasma species, different concentrations of the $O_2$ were added to the plasma pencil. Next, the emission spectra of the plasma with different $O_2$% in the discharge were collected and the emission lines of OH at 308 nm (transition $A^2\Sigma^+ \rightarrow X^2\Pi, \quad \Delta v = 0$), $N_2$ at 337 nm (transition $C^3\prod_u - B^3\prod_g$), $H_\alpha$ at 656 nm (transition $2p - 3d$), He at 706 nm (transition $1s3s\ ^3S - 1s2p\ ^3P^0$) and O I at 777 nm (transition $2s^2 2p^3(^4S^0)3s - 2s^2 2p^3(^4S^0)3p$) were chosen for space resolved analysis of the emission spectroscopy. The results of spatial distribution of the active species intensities show that the emission spectrum of $He/O_2$ (0.5 %) mixture is very similar to pure helium discharge when comparing identified species. Moreover, it is clearly recognizable that the addition of oxygen to the plasma pencil results in a decrease of the emission lines intensities. The main reason for decrease of the emission line intensities is the decreases of the plasma power with addition of the oxygen in the discharge..[15, 31] Similar observation has been reported previously by others on plasma containing oxygen or other electronegative molecular gases.[15, 21, 32]

the discharge in pure helium shows a higher intensity of OH radicals compared to the plasma pencil that contains $O_2$ gas mixture for both cases (the active zone and afterglow region) of the plasma pencil. In the active zone of the plasma, the most intensive emission line belongs to O I at 777 nm, while in the afterglow region of the plasma pencil, $N_2$ emission line at 337 nm is the most intensive emission line in the emission spectra. Furthermore, addition of higher amount of oxygen to the plasma results in a decrease of these emission lines in the discharge. Oxygen is an electronegative gas, hence, when oxygen is added to the plasma pencil, the added oxygen captures significant free electrons and produces $O^-$ and $O^{2-}$ ions. Thus, the electron attachment by oxygen results in a decrease of the electron density and electron mean energy.[33-35] The OH radicals are mainly produced by electron-water vapor collision process according to the following reaction, and therefore the decrease of the electron density leads to decrease of the intensities of OH and other atomic emission lines at a constant power.[28, 33, 34]

$$e + H_2O \rightarrow e + H + OH \quad (2)$$

The reason for increase of O I intensity in the active zone region of the plasma pencil is that when oxygen is added to the pure helium plasma pencil, the added oxygen can be dissociated according to the following reactions and results in a formation of singlet oxygen (O) and O ($^1$D).

$$e + O_2 \rightarrow O^- + O \quad (3)$$

$$e + O_2 \rightarrow e + O + O\ (^1D) \quad (4)$$

$$e + O_2 \rightarrow 2e + O^+ + O \quad (5)$$

In addition, in the afterglow region of the discharge when plasma pencil propagates in the open air, the OH radicals can be produced by the interaction of O ($^1$D) and $H_2O$ according to the following reaction:[35]

$$O\ (^1D) + H_2O \rightarrow 2\ OH \quad (6)$$

On the other hand, the singlet oxygen and ozone molecules generated in the discharge react with the produced OH radicals according to the following reactions and thus, the OH radicals intensity in the plasma pencil decreases with addition of oxygen percentage to the pure helium plasma pencil.[35]

$$OH + O \rightarrow H + O_2 \quad (7)$$

$$OH + O_3 \rightarrow HO_2 + O_2 \quad (8)$$

**Space resolved optical emission spectroscopy of the plasma pencil**

The spatial distribution characteristics of chemically active species are very important in developing the plasma pencil kinetic model and understanding the mechanism of biomedical applications of the plasma pencil. Here, we present the spatially resolved spectra of the afterglow region of the plasma pencil.

The spatially resolved optical emission spectra of the afterglow region were collected for pure helium and helium/oxygen mixture (0.5%), with resolution of 2.5 mm. Next, the intensities of the intensive reactive plasma species were chosen for deeper analysis of the space resolved emission spectroscopy. the emission intensity of the OH radicals ( $A^2\Sigma^+ \rightarrow X^2\Pi, \quad \Delta v = 0$ ) and $N_2$ ( $C^3\prod_u - B^3\prod_g$ ), $H_\alpha$ and O I and helium vary with distance from the edge of quartz capillary. that the emission intensity of helium, O I and $N_2$ ( $C^3\prod_u - B^3\prod_g$ ) rises initially up to 7 mm from the edge of capillary and then decreases, while the emission intensity of the OH ( $A^2\Sigma^+ \rightarrow X^2\Pi, \quad \Delta v = 0$ ) and $H_\alpha$ decreases with increase of distance from the capillary. The emission intensity of $N_2$ at 10 mm is almost 8-10 times larger than the intensity at the edge of the capillary. Moreover, the emission intensity of $N_2$ reaches a maximum value after OH radicals. The maximum intensity of $N_2$ is located at 10 mm while the OH radicals' maximum intensity is located at 7 mm. This behavior can be explained by the fact that $H_2O$ dissociation is initiated by electron

induced processes inside the discharge and in the short distance after the edge of capillary, where the electron exhibit required the energy.[15] In the case of the plasma pencil in helium/oxygen mixture (0.5%), the intensity decay of the helium in the plasma plume has an exponential decay, initially increasing up to 10 mm from the edge of capillary and after that again decreasing (FIG 8.b). The most intensive emission line belong to O I, which is located inside the quartz capillary. The $N_2$ emission intensity reaches to its maximum outside the capillary and at 5 mm distance from the edge of capillary. The identified excited nitrogen molecules are produced from electron impact reactions in the plasma plume as it propagates into the ambient air.[28] The main reason for the decrease of the emission intensities of the reactive plasma species with the distance from the edge of capillary is the decrease of the high energy electron density and mean energy.[32] Outside the capillary the increase of the $N_2$ (SPS) emission could be a result of energy transfer from metastables and decreasing of the OH emission by increasing $N_2$ in the plasma pencil and lower $H_2O$ density in the surrounding air compared to nitrogen.

The identified reactive plasma species such as the singlet oxygen, hydroxyl radicals, and neutral nitrogen molecules detected in the plasma pencil can play a significant role in biomedical applications especially operating at the atmospheric pressure.[36, 37] Similar significant generation of reactive oxygen species such as singlet oxygen (O) and $O_3$ were observed with $He/O_2$ gas mixture used in a plasma pencil which can result in enhanced efficacy of bacterial inactivation.[26, 38] It is believed that the oxygen species in the discharge contributes to the sterilization process due to its strong oxidative effect on the outer structure of the cells,[36, 37] while the OH radicals generated by the plasma plays a significant role through chemically attacking the outer structure of the cells and the production of the nitrogen containing group adds to the lethality of the process.[39]

**OH rotational temperature determination using Boltzmann plot method**

The plasma gas temperature has been derived from OH rotational temperatures. The OH rotational temperature is usually considered to be equal to the plasma gas temperature considering the low rotational level of the OH radicals OH (A-X) and small rotational quantum numbers *J*.[15, 40-42] The Boltzmann plot of the rotational population of the OH radicals has been widely used for this purpose.[15, 40, 43, 44]. We demonstrated the high resolution emission spectra of the OH radicals in pure helium and helium oxygen (0.5%), respectively. Using the OH emission spectra and assuming that the OH rotational states are Boltzmann distributed according to the following equation

$$I_{J'J''} \approx h\nu_{J'J''}(2J+1)A_{J'J''}\exp\left(-\frac{B_\nu hcJ(J+1)}{k_B T_{rot}}\right), \qquad (9)$$

where $\nu_{J'J''}$ is the frequency of transition from rotational level $J'$ to $J''$, $A_{J'J''}$ is the corresponding transition probability, $B_\nu$ is the rotational constant, $k_B$ is the Boltzmann constant and $h$ is the Planck constant. The rotational energy $E(cm^{-1})$ equals to $B_\nu J(J+1)$. The energy and probability data of OH transitions were taken from literature.[45, 46] The corresponding OH rotational temperature is equal with gas temperature when the rotational population distribution is in equilibrium with heavy species translational temperature in the discharge. In atmospheric pressure plasma, this assumption is valid on atmospheric pressure plasmas when high collisional reactions occur. A detailed description of the used method can be found in Sarani. et, al. 2010.[15]

We presented $\ln(I\lambda/(2J+1)A_{JJ})$ for transition $OH(A^2\Sigma - X^2\Pi)$ as a function of levels energy for *J<13*. This plot describing distribution of $OH(A^2\Sigma)$ radicals among rotational levels for pure helium and helium/oxygen mixture (0.5%) at discharge generated at fixed power of 18 W. Based

on the Boltzmann plot method, the OH rotational temperature in the active zone region of the plasma pencil was measured to be 309.52 K and 366.48 K, for pure helium and helium/oxygen gas mixture (0.5% oxygen), respectively. Whereas the measured rotational temperature in the afterglow region at 5 mm away from the capillary edge was increased to 315.66 K and 362 K, for pure helium and helium/oxygen gas mixture (0.5% oxygen), respectively. As can be seen, the addition of the oxygen to the plasma pencil results in an increase of the OH rotational temperature. The excited OH radicals characterized by low rotational temperature are produced by electron impact excitation of ground state OH according to flowing reaction.[15]

$$OH(X^2\Pi) + e \rightarrow OH(A^2\Sigma)^* + e, \qquad (E_{threshold} = 4\,eV), \tag{10}$$

The results of the OH rotational temperature obtained in this work by using Boltzmann plot method are in a good agreement with those data obtained by fitting of the OH spectra using LIFBASE software in our previous publication [47]. The OH rotational temperatures for active zone of the pure helium plasmas are 309.52 ± 25 K and 310 ± 25 K by using Boltzmann plot method and fitting of the OH rotational spectra by LIFBASE software [47], respectively.

**Electron density determination using line broadening**

The analysis of the stark broadened line profiles is a well-established technique for plasma diagnostics. Plasma electron density can be obtained from the full width at half maximum (FWHM) of the stark broadened profile of the hydrogen lines.[48-50] One of the most common methods for determination of the electron density is using the hydrogen Balmer full width at half maximum.[48]

At atmospheric pressure, the profile of atomic spectral lines emitted from the plasma can be approximated by a Voigt function. In this work, the line shape of the hydrogen alpha transition is

determined by Lorentzian and Gaussian broadening mechanisms that results in a Voigt function.[41] The Lorentzian part of the profile correspond to the contribution of the Stark and Van der Waals collisional broadening that have their origin in the interaction between the emitting particles and the particles around them. The Gaussian part of the profile corresponds to the contribution of the Doppler and instrumental broadening. The Doppler broadening is due to the thermal speed of the emitting particle and instrumental broadening caused by measurement devices.[41] The broadening due to the natural lifetime is too small and is not taken into account in the present work.

For atmospheric pressure plasmas, low gas temperature condition, and electron densities around $10^{14}$ $cm^3$, the Van der Waals broadening has to be taken into account. The van der Waals broadening is caused by the neutral perturbers and its FWHM can be estimated as[51]

$$\Delta\lambda_{vdW} = 8.18 * 10^{-26}\lambda_0^2(\bar{R}^2)^{\frac{2}{5}}T_{gas}^{\frac{3}{10}}N\sum_i\left(\frac{\alpha_i^{\frac{2}{5}}\chi_i}{\mu_i^{\frac{3}{10}}}\right) \quad (11)$$

where $\lambda_0$ is the wavelength in nm, μ is the reduced mass in atomic mass unit, N is the neutral particle density in $cm^{-3}$ , $i$ is the helium gas and χ is the fraction of the perturber.[51] The value of the polarizability of the α pertuber for helium gas is $2.05\times10^{-25}$ $cm^3$.[52] After considering the fine structure and calculating the value for atomic lines, the FWHM can be estimated as

$$\Delta\lambda_{vdW}(nm) = \frac{C}{T^{\frac{7}{10}}} \quad (12)$$

where C is equal to 2.42, the Van der Waals broadening constant for hydrogen alpha line in helium plasma.[52] Using the above equation the Van der Waals broadening was estimated as 0.0393 nm.

The Doppler broadening and Resonance broadening are not taken into account in the present work because their values are negligible due to the low gas temperature and atmospheric pressure conditions. In this work, the instrumental slit function is well approximated by a Gaussian profile due to the fact that monochromator slits with equal width were used. The shape and the broadening caused by instrumental were determined by using a Mercury-Argon pen lamp and considering the emission line at 435 nm. The instrumental profile resulted after using our experimental device very well fitted with a Gaussian function with an instrumental width of 0.17 nm. The convolution of the above Lorentzian and Gaussian line shapes results in a Voigt profile with FWHM, $\Delta\lambda_V$ of [53]

$$\Delta\lambda_V \approx \sqrt{\left(\frac{\Delta\lambda_L}{2}\right) + {\Delta\lambda_G}^2} + \frac{\Delta\lambda_L}{2} \tag{13}$$

The Lorentzian full width at half maximum (FWHM) is the sum of the Lorentzian FWHMs, while the Gaussian FWHM is the square root of the sum of the squared Gaussian FWHMs.[41] In order to determine the electron density, the measured line of the $H_\alpha$ is fitted with a Voigt function with FWHM of 0.22 nm. We demonstrated the measured line broadening of $H_\alpha$ line for the helium plasma fitted with a Voigt function along with the instrumental broadening of the line at 435 nm of the Mercury-Argon pen lamp fitted with Gaussian function. The Lorentzian part of the FWHM is used to estimate the Stark broadening which results in a $\Delta\lambda_s$ of 0.014 nm. Using Eq. (14) for Stark broadening of the $H_\alpha$,[52] the electron density in the afterglow region of the plasma pencil was estimated as $2.1 \times 10^{14}$ $cm^3$.

$$\Delta\lambda_s = 1.78\left(\frac{n_e}{10^{23}m^{-3}}\right)^{\frac{2}{3}} \tag{14}$$

**Plasma pencil treatment of *S. pneumoniae* on blood agar and in liquid media**

The plasma treatment of the pneumococcus on the solid blood agar plates caused inactivation within the treated surface area. A time-dependent and input gas-dependent response was observed in the pneumococcal inactivation on the solid blood agar surface. A mean inactivation of $4.0 \times 10^4$ CFU and $1.3 \times 10^5$ CFU was observed after treatment for 60s with He plasma and He/0.1% $O_2$, respectively. By increasing the treatment time to 120s, a mean inactivation of $5.2 \times 10^5$ CFU and $1.0 \times 10^6$ CFU was identified for He and He/0.1% $O_2$ plasma, respectively. It was interesting that a mere 0.1% addition of oxygen gas was able to double the inactivation rate of the plasma treatment. In a similar study using *Streptococcus mutans*, a close relative to the pneumococcus, investigators identified an increase in the inactivation by injection of $O_2$ into the He plasma.[54] It has been known for some time now that oxygen radicals play a role in bactericidal activity.[55] This has further been demonstrated with several other plasma systems.[7, 56, 57] Another aspect of this research identified that doubling of the treatment time allowed for the formation of widespread inactivation zones. The respiratory tract is covered with a mucous membrane that secretes mucous to lubricate and protect the membrane.[58] During pneumococcal infection, fluid buildup occurs around the mucous membranes due to increased swelling.[59] To identify the effectives of the plasma pencil for inactivation of *S. pneumoniae* in liquid, we treated pneumococcal suspensions in liquid media. As was identified with treatment of solid surfaces, we observed a time-dependent and input gas dependent response to plasma treatment. Pneumococcal suspensions in liquid media treated with He plasma for 60s, 120s, and 300s did not show a significant inactivation as compared to untreated samples. However, the addition of 0.1% $O_2$ to the admixture allowed for a 40% inactivation from $1.8 \times 10^7$ CFU $ml^{-1}$ to $7.1 \times 10^6$ CFU $ml^{-1}$ ± SEM $2.9 \times 10^6$ of the pneumococcal suspension after 300s of treatment.

We have designed, constructed and investigated a low temperature plasma pencil driven by a kHz AC power supply. The electrical and optical characteristics of the plasma pencil in helium and helium/oxygen gas mixture have been investigated using electrical characterization and optical emission spectroscopy diagnostic techniques. The effects of oxygen at various concentrations on the helium plasma pencil were investigated. The plasma power was estimated to be in the range of 8-20 W for different applied voltages and gas mixtures. Identification of the different radicals and excited species produced in the active zone and afterglow region of the plasma pencil have been carried out. The emission spectroscopy analysis revealed that the most intensive emission lines belong to OH transition $A^2\Sigma^+(\nu = 0,1) \rightarrow X^2\Pi(\Delta\nu = 0)$ at 308 nm and OH transition $A^2\Sigma^+(\nu = 0,1) \rightarrow X^2\Pi(\Delta\nu = 1)$ at 287 nm, O I transition $3p^5P \rightarrow 3s^5S^0$ at 777.41 nm, O I transition $3p^3P \rightarrow 3s^3S^0$ at 844.6 nm and $N_2$(C-B) second positive system (SPS) with electronic transition $C^3\Pi_u \rightarrow B^3\Pi_g$ in the range of 300-450 nm. Also, different atomic emission lines include He I transition 3p3 P0→2s3S at 388.8 nm, He I transition $3p^1P^0 \rightarrow 2s^1S$ at 501.6 nm, He I transition $3d^3D \rightarrow 2p^3P^0$ at 587.6 nm, He I transition $3d^1D \rightarrow 2p^1P^0$ at 667.8 nm, He I transition $3s^3S^1 \rightarrow 2p^3P^0$ at 706.5 nm, He I transition $3s^1S^0 \rightarrow 2p^1P^0$ at 728.1 nm and $H_\alpha$ transition 2p-3d at 656.3 nm have been identified. The effect of adding oxygen on electrical and spectral properties of the plasma pencil has been investigated. Addition of oxygen to the plasma pencil resulted in a decrease in plasma power and therefore decreased the electron density and also the intensity of emission lines. Plasma density has been estimated from Stark broadening of the hydrogen line at 656 nm and is in order of $2.1\times10^{14}$ $cm^{-3}$. The plasma gas temperature was evaluated using OH rotational temperature. The OH rotational temperature for pure He plasma is 315.66 K and is 362 K for pure helium and helium/oxygen gas mixture (0.5% oxygen), respectively. The plasma pencil generates significant amounts of reactive species at low gas temperatures which promises its great potential for a range of biomedical

applications. The preliminary work with inactivation of *S. pneumoniae* on solid surface and liquid suspension using the plasma pencil suggests this as a potential tool for biomedical applications. Further studies on the biological side such as the effects on inactivation on mucosal tissue need to be assessed.

**Progress of Tasks 10 and 11: Testing and characterization phase: Portable plasma source will be tested and characterized for its operating parameters and plasma parameters, and (Task 11) Biological testing: In-vitro biological testing.**

## I. Inactivation of bacteria in aqueous media in direct and indirect treatment modes

An atmospheric pressure resistive barrier air plasma jet is designed to inactivate bacteria in aqueous media in direct and indirect exposure modes of treatment. The resistive barrier plasma jet is designed to operate at both DC and standard 50-60 Hz low frequency AC power input and the ambient air at 50% humidity level was used as the operating gas. The voltage-current characteristics of the plasma jet were analyzed and the plasma power was measured to be 26 Watt. The plasma jet rotational temperatures ($T_{rot}$) are obtained from the optical emission spectra, from the N2C-B(2+) transitions by matching the experimental spectrum results with the SPECAIR simulation spectra. The reactive oxygen and nitrogen species were measured using optical emission spectroscopy and gas analyzers, for direct and indirect treatment modes. The nitric oxides (NO) were observed to be the predominant long lived reactive nitrogen species produced by the plasma. Three different bacteria including Staphylococcus aureus (Gram-positive), Escherichia coli (Gram-negative) and Neisseria meningitidis (Gram-negative) were suspended in an aqueous media and treated by the resistive barrier air plasma jet in direct and indirect exposure modes. The results show that a near complete bacterial inactivation was achieved within 120 second for both

direct and indirect plasma treatment of S. aureus and E. coli bacteria. Conversely, a partial inactivation of N. meningitidis was observed by 120 second direct plasma exposure and insignificant inactivation was observed for the indirect plasma exposure treatment. Plasma induced shifts in N. meningitidis gene expression was analyzed using pilC gene expression as a representative gene and the results showed a reduction in the expression of the pilC gene compared to untreated samples suggesting that the observed protection against NO may be regulated by other genes.

## A. Experiment

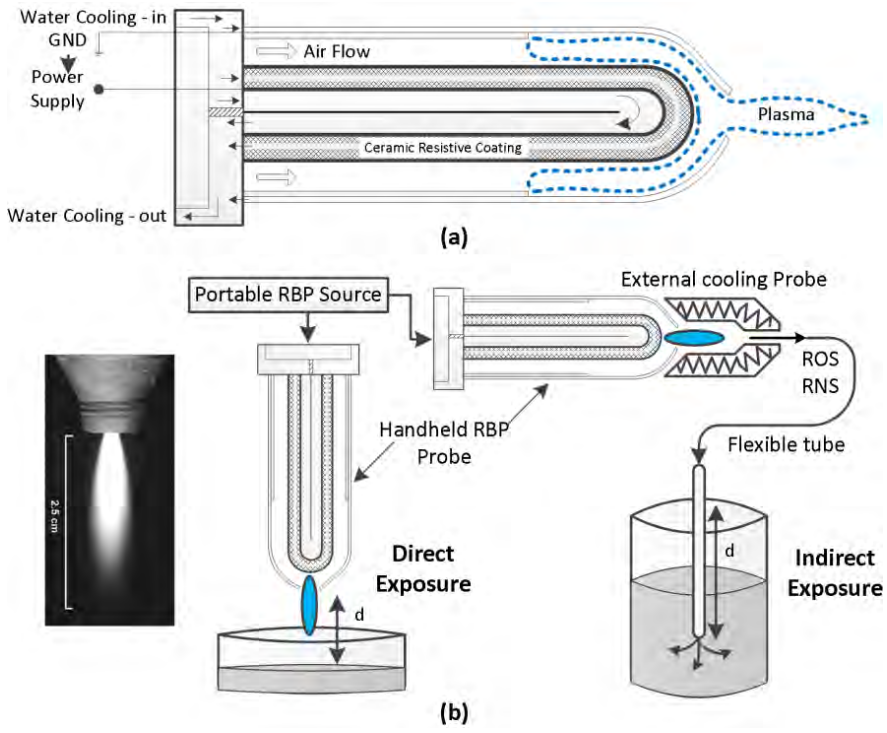


FIG 1. The schematic set up of: (a) the RB air plasma jet, (b) direct and indirect plasma exposure.

The schematic representation of the atmospheric pressure resistive barrier (RB) air plasma jet together with an image of the air plasma jet. Basically, the RB plasma jet consists of central

deionized water cooled cylindrical electrode surrounded by deionized water cooled high density alumina ceramic resistive coating. The central electrode which is approximately 1 cm diameter and 10 cm long is surrounded by a double layer hollow ground electrode separated by an electrode gap space of 2 mm. Discharge streamers are formed between the high-voltage resistive electrode and the ground electrode. With applying enough voltage, the air passing through the RB plasma jet gets ionized and exits through a 2 mm pinhole type opening at the tip of the plasma source generating a stable plasma jet and a continuous flow of active species such as ROS and RNS. The discharge streamers formed in the cylindrical hollow electrode configuration are dynamic with respect to its location between the electrodes, which also assists in preventing localized heating and arc formation. The presented RB plasma jet is developed based on the principles of large volume non-thermal resistive barrier discharge (RBD)23-25 and can be used in both direct and indirect plasma exposure modes Direct exposure of plasma involves, exposure of plasma directly on to a target treatment surface whereas the indirect plasma exposure involves, exposure of only the ROS and RNS generated by the plasma instead of the plasma itself, thus eliminating the effect of any possible UV radiation produced by plasma. For the indirect exposure method the concentrations of the nitric oxides are preserved by reducing the plasma temperature rapidly through a separate external small efficient cooling unit.

The RB plasma jet operates in both DC and low frequency AC, such as the standard operating voltages 120 V/60 Hz and 230 V/50 Hz. The power supply is stepped-up with using a transformer (6 kV, 30 mA (max)). In addition, the power supply unit also houses transistor-transistor logic (TTL) and relay controls to select between AC and DC, and power levels and flow controls. The RB plasma jet uses atmospheric pressure air as the operating gas. A 12 V DC air compressor is used to force the air through the electrode gap space of the RB plasma jet. Thus, the

plume length, plasma power and ROS including nitric oxides at the tip of the handheld plasma jet tip are controlled and maintained. The power supply unit also contains a mini 12 V DC water pump (Geo-Inline) for cooling the electrodes in the handheld plasma probe unit as well as the optional external cooling unit. The entire RB plasma source is very compact, portable and light weight. It is constructed to fit within 12 × 10 × 10 inch3 portable metallic case and the entire power supply and RBS plasma source weighs approx. 20 lbs.

**B. Diagnostics**

The voltage applied to the high-voltage electrode is measured using a high voltage probe (Tektronix P6015A) and the discharge current is measured using a current probe (Tektronix TCP202). The voltage–current waveforms are recorded using a 2 GHz digital oscilloscope (Tektronix TDS3034C). Accurate measurement of gas temperatures of the RB plasma jet is a significant experimental challenge. Due to electrical interference using conventional thermocouple inside the discharge can lead to inaccurate measurements. Therefore, the optical emission spectroscopy26,27 was employed to measure the rotational gas temperature ($T_{rot}$) of the plasma jet using a high resolution narrow band (0.004 nm resolution) monochromator (Acton Research, Model: SP-2750) coupled with a fast gating Andor iStar ICCD (ANDOR, DH 734). This system has a near-Lorentzian slit function with a half-maximum width of 0.2 nm when the grating density was set to 1200 lines/mm. A high-temperature ceramic fiber-insulated-wire thermocouple probe capable of measuring temperatures up to 1400 °C was used to measure the temperature of the downstream jet when plasma emission ends after approximately 2.5 cm. The parts per million (ppm) concentration of the ROS and RNS including nitric oxides at different spatial distances from the tip of the plasma jet was measured using two gas sensors namely NOXCANg and Testo 350 M/XL gas analyzers.

**C. Bacterial sample preparation and plasma treatment procedure**

Bacterial samples of S. aureus (ATCC 259231), E. coli (ATCC 117751), and N. meningitidis serogroup C (ATCC 700532) were obtained from ATCC (Manasses, VA). Bacterial cultures of S. aureus (ATCC 259231) and E. coli (ATCC 117751) were grown overnight on Tryptic Soy agar (BD, Franklin Lakes, NJ) plate overnight at 37°C in 5% CO2. N. meningitidis was grown overnight on GC medium (BD, Franklin Lakes, NJ) plate supplemented with Thayer-Martin supplement I and supplement II (Sigma-Aldrich, St. Louis MO) overnight at 37°C in 5% CO2. Bacteria was collected from overnight cultures using an inoculating loop and placed into 20 ml of Mueller Hinton broth (MHB) (BD, Franklin Lakes, NJ). Bacterial cultures in suspension were adjusted with sterile MHB to an OD at 595 nm (OD595) = 0.2 (Spectronic Genesys 5 Spectrophotometer, Madison, WI) and allowed to incubate (37°C, 5% CO2) till reaching an OD595 = 0.4. N. meningitidis suspensions included agitation by a plate mixer (~100 rpm). After reaching the selected density, 13x100 glass culture tube were filled with 5ml of bacterial suspension and treated to regime of either 0, 30, 60, or 120 seconds of maximum power and flow rate of RB plasma jet in direct or indirect treatment modes by fixing the plasma jet exit above the surface of the media at a distance of approximately 5cm. Control suspension samples pH was monitored before and after 30, 60, and 120 seconds of direct and indirect RB plasma jet treatment using S20 SevenEasy pH meter (Mettler-Toledo, Columbus, OH). Bacterial density was monitored over a period of 24 hours and OD595 readings were recorded. The efficacy of the inactivation was determined by making serial dilutions of untreated and treated samples and plating them on agar plates. Three independent experiments were performed and data were collected for the analysis of post-treatment bacterial growth means over time.

**D. Messenger RNA analysis by quantitative real time-PCR**

Real time polymerase chain reaction (RT-PCR) analysis can provide information about the presence and quantity of a specific gene within a cell. Cells such as bacteria can recognize external stimuli such as NO produced by the RB plasma jet and react accordingly to alter its metabolic processes through gene regulation to respond to the stimuli. Cultures of N. meningitidis were prepared as described above and the untreated and 60 second direct plasma treated samples were incubated at 37°C, 5% CO2. Bacterial RNA was harvested from each sample culture at 2 hour post treatment using a Qiagen RNeasy minikit. Purified mRNA was quantitated via Nanodrop with appropriate standards. cDNA synthesis and quantitative PCR were done using the Superscript III Platinum SYBR Green two-step qRT-PCR kit (Invitrogen) on an Cepheid Smart Cycler. The relative expression of pilC was normalized to that of 16S gene, which served as an internal control. The qRT-PCR experiments were done in triplicate with independently isolated RNA samples.

**E. Electrical characterization of the RB plasma jet**

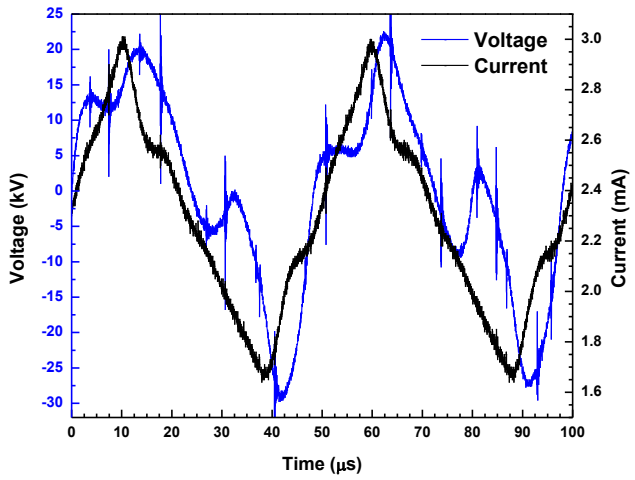


FIG 2. Voltage-current waveform of the RB air plasma jet.

The electrical properties of the discharge are obtained using voltage-current characterization. The discharge is initiated by applying a sufficient voltage between electrodes at which the air between electrodes breaks down and results in a self-sustained plasma jet maintained by applied voltage of the power supply. We demonstrated the voltage-current waveform of the RB plasma jet. The positive and negative half periods of the applied voltage are not symmetrical due to the existence of only one resistance between the electrodes. that breakdown of air in atmospheric pressure resistive barrier plasma jet resulting in several current filaments called micro-discharges which are randomly spread in time and space. The maximum voltage and current values are approximately 20 kV and 3 mA on the positive half period of the applied voltage, correspondingly. Using the voltage–current waveforms, the average power dissipated in the discharge is calculated by integrating the product of the discharge voltage and current over one cycle; according to the following equation ($T$ = period of the discharge).28

$$W = \frac{1}{T}\int_{t}^{t+T} I(t)V(t)dt \qquad (1)$$

and the average plasma power is measured to be 26 W.

**F. Optical emission spectroscopy**

The rotational temperature ($T_{rot}$) of the RB plasma jet was measured using the optical emission spectroscopy. The rotational temperature and plasma gas temperature can be considered equivalent if there is a small energy gap between the rotational levels compared with that of the vibrational or electronic energy levels and in the presence of thermal equilibrium between the translational and rotational degrees of freedom.29 A local thermodynamic equilibrium (LTE) condition has been assumed and emission spectra of the plasma jet were used for gas temperature determination.

The commonly used technique to estimate rotational temperature is based on finding the best fit between experimental and simulated emission spectra of the second positive system of N2 and considering the plasma gas temperature equivalent with rotational temperature of N2 (Trot).

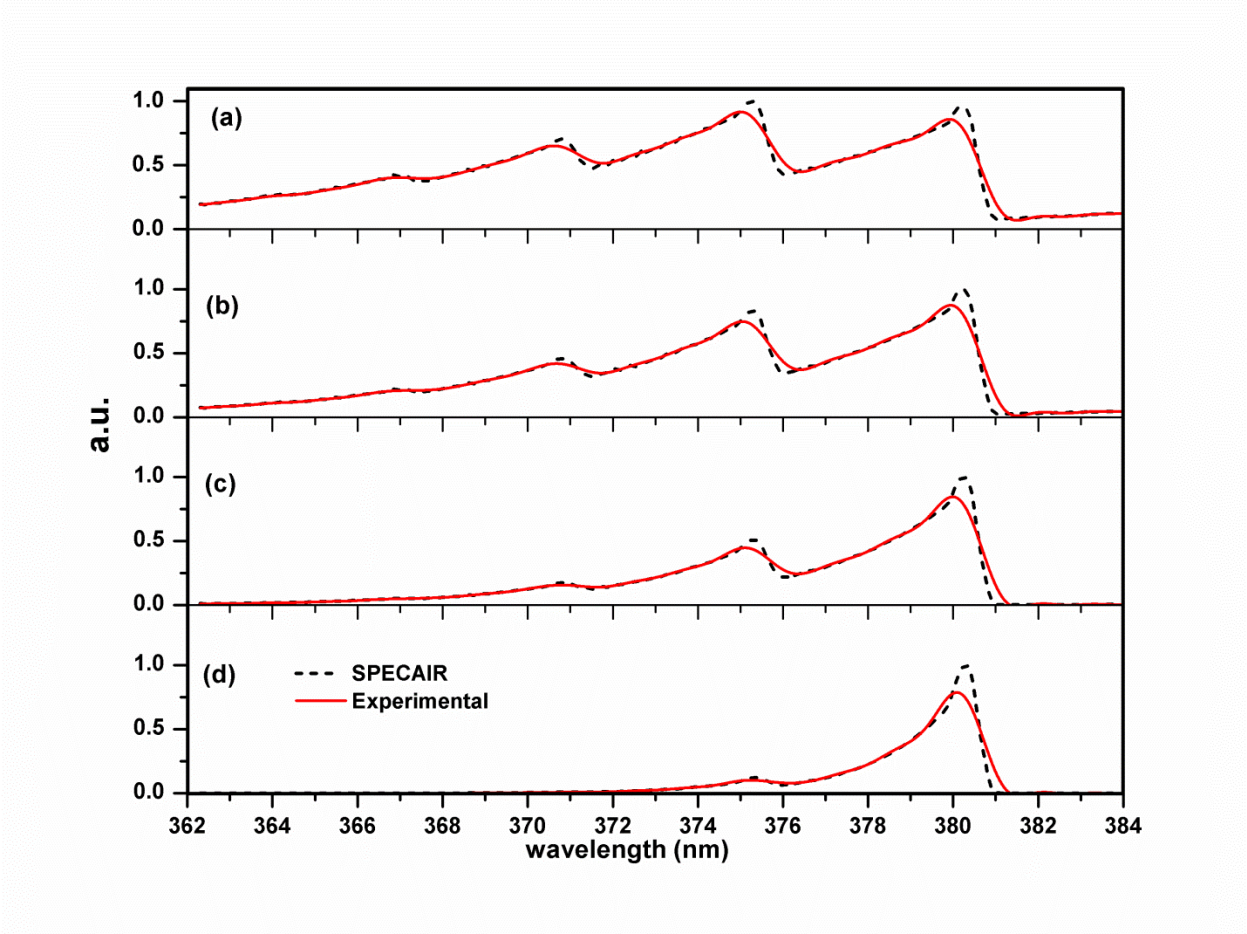


Experimental and simulated air plasma emission spectra of N2 SPS for fixed power of 26 watt without cooling unit and at distances: (a) 0.2 cm, (b) 0.8 cm, (c) 1.5 cm, and (d) 2 cm after the nozzle.

In this section, the spectral lines of the nitrogen second positive system (SPS), (N2(C-B) (C 3∏ B 3∏) (2+)), is used to determine the rotational temperature distribution of nitrogen SPS

with SPECAIR software.30 SPECAIR is computer simulation software developed by Laux et. al. on the basis of the Non-Equilibrium Air Radiation code (NEQAIR) by Park.30 The rotational temperature distribution of the N2 SPS, in the afterglow of the RB plasma jet was determined on the basis of simulation of experimental spectra in the range of region 364-383 nm. Fitting of the spectra is carried out with one rotational temperature, and taking into account the instrumental function of the spectrometer. The experimental spectra were compared to the simulated spectra with various rotational temperatures. The rotational temperature for the best fitting between simulated and experimental spectra was determined as the gas temperature. The experimental and simulated spectra of N2 second positive system

The results indicate the rotational temperature for air discharge at a distance of 0.2 cm from the nozzle is 3050 ◦C. The $T_{rot}$ drops to 2100 ◦C at 0.8 cm and continue to decrease to 1500 C at 1.5 cm and to 1050 ◦C at 2 cm away from the nozzle. The rotational temperature of nitrogen is significantly smaller at 2 cm away from the nozzle than the one of 0.2 cm from the jet exit. This clearly indicates that the nozzle acts as an efficient heat source for the plasma jet. Nitrogen line emissions drop significantly after 2 cm (plasma plume length is 2.5 cm) from the tip of electrode along the axis and beyond which the gas temperature estimation by OES based rotational temperature estimation is challenging. However, the long life active species such as the ROS and RNS produced by the plasma jet can still propagate further in to the surrounding air (NOx concentration was measured to be ~900 ppm at 10 cm away from nozzle) and are important active species particularly for the biomedical applications. Therefore the downstream gas temperatures beyond the plasma emission, which is from 2 cm of the plasma jet exit onwards, were measured by using a high-temperature ceramic fiber-insulated-wire thermocouple probe.

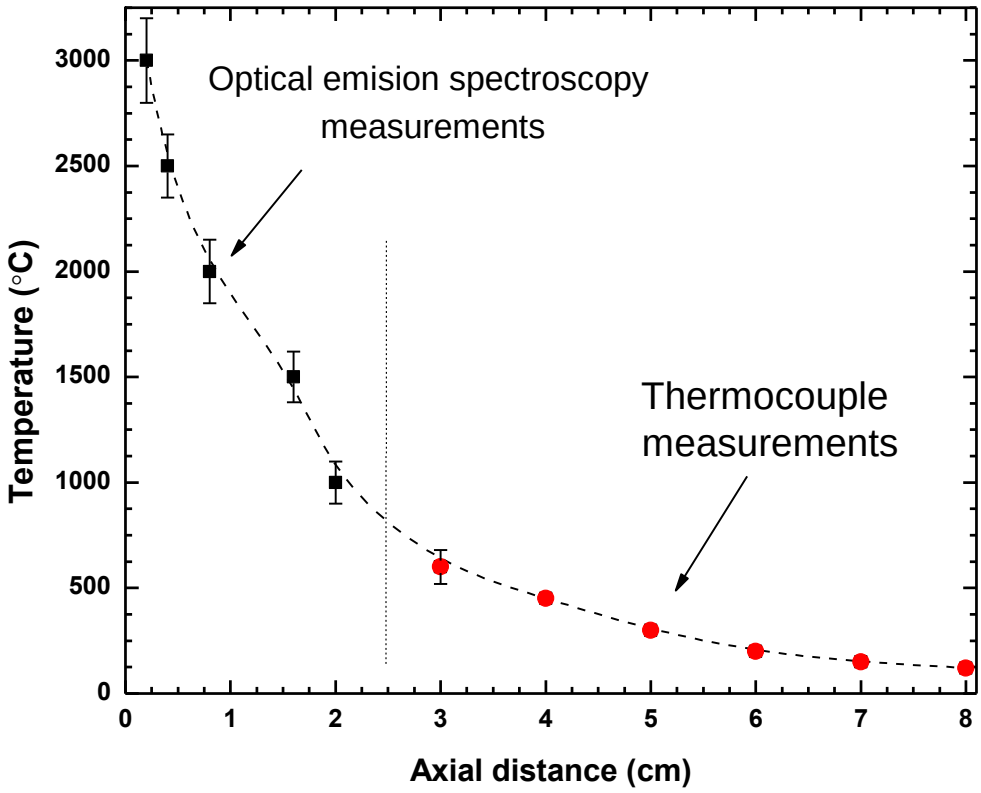


Gas temperature as a function of distance from the tip of the RB plasma jet. Air discharge and fixed power of 26 watt (No cooling unit).

the axial temperature measurements of the RB plasma jet before attaching the cooling unit. the gas temperatures decrease at a much slower rate after approximately 5 cm from the nozzle. The high gas temperatures obtained from N2 rotational temperature is due to excitation of N2 to high rotational/vibrational levels and the excited N2 species are generated in the plasma jet. However, plasma gas temperature drops down very fast at the end of the jet's plume. The temperature of the plasma plume at the exit reaches >2500 °C sufficient enough to generate nitric oxides. When the

external cooling units were added the gas temperatures were brought close to room temperature at the tip of the handheld plasma source unit.

### G. Measurements of long lived active plasma species

RB plasma jet produces wide range of active species such as radicals, electrons, atoms, ions, molecules, ROS and RNS etc. These plasma species contributes to the biological cell interactions and inactivation of the bacteria. The concentrations of the ROS and RNS produced by the plasma jet with and without the cooling unit are measured using gas analyzers. The majority of the short lived ions will recombine before it exits through the cooling unit and at this stage several long lived gas species and other parameters were monitored, including O2, O3, CO, COlow, NO/NO2, NOlow, NOX, CO2(Infrared), SO2, HC, H2S, temperature, pressure, flow, velocity, efficiency, mass, etc. Based on the results we observed that nitric oxides are the predominant long lives species produced by the RB plasma jet and some trace of O3. The nitric oxide formation is a reversible plasma chemical reaction and it can be expressed as

$$N_2 + O_2 \Leftrightarrow 2NO - \Delta E \qquad (2)$$

The decaying concentration of the nitric oxides from the plasma jet can be used as reference for the treatment distance between the biological cells and the plasma source tip. The background NOx concentration are measured using NOxCANg module at various timings and at standard laboratory conditions well before the plasma source was operated and it was measured to be less than 0.5 ppm.

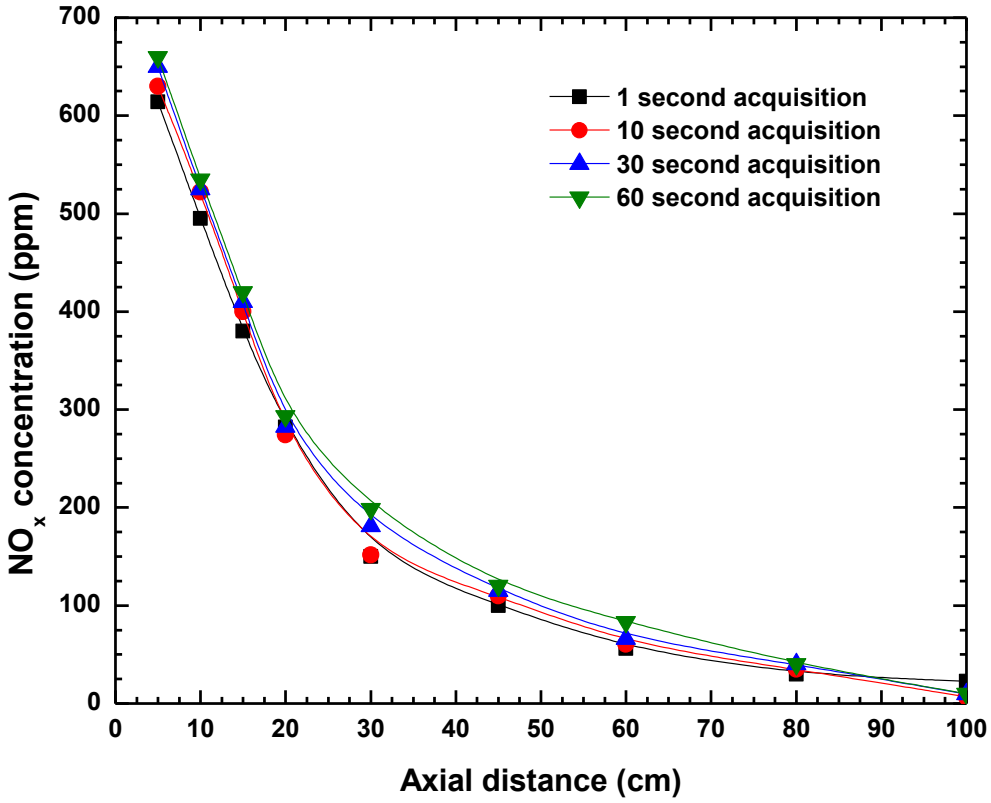


NOx concentration (ppm) at different distances from plasma jet's nozzle without the cooling unit.

The NOx concentration measurements are carried out at 20 data sets separated by 1 min with 1 second acquisition time at different distances. For consistency in the concentration measurements, three other sampling timings such as 10, 30 and 60 second are tested in addition to 1 second acquisition time. We demonstrated the NOx concentration at different distance with different acquisition times. As can be seen, the concentration of NOx species is consistent for various gas acquisition integration times at various distances from plasma jet's nozzle.

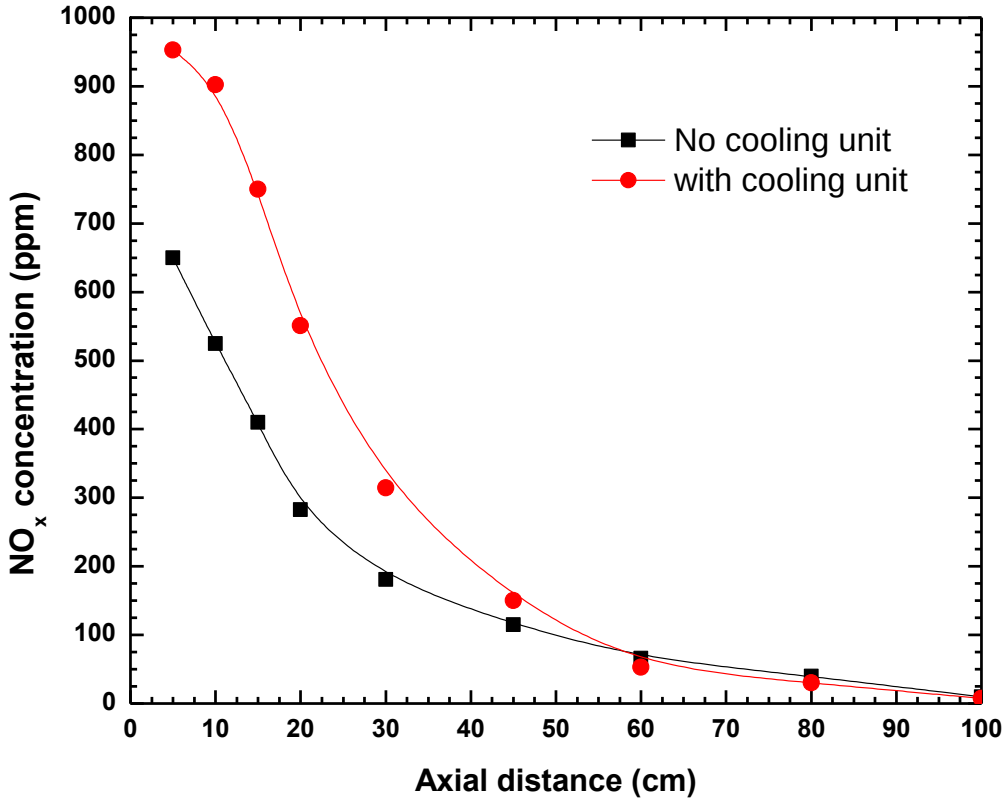


NOx concentrations of the RB plasma jet with and without cooling unit.

The NOx concentrations of the plasma jet with and without the cooling unit are measured at various axial distances from the tip and the results The measurements shows that the NOx concentration peaks at the electrode tip as expected and the NOx concentration was measured to be in the rage of 500-660 ppm at 5 cm from the plasma jet exit without the cooling unit. The concentration drops to half of its initial value at ~20cm and it continue to drop to ~100 ppm at 60 cm and at 100 cm distance from the tip the concentration was very low (<10 ppm). the NOx concentrations for plasma jet with cooling unit (circles) and it was observed that the NOx concentration after the cooling unit was higher (~950 ppm) compared to that of plasma jet without

cooling unit (~615 ppm), this was due to the fact that plasma jet diffuses out after it exits from the nozzle whereas the probe diameter after the cooling unit is very small like a pinhole arrangement with 1 mm diameter opening leading to increased concentration.

NOx is composed of two components such as the mono-nitrogen oxides or nitric oxides (NO) and nitrogen dioxide (NO2). In order to measure the individual concentration levels of NO and NO2 a different diagnostic tool was realized using a gas analyzer (Testo 350 M/XL) capable of identifying and characterizing over several molecular gases including NO and NO2. Table 1 shows the concentrations of NO and NO2 produced by the plasma jet without the cooling unit and the Table 2 shows the concentrations of NO and NO2 produced by the plasma jet with external cooling unit. In both cases, the concentration of NO2 was much lesser compared to that of NO by an order of magnitude or higher.

**Table 1. The direct exposure NO and NO2 (ppm) concentrations of the RB plasma jet at various axial distances d (cm) from the jet exit tip. (without the external cooling unit)**

| d | 5 | 10 | 15 | 20 | 25 | 30 | 35 | 40 | 45 | 50 | 55 | 60 | 70 | 80 | 90 | 100 |
|---|---|---|---|---|---|---|---|---|---|---|---|---|---|---|---|---|
| NO | 1555.6 | 631.6 | 450.8 | 288 | 239.7 | 193 | 140.2 | 116 | 81 | 90.1 | 86 | 54.8 | 44.3 | 27.3 | 10 | 5.2 |
| NO2 | 191.1 | 57.2 | 35 | 21.8 | 16.7 | 13 | 9.3 | 7.5 | 5.1 | 5.4 | 4.9 | 3.1 | 2.4 | - | - | - |

**Table 2. The indirect exposure NO and NO2 (ppm) concentrations of the RB plasma jet at various axial distances d (cm) from the jet exit tip. (with the external cooling unit).**

| d | 5 | 10 | 15 | 20 | 25 | 30 | 35 | 40 | 45 | 50 | 55 | 60 | 70 | 80 | 90 | 100 |
|---|---|---|---|---|---|---|---|---|---|---|---|---|---|---|---|---|
| NO | 2469.2 | 1110 | 651.6 | 389.3 | 341.6 | 200 | 180 | 160 | 90 | 85 | 80 | 49.6 | 25 | 12.8 | 9.5 | 7.1 |
| NO2 | 218 | 120 | 79.3 | 46.4 | 28.3 | 25 | 15.4 | 13 | 9.1 | 7 | 8 | 3.9 | 2 | 1.5 | - | - |

The ppm concentration of NO is at the preferred level for a wide range of standard biomedical treatment applications. The ppm concentration of NO2 is below the OSHA safety standards. The formation of different active species produced in air plasmas involves very complex plasma chemistries. At such a relatively high gas temperature different nitrogen oxides products are formed from N2 and O2 reactions.31 The O2 concentration affects the production of NOx species air discharges and tt has been shown that a threshold value of O2 concentration (5%) is necessary for production of different NOx species.31,32 In such a plasma condition, NO2 will be produced from N2 and O2 in the discharge based on the following reactions.

$$N_2 \rightarrow 2N \qquad \Delta G^\circ = +911.1\ \text{kJ}.mol^{-1} \tag{3}$$

$$N + O_2 \rightarrow NO_2 \qquad \Delta G^\circ = -404.3\ \text{kJ}.mol^{-1} \tag{4}$$

$$N + O_2 \rightarrow NO + O \qquad \Delta G^\circ = -137.3\ \text{kJ}.mol^{-1} \tag{5}$$

Although NO2 production is more favorable than NO production, NO2 decomposes according to following reactions and produces additional NO species.

$$NO_2 \rightarrow N + O_2 \qquad \Delta G^\circ = +404.3\ \text{kJ}.mol^{-1} \tag{6}$$

$$NO_2 \rightarrow NO + O \qquad \Delta G^\circ = +267.0\ \text{kJ}.mol^{-1} \tag{7}$$

Thus, considering both process of NO formation; such as from N2 and O2 (according to reactions 3 and 5) and from decomposition of NO2 (reaction 7), results in a higher NO concentration compared to NO2 along the plasma jet (see Table 1-2). Such processes are observed in other thermal plasmas as well.32

**H. Direct versus indirect bacterial inactivation in liquid environment**

Plasma treatments on bacterial cultures of S. aureus, E. coli, and N. meningitidis were done using direct and indirect methods. The demonstration of bacterial inactivation and its quantitative analysis were done by optical density (OD) measurements using UV-VIS spectrometer tested at 595 nm. Considering the OD value proportional with the concentration of the detected bacteria, we determined the inactivation of the bacterial growth. The pH measurements of the plasma treated samples showed similar values as the untreated samples.

demonstrate that with direct plasma treatment, S. aureus suspensions reached a mean maximum density over a 24 hour period of OD595 = 1.418, OD595 = 1.283, and OD595 = 0.137, with increasing direct treatment of RB plasma jet times of 30s, 60s, and 120s, respectively, while untreated S. aureus bacterial suspensions resulted with a mean maximum density measurement of OD595 =1.964. The results show that the S. aureus suspended in aqueous media were inactivated with 60s of direct exposure of RB plasma jet. Similarly, E. coli displayed similar trends as S. aureus suspensions as shown

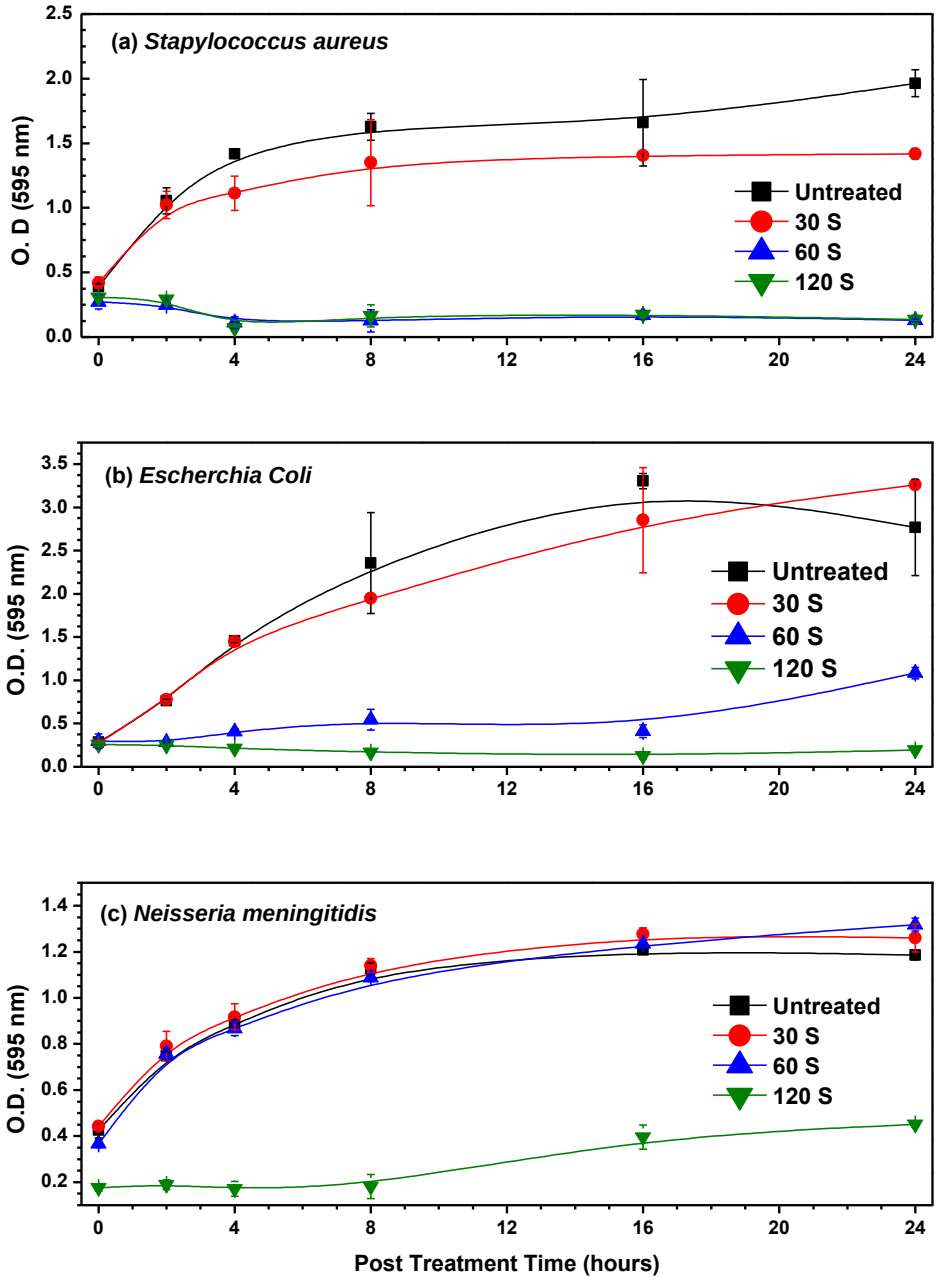


Inactivation efficacies of RB plasma jet as a function of direct plasma exposure treatment. Density measurements over 24 hr post treatment on: (a) S. aureus, (b) E. coli, (c) N. meningitidis.

The untreated E. coli suspensions reached a mean maximum density over a 24 hour period of OD595 = 3.305. The OD595 mean maximum density readings over a 24 hour period of E. coli with 30s and 60s of direct treatment of RB plasma jet reached OD595 = 2.77 and OD595 = 1.084, respectively, showing partial inactivation. Whereas, the E. coli suspensions with direct treatment of RB plasma jet for 120s displayed a radically lower OD595 with the mean maximum density reading over a 24 hour period reaching OD595 = 0.259. The inactivation efficacy of the S. aureus and E. coli by the RB plasma jet direct treatment of 120s at 5 cm distance was further corroborated with 1 x 10-6 serial dilution and 100 µl plating of cultures on agar plates as shown As shown the direct treatment of RB plasma jet on N. meningitidis suspensions showed a different density pattern compared to E. coli and S. aureus suspensions. The OD595 mean maximum density readings over 24 hour period of N. meningitidis with 30s, 60s, and 120s of direct treatment of RB plasma jet reached OD595 = 1.26, OD595 = 1.32, and OD595 = 0.451, respectively. Untreated suspensions of N. meningitidis displayed a mean maximum density measurement of OD595 = 1.185. The indirect plasma treatment involves exposure of only the long lived active species (ROS and RNS) generated by the plasma instead of the plasma itself, thus excluding the effect of any possible UV radiation produced by plasma. It has been researched that under same treatment condition, a direct plasma treatment is an order of magnitude faster than indirect treatment by plasma active agents such as bombardment of the surface of a microorganism by charged particles in the primary inactivation mechanism.33 In the RB plasma jet indirect exposure method the concentrations of the nitric oxides are preserved by reducing the plasma temperature rapidly through a separate external small efficient cooling unit.

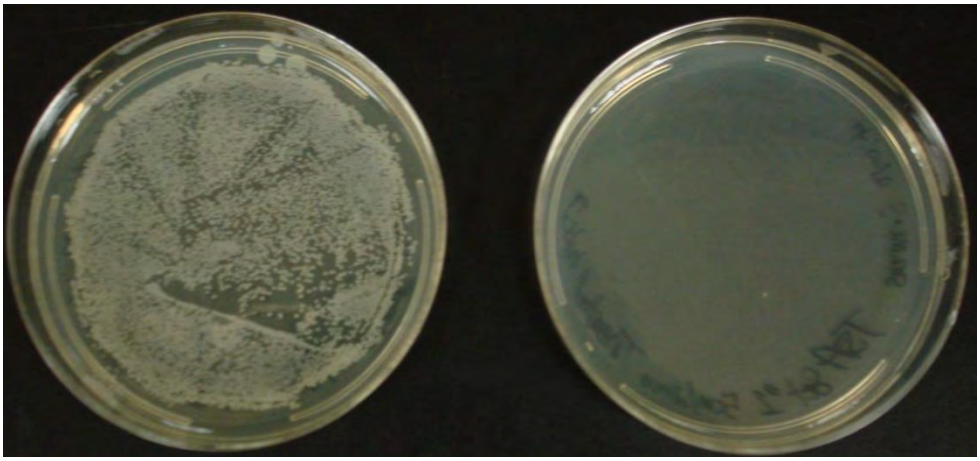

(a)

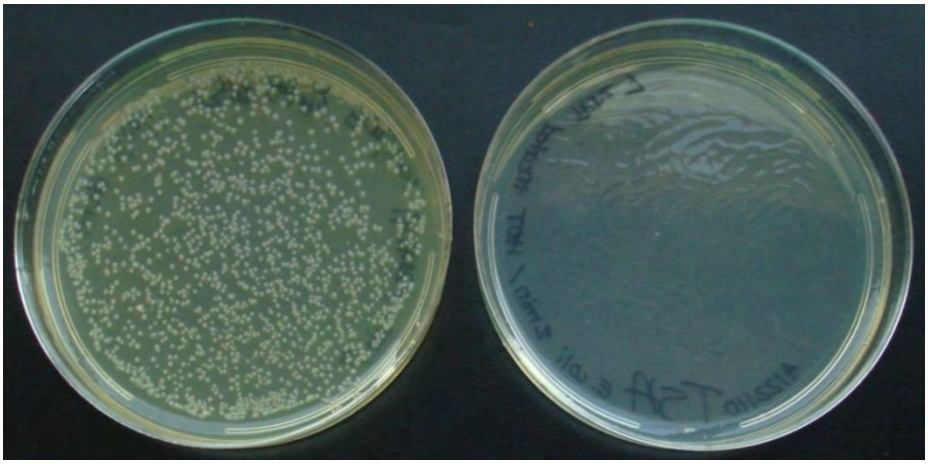

(b)

Bacterial growth represented in terms of CFUs on agar plates for (a) S. aureus, (b) E. coli. (left)-control without plasma treatment, (right)-120s direct RB plasma jet treated.

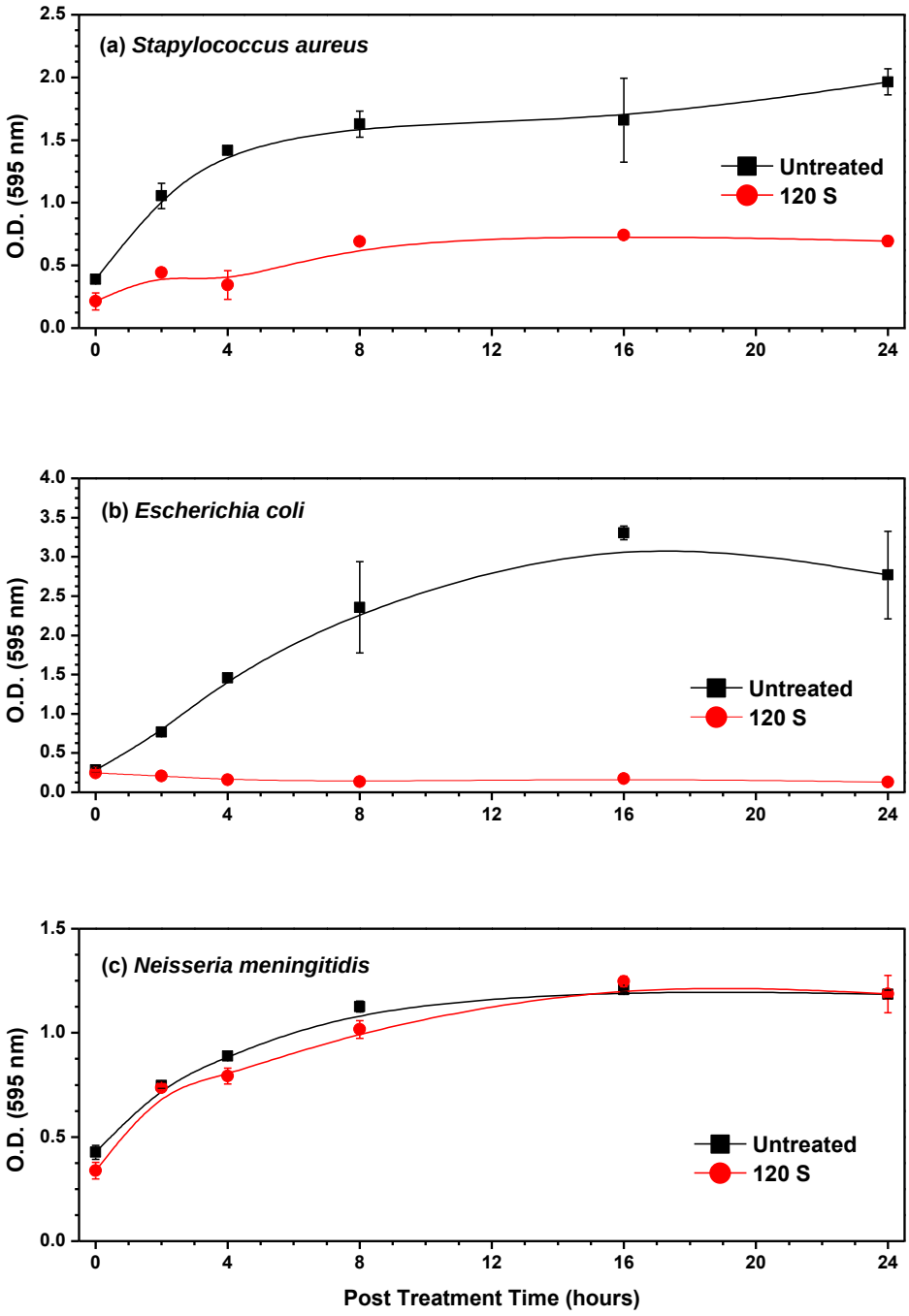


Inactivation efficacies of RB plasma jet as a function of indirect plasma exposure treatment. Density measurements over 24 hr post treatment on: (a) S. aureus, (b) E. coli, (c) N. meningitidis.

Utilizing the maximum time of direct exposure of RB plasma jet treatment at which the lowest densities were seen in S. aureus, E. coli, and N. meningitidis suspensions, we found that 120s of indirect exposure of RB plasma jet treatment greatly reduced the densities of S. aureus and E.coli and with mean maximum densities over a 24 hour period reaching OD595 = 0.693 and OD595 = 0.130, respectively; as compared to untreated controls as shownAs suspected, the 120s of indirect RB plasma jet treatment of N. meningitidis suspensions did not impact the density as determined with the mean maximum density over a 24 hour period reading of OD595 = 1.187, similar to the untreated control as shown in Fig 9(c). Eventually the inactivation of N. meningitidis can be expected since its close relative N. gonnorhea with similar characteristics was effectively inactivated after at least 4 min of plasma treatment.34

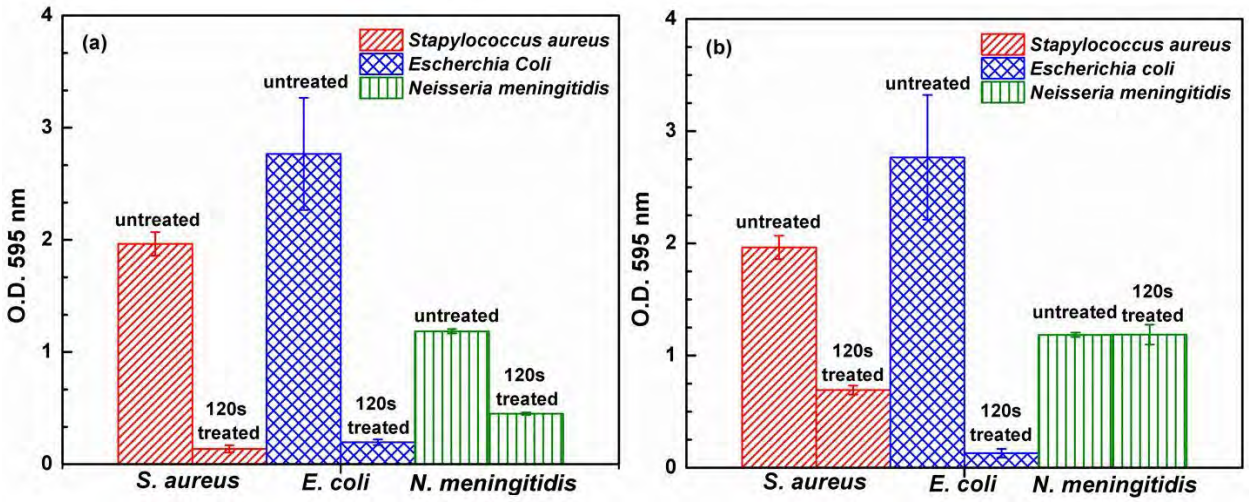


Comparative 24-hr post treatment inactivation results for S. aureus, E. coli and N. meningitidis by RB plasma jet exposure in: (a) direct plasma treatment, (b) indirect plasma treatment –modes.

The comparative bacterial growth inactivation results by the direct and indirect RB plasma jet treatments are presented Variable differences in the amount of plasma exposure required to inactivate different strains of bacteria has been repeatedly reported but of greater interest is variable resistance to inactivation amongst bacteria of the same species as seen with S. aureus35 and determined in N. gonnorhea36. The identified variability in bacterial resistance to plasma as seen in this study and previously reported studies suggest that some bacteria may be incorporating mechanisms to ameliorate some of the plasma effect. In the use of direct plasma inactivation of bacterial growth, N. meningitidis required greater plasma exposure to allow for its inactivation, while there was no apparent inactivation by indirect plasma treatment. As indicated in Table 1 and 2, NO is a major component of the long lived species produced by the RB plasma jet. N. meningitidis is normally found in the moist tissues of the NO rich environment of the nasal passages.37 Furthermore N. meningitidis is known for its ability to impede host cell defenses against removing the bacteria through inhibition of NO induction cell suicide.38 We can only allude to the incorporation of these mechanisms as a factor that provided tolerance toward indirect plasma treatment consisting of high levels of nitric oxide for N. meningitidis as compared to successful decreases in densities seen in E. coli and S. aureus. Although the results signify that N. meningitidis might be metabolizing NO, further metabolic measurements may be required in order to confirm. Alternately, the ability of plasma to affect bacterial gene expression has been previously described with E. coli treated with direct plasma demonstrating significant changes in gene expression of genes that control the bacterial defense against oxidative stress.39,40 Similarly, a pilC gene expression analysis of N. meningitidis was performed for 60 second direct treatment of RB plasma jet. The pilC gene is widely known for directing the production of PilC protein that

is the primary adhesin allowing for the bacteria to bind to the semi-aqueous mucosal layer inside the nose and throat.41

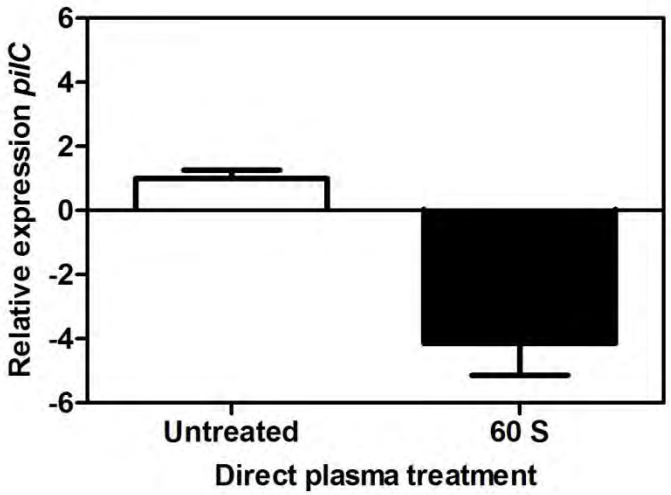


FIG 11. Quantitative PCR analysis of relative expression of pilC in N. meningitidis untreated and 60 second of RB plasma jet direct treatment.

The results indicate that, 60 seconds of direct plasma treatment has a 4 fold reduction in the relative expression of the pilC gene as compared to the untreated sample as shown. The values were determined after correcting the gene expression using the internal 16S control. The 16S control gene is a standard functional gene within the bacteria whose expression level is normally constant. The values represent mean ± standard deviations. We can derive from previous reports that demonstrated an increase in the levels of NO in cultures of N. meningitidis results in an increase in expression of genes involved with protection against NO.42 Therefore, the change in gene expression of pilC suggests that other genes involved with protection against NO are also variably affected by direct plasma treatment. The NO detoxification mechanisms found in the bacterial species used in this study were originally detected as a bacterial defense response against

host cell nitrosative stress.4,43 The presence of bacterial bio-physical mechanisms that may provide the capabilities to resist specific plasma chemistries as observed with N. meningitidis highlights a research prospect for plasma treatment of infected wounds. The authors have suggested the potential use of RB plasma jet for wound sterilization, although the increasing levels of NO may concern to treating wound tissue. So far, there have been no report of plasma treatment on bacterial infected wounds being negatively impacted in rodent44 and porcine2 models or human clinical trials45. The RB plasma source can be extended further to personal and small scale treatment of wound infections, medical instrumentation sterilization, along with food and agricultural product sterilization and detoxification.

In conclusion, we have developed a portable, light weight resistive barrier (RB) plasma jet applicable for a range of biomedical applications including bacterial inactivation in aqueous media. The RB plasma jet can be operated at both DC and standard low frequency AC, and also able to function effectively in both direct and indirect plasma exposure configurations based on the type of treatment targets and applications. The characteristics of the RB plasma jet such as the voltage-current curves, plasma power, plasma gas temperature and RNS concentrations were characterized. The voltage-current waveform analysis resulted the plasma power to be 26 W. A high resolution optical emission spectroscopy diagnostic analysis of the N2 second positive band system N2C-B(2+) rotational transitions in the 364-383 nm range showed the gas temperatures equivalent to the rotational (Trot) temperatures to be as 3000 ○C at 0.2 cm from the exit and decayed to 2000 ○C at 0.8 cm and continued to decay to 1500 ○C at 1.5 cm and to 1000 ○C at 2 cm and the jet temperature reached room temperature with the addition of external cooling unit for the indirect treatment mode. The parts per million (ppm) concentration of the nitric oxide (NO) at different spatial distances from the tip of the plasma jet were measured to be in the rage of 500-

660 ppm at 5 cm distance from the electrode and drops to ~100 ppm at 60 cm. The RB plasma jet was effective in inactivating the S. aureus and E. coli in less than 120 seconds determined by measuring the density of bacteria growing in liquid cultures, in both direct and indirect exposure treatment modes. The N. meningitidis appeared to show some resistance to inactivation and required extended plasma exposure as compared to S. aureus and E. coli, especially when the RB plasma jet was used in the indirect mode. The RT-PCR based pilC gene expression analysis was done on 60 second direct plasma treated N. meningitidis samples at which only partial inactivation was achieved. The results revealed that although a significant inactivation was not observed as determined by bacterial growth, the genes that control the ability of bacteria to cause an infection were being inhibited by at least 4 fold differences as compared to untreated bacteria. However, the ability of N. meningitidis to partially resist direct plasma and completely resist indirect plasma treatment suggest that it has incorporated processes that are regulated by genes that are directed by external stimuli such as NO from the RB plasma jet. The findings indicate that N. meningitidis displayed some tolerance to plasma and the long lived reactive nitrogen species, indicating the need for further research toward the specific bacterial inactivation mechanisms of plasma derived reactive nitrogen species.

## II. Characterization of a non-thermal atmospheric pressure helium plasma jet

In this project period, we have also applied optical emission spectroscopy diagnostics to investigate the characteristics of a non-thermal atmospheric pressure helium plasma jet. The discharge characteristics in the active and afterglow region of the plasma jet, that are critical for biomedical applications, have been investigated. The voltage-current characteristics of the plasma discharge were analyzed and the average plasma power was measured to be around 18 W. The

effect of addition of small fractions of oxygen at 0.1 - 0.5% on the plasma jet characteristics were studied. The addition of oxygen resulted in a decrease in plasma plume length due to the electronegativity property of oxygen. Atomic and molecular lines of selected reactive plasma species that are considered to be useful to induce biochemical reactions such as OH transitions $A^2\Sigma^+(\nu = 0,1) \rightarrow X^2\Pi(\Delta\nu = 0)$ at 308 nm and $A^2\Sigma^+(\nu = 0,1) \rightarrow X^2\Pi(\Delta\nu = 1)$ at 287 nm, O I transitions $3p^5P \rightarrow 3s^5S^0$ at 777.41 nm and $3p^3P \rightarrow 3s^3S^0$ at 844.6 nm, $N_2$(C-B) second positive system (SPS) with electronic transition $C^3\Pi_u \rightarrow B^3\Pi_g$ in the range of 300-450 nm and $N_2^+$(B-X) first negative system (FNS) with electronic transition $B^2\Sigma_u^+ \rightarrow X^2\Sigma_g^+(\Delta\nu = 0)$ at 391.4 nm have been studied. The atomic emission lines of helium were identified, including the He I transitions $3p^3P^0 \rightarrow 2s^3S$ at 388.8 nm, $3p^1P^0 \rightarrow 2s^1S$ at 501.6 nm, $3d^3D \rightarrow 2p^3P^0$ at 587.6 nm, $3d^1D \rightarrow 2p^1P^0$ at 667.8 nm, $3s^3S^1 \rightarrow 2p^3P^0$ at 706.5 nm, $3s^1S^0 \rightarrow 2p^1P^0$ at 728.1 nm, and $H_\alpha$ transition 2p-3d at 656.3 nm. Using a spectral fitting method the OH radicals at 306-312 nm, the rotational and vibrational temperatures equivalent to gas temperatures of the discharge was measured and the effective non-equilibrium nature of the plasma jet was demonstrated. Our results show that, in the entire active plasma region, the gas temperature remains at 310±25 K and 340±25 K and it increases to 320±25 K and 360±25 K in the afterglow region of the plasma jet for pure helium and helium/oxygen (0.1%) mixture, respectively. Additionally, the vibrational temperatures range from 2200±100 K and 2500±100 K for pure helium and helium/oxygen (0.1%) mixture, respectively. The plasma jet was tested on heat sensitive polymer films used in biomedical applications such as polyethylene terephthalate (PET) and poly-L-lactide (PLLA) samples continuously for several minutes without causing any physical or thermal damage to the films. The plasma jet produces significant reactive species of interest while the gas temperatures remain very low demonstrating its potential for a range of biomedical applications.

Non-thermal plasma jets that are operated in atmospheric pressure have been proven to be an effective plasma sources because of their feasibility to be used in a range of applications such as sterilization,[1, 2] surface modification of the polymers[3-5] environmental and industrial applications[6] and more recently in medicine.[7-9] In such plasmas, the high electron temperature enhances the plasma chemistry processes which lead to the generation of highly reactive chemical species e.g. hydroxyl radicals and ozone, while the plasma gas temperature remaining close to the room temperature. Atmospheric pressure plasma jets with lower gas temperatures are suitable for treating temperature sensitive materials without causing damage, and they are also found to be easily adaptable to complex geometries and conventional processes.

Atmospheric pressure plasma jets (APPJs) are capacitively coupled dielectric barrier discharge (DBD) sources typically operated in the radio frequency range, e.g. at 13.56 MHz[10] or 27.12 MHz[11] and it can be generated in various electrode arrangements.[12] In general the APPJs consist of two electrodes in different arrangements. In some studies, a simple nozzle configuration with a dielectric tube surrounded by ground electrode has been used. A pulsed or AC power supply with frequency of several kHz was applied between the electrodes to generate plasma from working gases such as helium, argon and nitrogen.[6, 13, 14] In most of the APPJ applications, gas temperatures significantly influence the application, thus it needs to be precisely diagnosed. However, determination of the gas temperature in the DBD plasma jets is a significant experimental challenge due to electrical interferences caused by conventional thermocouples inside the discharge leading to inaccurate measurements. Another problem is that the quartz capillary in such plasma jets is generally narrow. Therefore a convenient way to measure the gas temperature inside or near the discharge volume is to place the thermocouples outside the discharge or measure the temperature after switching off the discharge. Both techniques are inaccurate; the

DBD plasma jets are made of quartz, which is an insulating material and it yields a poor heat transfer from the gas to the plasma jet's wall, therefore, rendering the temperature of quartz capillary wall rather the needed gas temperature. Among different plasma diagnostic methods, optical emission spectroscopy (OES) diagnostics acts as a viable technique for determining discharge parameters.[6, 15, 16] OES is a non-invasive and non-perturbing plasma diagnostic technique that is easy to use and widely applied for investigation of plasma species and characterization of its gas temperatures. OES enables to identify the reactive plasma species such as radicals, atomic and molecular species and therefore it provides the insight of the plasma chemical processes.[6, 16] In addition, OES provides valuable information on excited atomic or molecular plasma species, which enables us to determine the rotational and vibrational temperatures of the plasma and thus the non-equilibrium nature of the plasma jet and the plasma gas temperatures.[6, 16-18]

The plasma jet developed in this work aimed to produce reactive plasma species, such as hydroxyl radicals, excited nitrogen species, singlet oxygen and helium metastable that can be applied for bio-medical applications including inactivation of bacteria, sterilization, and treatment of cancer. This work is aimed on applying optical emission spectroscopy to identify plasma species that are critical for several biomedical applications and determining the plasma gas temperatures. In addition, the effect of addition of oxygen in the plasma jet characteristics is of focus in this work due to the significance of singlet oxygen radicals in biomedical applications. This work also aimed to produce increased amounts of active species by adding oxygen without significant increase in the plasma jet gas temperature and produce the plasma jet at low temperatures suitable for treating heat sensitive surfaces.

In this paper, the consumed power for plasma generation (plasma power) has been estimated from voltage-current waveform analysis in order to optimize the plasma jet operation. The effects of addition of small fractions of oxygen on the plasma jet are presented. Subsequently, we present the optical emission spectroscopy results of the plasma jet in helium and helium/oxygen mixtures (0.1-0.5% oxygen). The results of our investigation on the plasma jet includes the analysis of optical emission spectra measured in the active region, the region between the electrodes where plasma is formed inside quartz capillary, and also in the jet's afterglow region where the plasma jet propagates in to the surrounding air. In addition, using a high resolution spectrometer, the OH rotational and vibrational temperatures were determined by fitting the experimental and simulated spectra. The result of this work are useful for a range of atmospheric pressure plasma jet applications, such as surface treatment of polymers, biomedical and environmental applications where OES act as a key diagnostic for investigating the plasma chemical processes.

## A. EXPERIMENTAL SETUP

In our investigation, we have designed and constructed an atmospheric pressure dielectric barrier plasma system that can produce a long plasma jet aimed for materials processing and biomedical applications. The schematic of our plasma system is shown. The plasma jet was produced in a quartz capillary with inside and outside diameters of 1.3 and 3.0 mm, respectively. A 0.5 mm diameter tungsten rod was used as the central high voltage electrode which is positioned inside the quartz capillary.

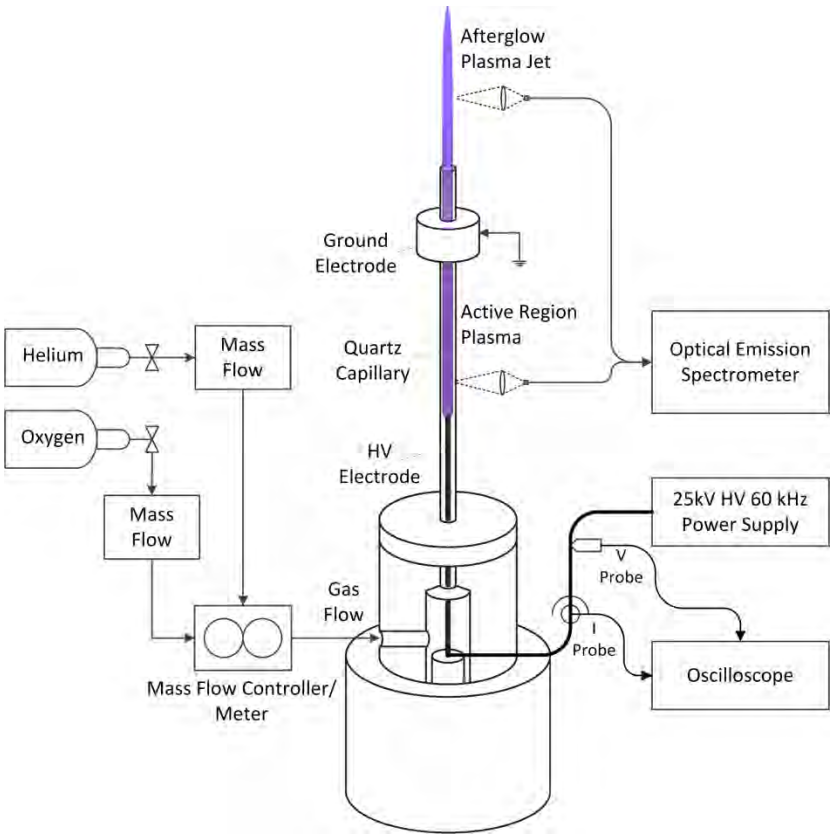


Schematic of the plasma jet system along with V-I and OES diagnostics.

A 10 mm long ring type copper ground electrode positioned outside the quartz capillary at a distance of 40 mm away from the tip of the central high voltage electrode. The primary operating gas for the plasma jet used in this work is Helium and small fractions of oxygen (0.1 - 0.5%) were used as the secondary gas. The gas flow rate was monitored by a two channel power supply/readout (model: MKSPR400) and controlled by two mass flow meters (Model: MKS 1179A). The total gas flow rate was maintained at 3 slm.

A variable sine-wave AC high-voltage power supply ($V_{pp}$: 0-25 kV) operating at 60 kHz was used to generate the plasma jet. The applied voltage waveform was monitored using high voltage probe (Tektronix P6015A) and the current waveform was monitored by current probe (Tektronix TCP202). The current and voltage signals are recorded using digital oscilloscope

(Tektronix TDS 3034C). The peak to peak applied voltage value was varied between 6 to 14 kV. The input power was fixed at an optimal value of 18 W for all the experiments.

Optical emission spectra of the plasma jet were measured in order to identify various reactive plasma species in the active and afterglow region of plasma jet and to determine the plasma gas temperatures. The spectra were collected with an optical fiber (diameter of 0.6 mm), placed near to the active zone and the afterglow region of the plasma jet. Two spectrometers of different resolution were used. The optical emission spectra of the discharge in the 200–900 nm region were recorded by broadband Ocean Optics HR2000 spectrometer with a resolution 0.83 nm and the emission of OH radicals in the range of 306-312 nm was recorded with 500 $\mu$s integration time using a 0.08 nm resolution spectrometer system which is a combination of monochromator (Princeton Instruments Acton SP2750) and fast gated CCD (ACTON IStar).

**B. Plasma jet length, voltage-current and plasma power measurements**

A complete gas breakdown between the electrodes with a formation of bright glow discharge was achieved by applying a high voltage of approximately 6 kV ($V_{pp}$). A long afterglow plasma jet of length up to 40 mm was achieved with a gas flow rate of 3 slm. We were able to vary the plasma jet length by varying the gas flow rates, applied voltage and gas compositions. As shown in the visual view of the plasma jet the plasma jet creates a long plume length which propagates in to the surrounding air.

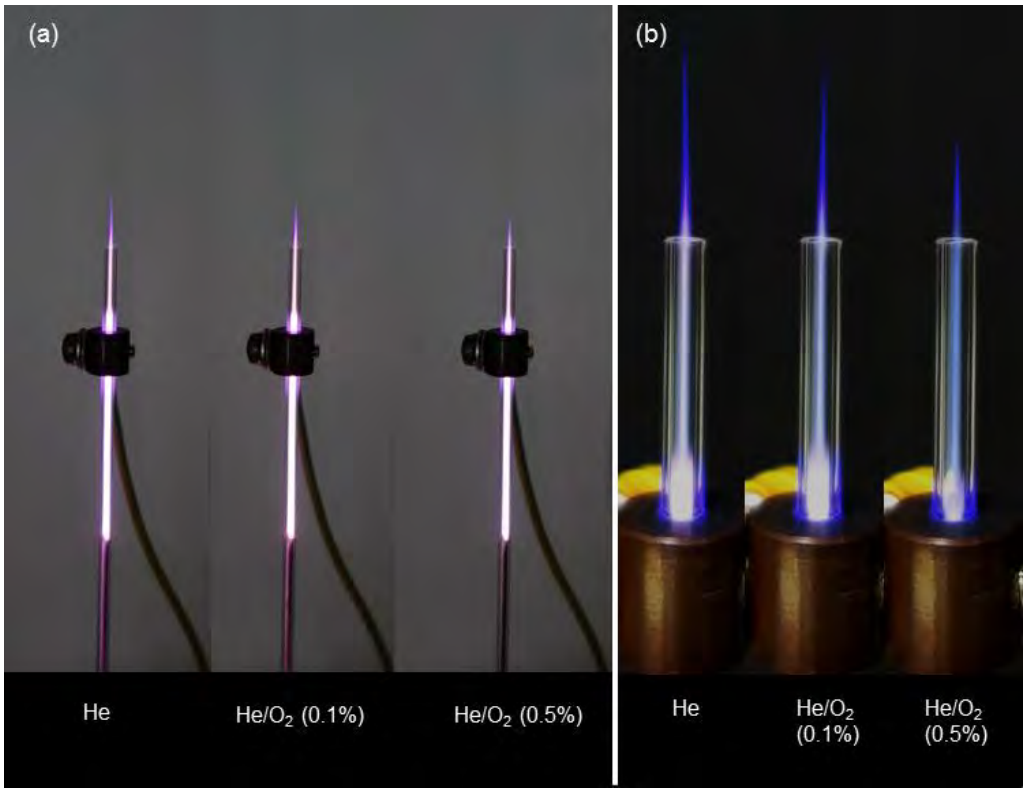


Visual view of the plasma system. (b) Images of afterglow region of the plasma jet in pure helium and $He/O_2$ mixtures. Total gas flow rate is 3 slm and plasma power is 18 Watt.

the photograph of the afterglow region of the plasma jet operating in pure helium at 3 slm and helium/oxygen (0.1% and 0.5% $O_2$) mixtures. The images were taken by a Sony RX100 digital camera and the exposure time for all of the images was fixed at 1/30 s. The length of plasma plume from the tip of the quartz capillary for pure helium discharge is 25 mm. With 0.1% oxygen added to the Helium gas, the plasma plume length decreased to 17 mm. It was observed that the addition of oxygen in to the plasma jet results in a decreased plasma jet length. Since oxygen is an electronegative molecular gas, the decrease in plasma jet length is believed to be caused by decrease in electron densities and helium metastable densities with the addition of oxygen.

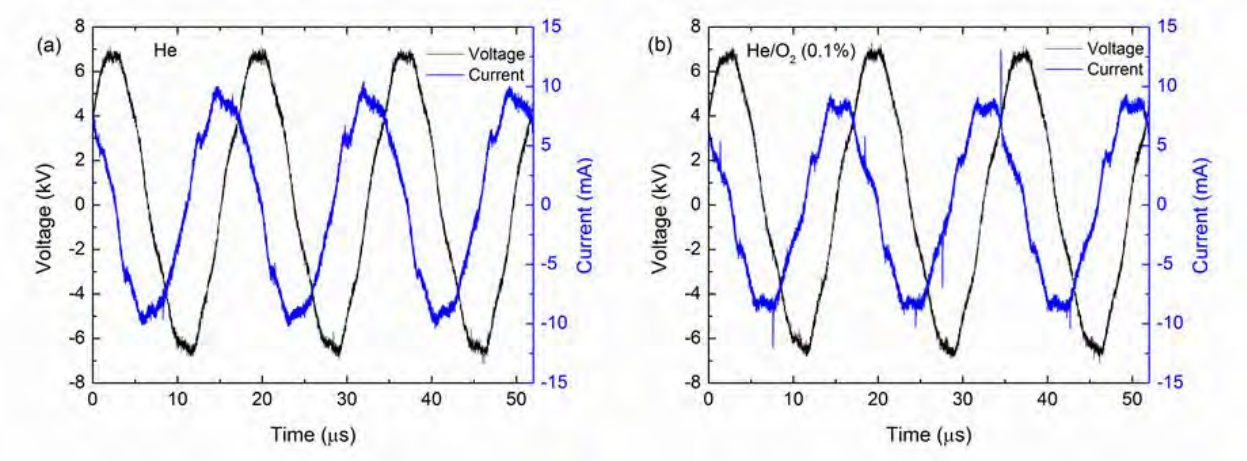


Voltage-current waveforms of the plasma jet. (a) Discharge in pure Helium and (b) Discharge in $He/O_2$ mixture (0.1% Oxygen).

The voltage and current waveforms were obtained for various applied voltages ranging from 6 to 14 kV ($V_{pp}$) and gas compositions of He and He + $O_2$ (0.1 - 0.5% $O_2$). A typical example of voltage-current waveform of the plasma discharge in He and He + 0.1 % $O_2$ is shown in which the applied voltage and gas flow rate was set at 12 kV ($V_{pp}$) and 3 slm respectively. The DBD plasma jet generates a very uniform discharge in pure helium gas and only two small current peaks exist on the current waveform during each half period of the applied voltage. Both peaks are smooth and the maximum current is ~10 mA and the duration of the current peaks are approximately 0.8 $\mu$s. A clear change in the voltage-current waveform was observed when oxygen was added to the plasma jet. Addition of the oxygen to the plasma jet results in a small increase of the current peak intensity to ~12 mA and decrease of the current peaks duration to 0.5 $\mu$s. The results indicate that the voltage slightly decreases with increase of the current peaks. The consumed power for plasma generation is calculated by integrating the product of the discharge voltage and current over one cycle; according to the following equation ($T$ = period of the discharge)[19]

$$W = \frac{1}{T}\int_{t}^{t+T} I(t)V(t)dt \quad (1)$$

and the average plasma power is measured to be 18 W.

**C. Plasma species identification using optical emission spectroscopy**

Optical emission spectroscopy was used to study the plasma jet in He and He/$O_2$ gas mixtures in terms of identifying the reactive plasma species produced by the plasma jet as well as determining the plasma gas temperatures. The emission spectra were measured at two locations, first in between the high voltage and ground electrodes (active region) and the second was at 5 mm away from capillary exit tip and into the plasma jet's plume (afterglow region). the time resolved optical emission spectra in the range of 200 - 900 nm measured in the active region for pure helium and helium/0.1% oxygen mixture respectively.

The emission spectra in the active region of the plasma jet is composed of OH transition $A^2\Sigma^+(\nu = 0,1) \rightarrow X^2\Pi(\Delta\nu = 0)$ at 308 nm, and OH transition $A^2\Sigma^+(\nu = 0,1) \rightarrow X^2\Pi(\Delta\nu = 1)$ at 287 nm; He I transition $3p^3P^0 \rightarrow 2s^3S$ at 388.8 nm, He I transition $3p^1P^0 \rightarrow 2s^1S$ at 501.6 nm, He I transition $3d^3D \rightarrow 2p^3P^0$ at 587.6 nm, He I transition $3d^1D \rightarrow 2p^1P^0$ at 667.8 nm, He I transition $3s^3S^1 \rightarrow 2p^3P^0$ at 706.5 nm, and He I transition $3s^1S^0 \rightarrow 2p^1P^0$ at 728.1 nm; $H_\alpha$ transition 2p-3d at 656.3 nm, O I transition $3p^5P \rightarrow 3s^5S^0$ at 777.41 nm, O I transition $3p^3P \rightarrow 3s^3S^0$ at 844.6 nm and spectral band of the $N_2$ transition $C^3\Pi_u \rightarrow B^3\Pi_g(\Delta\nu = 0)$ at 337.1 nm. Discharge in pure helium shows a higher intensity of OH radicals compared to the plasma with He/0.1% $O_2$ gas mixture at 308 nm. The presence of OH and $N_2$ emission lines in the active region of the discharge is due to the presence of residual $H_2O$ and $N_2$ impurities in helium gas. Addition of small amount of oxygen (0.1%) to plasma jet results in an increase in the intensity of singlet oxygen lines at 777.41 nm and

844.6 nm, while the intensity of the other emission lines has decreased. Oxygen is an electronegative gas, hence, addition of oxygen to the plasma produces $O^-$ and $O^{2-}$ ions by electron attachment mechanisms which results in a decrease of electron density and consequently decrease in the intensity of the other lines at a constant power.[6]

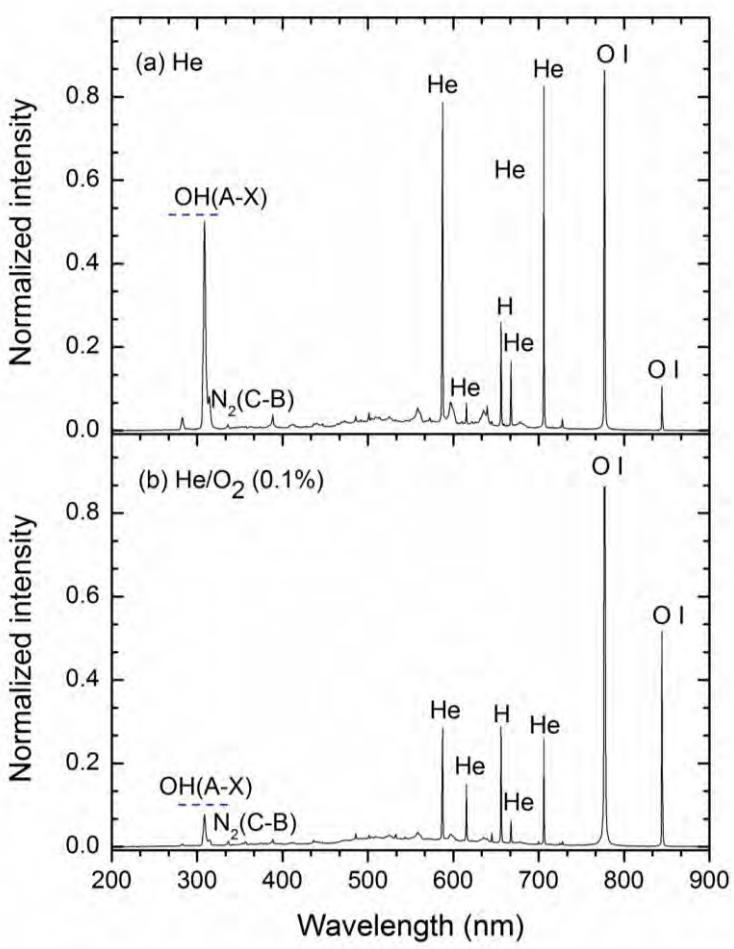


Optical emission spectra of the active zone region of plasma jet. (a) Discharge in pure helium. (b) Discharge in helium/oxygen mixture (0.1%). Total gas flow rate is 3 slm and plasma power is fixed at 18 W.

The emission spectra of the afterglow region of the plasma jet in pure helium and helium/oxygen mixtures are shown respectively. The optical emission spectra of the plasma jet in

the afterglow region are significantly different from the emission spectra measured in the active region as shown The emission spectra in the afterglow region of the plasma jet where plasma propagates in to the surrounding air is composed of molecular nitrogen $N_2$(C-B) second positive system (SPS) with electronic transition $C^3\Pi_u \rightarrow B^3\Pi_g$ in the range of 300-450 nm. $N_2^+$(B-X), first negative system (FNS), has a spectral band at 391.4 nm with electronic transition $B^2\Sigma_u^+ \rightarrow X^2\Sigma_g^+(\Delta v = 0)$, which is clearly visible in the measured emission spectra. Other emission lines belongs to OH emission lines at 308 nm, transition $A^2\Sigma^+(\nu = 0,1) \rightarrow X^2\Pi(\Delta v = 0)$ and OH transition $A^2\Sigma^+(\nu = 0,1) \rightarrow X^2\Pi(\Delta v = 1)$ at 287 nm, and the spectral lines of helium atoms including, He I transition $3p^3P^0 \rightarrow 2s^3S$ at 388.8 nm, He I transition $3p^1P^0 \rightarrow 2s^1S$ at 501.6 nm, He I transition $3d^3D \rightarrow 2p^3P^0$ at 587.6 nm, He I transition $3d^1D \rightarrow 2p^1P^0$ at 667.8 nm, He I transition $3s^3S^1 \rightarrow 2p^3P^0$ at 706.5 nm, He I transition $3s^1S^0 \rightarrow 2p^1P^0$ at 728.1 nm, and $H_\alpha$ transition 2p-3d at 656.3 nm, O I transition $3p^5P \rightarrow 3s^5S^0$ at 777.41 nm and O I transition $3p^3P \rightarrow 3s^3S^0$ at 844.6 nm. Strong $N_2$ emission lines are commonly observed in atmospheric pressure non-equilibrium air discharges.[6] The identified excited nitrogen molecules are produced from electron impact reactions in the plasma plume as it propagates in to the ambient air. In the emission spectrum of $He/O_2$ (0.1%) mixture is very similar to pure helium discharge in the case of identified species. The intensity of molecular nitrogen emission bands is less intense compared to atomic lines when a small amount of oxygen (0.1%) is added to the plasma jet. In addition the intensity of atomic lines such as He I transition $3d^1D \rightarrow 2p^1P^0$ at 667.8 nm, He I transition $3s^3S^1 \rightarrow 2p^3P^0$ at 706.5 nm, He I transition $3s^1S^0 \rightarrow 2p^1P^0$ at 728.1 nm and O I transition $3p^5P \rightarrow 3s^5S^0$ at 777.41 nm is also decreased. The corresponding emission lines are identified using the NIST atomic spectra database[20] and Lofthus et. al.[21]

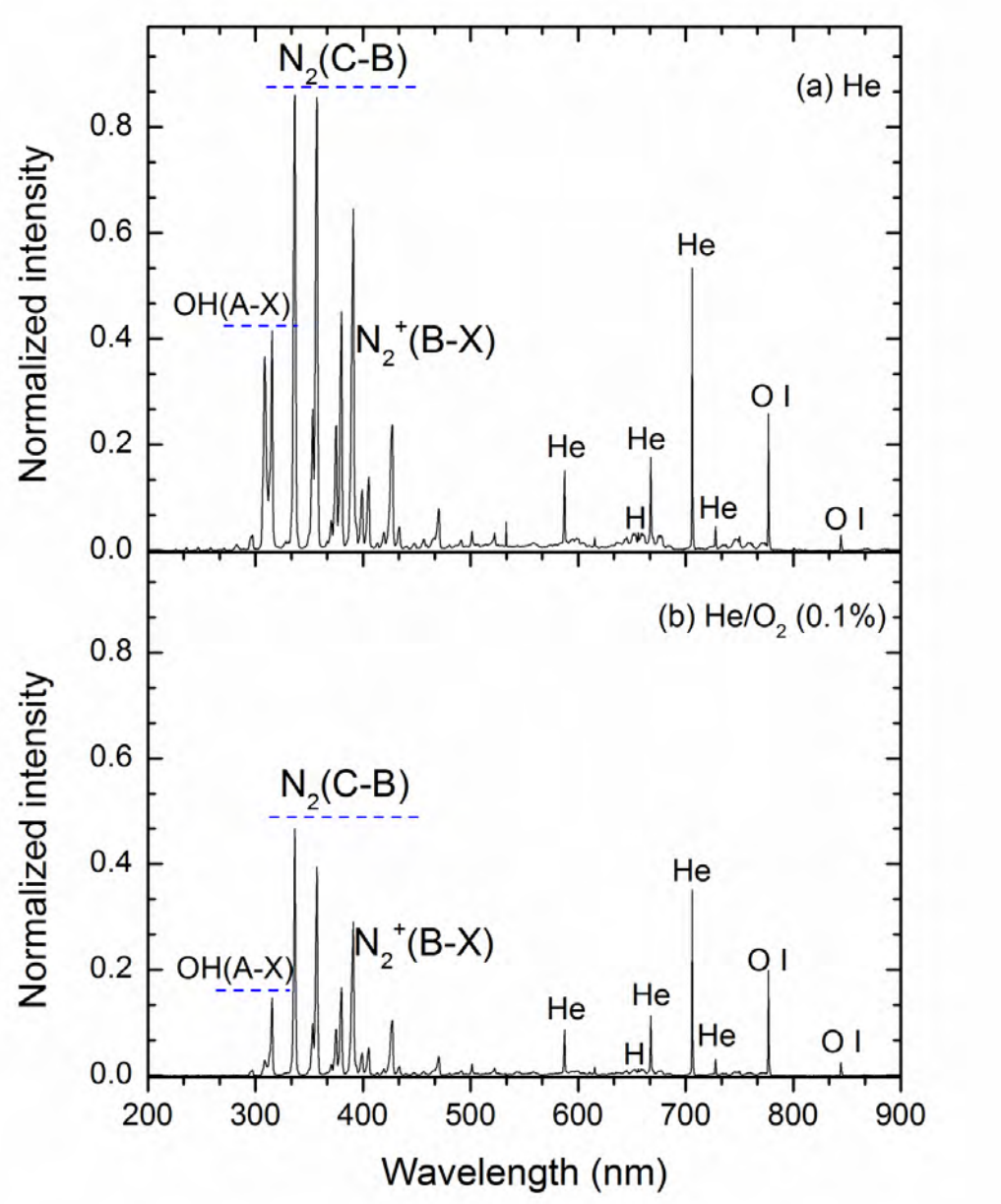


Optical emission spectra of the afterglow region of plasma jet. (a) Discharge in pure helium. (b) Discharge in helium/oxygen mixture (0.1%). Total gas flow rate is 3 slm and plasma power is fixed at 18 W. Emission spectra are recorded at 5 mm after the edge of capillary.

The identified reactive plasma species such as the singlet oxygen, hydroxyl radicals, and neutral nitrogen molecules generated by the plasma jet are measured with the OES diagnostics and these reactive plasma species can play a significant role in biomedical applications especially

operating at the atmospheric pressure.[7, 22] Similar significant generation of reactive oxygen species such as singlet oxygen O and $O_3$ were observed with $He/O_2$ gas mixture used in a plasma jet which resulted in enhanced efficacy of bacterial inactivation.[23] It is believed that the oxygen species in the discharge contributes to the sterilization process due to its strong oxidative effect on the outer structure of the cells.[7, 22] The OH radicals generated by the plasma plays a significant role through chemically attacking the outer structure of the cells and the production of the nitrogen containing group adds to the lethality of the process.[24]

**D. Rotational and vibrational temperature measurements**

The emission spectra of OH (A-X) radicals are widely used for plasma diagnostics, since they enable us to determine the rotational ($T_{rot}$) and vibrational temperature ($T_{vib}$) by fitting the experimental spectra on to a simulated spectra.[25] For all spectral simulations, a LIFBASE software[26] has been used. The emission intensity of the OH radicals is a function of the concentration of excited hydroxyl species, rotational and vibrational energy distributions, and the volume of plasma being analyzed. The OH rotational temperature in the active zone and afterglow region of the DBD plasma jet have been determined based on the simulation of emission spectra in the range of 306-312 nm with transition $A^2\Sigma^+(\nu = 0) \rightarrow X^2\Pi(\Delta\nu = 0)$. A spectral emission line can be characterized as a function of intensity, wavelength, profile and its width as expressed by[27]

$$I^{n',\upsilon',J'}_{n'',\upsilon'',J''} = N_{n',\upsilon',J'} A^{n',\upsilon',J'}_{n'',\upsilon'',J''} h\nu^{n',\upsilon',J'}_{n'',\upsilon'',J''} \quad (2)$$

where *n*, *v* and *J* represents quantum numbers of electronic, vibrational and rotational levels respectively.

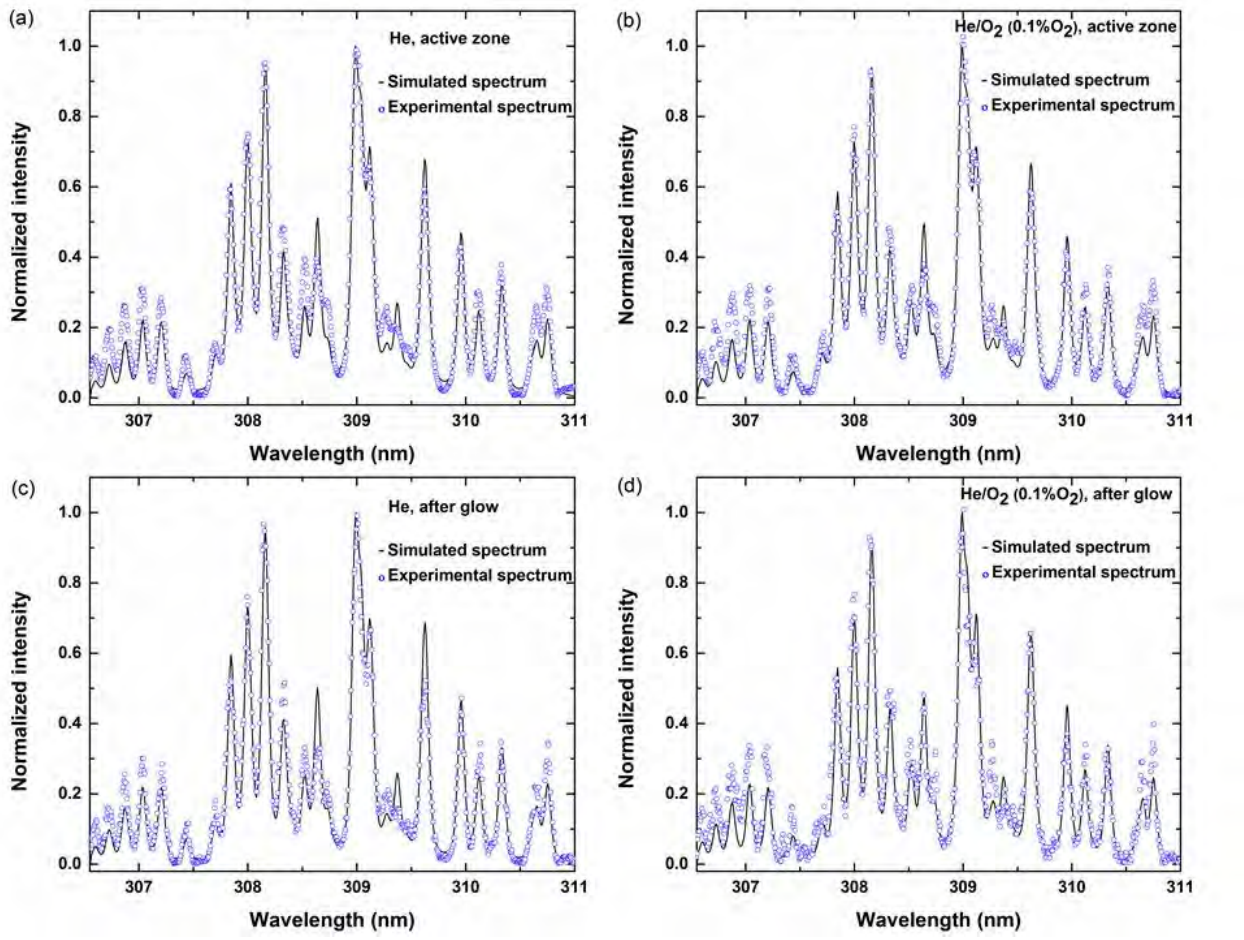


Experimental and simulated spectra of OH radicals. (a) Discharge in Pure He and in active zone region (between HV and ground electrodes). (b) Discharge in $He/O_2$ mixture (0.1%) and in active zone region (between HV and ground electrodes). (c) Discharge in Pure He and in the afterglow region. (d) Discharge in $He/O_2$ mixture (0.1%) and in the afterglow region. Plasma power was fixed at 18 Watt.

The single prime (′) signifies the upper level magnitudes and a double prime (″) signifies the lower level magnitudes. $N_{n',\upsilon',J'}$ is the density of the upper level of the molecule, $\nu$ is the frequency of the transition and $A^{n',\upsilon',J'}_{n'',\upsilon'',J''}$ is Einstein's transition probability of emission. The equation (2) can be modified as

$$I_{n'',\upsilon'',J''}^{n',\upsilon',J'} = C(\nu_{n'',\upsilon'',J''}^{n',\upsilon',J'})^4 N_{n'} S_{\upsilon'\upsilon''} S_{J'J''} \frac{\exp(-(hc/k)(G_{n'}(\upsilon')/T_{vib}))}{Q_{vib,n'}(T_{vib})} \frac{\exp(-(hc/k)(F_{\upsilon'}^{(i)}(J')/T_{rot}))}{Q_{rot,n',\upsilon'}^{(i)}(T_{rot})} \quad (3)$$

where $C$ is a constant, $h$ is the Planck's constant, $k$ is the Boltzmann constant, $c$ is the velocity of light and $N_{n'}$ is the density per volume of the molecules in electronic state of $n'$. The line strengths $S_{J'J''}$ are calculated from[28] and $S_{\upsilon'\upsilon''}$ are the band strengths. Furthermore, considering the non-Gaussian experimental line shape, a contribution of the Lorentzian function is taken into account. In this case, best fitted line shape was a mixture of a Voight and a Lorentzian profile. The line intensity as function of wavelength ($\lambda$) can be expressed as:

$$I(\lambda) = I_{n'',\upsilon'',J''}^{n',\upsilon',J'} \left( 1 - M \exp\left[ \left( -\frac{\lambda - \lambda_{n'',\upsilon'',J''}^{n',\upsilon',J'}}{FWHM} \right)^2 4\ln 2 \right] + M \frac{1}{4(\lambda - \lambda_{n'',\upsilon'',J''}^{n',\upsilon',J'} / FWHM)^2 + 1} \right) \quad (4)$$

where, $\lambda_{n'',\upsilon'',J''}^{n',\upsilon',J'}$ is the wavelength of the transition $n',\upsilon',J' \rightarrow n'',\upsilon'',J''$ and $M$ is a fraction of the Lorentzian contribution to the Voight profile of the instrumental function. The rotational ($T_{rot}$) and vibrational temperatures ($T_{vib}$) of the plasma jet were estimated by matching the experimental spectra on to the LIFBASE software simulated spectra.[26] In order to make the comparison, the intensity of both simulated and experimental spectra are normalized based on the (0-0) band and when a good agreement between experimental and simulated spectra were achieved, the corresponding OH rotational and vibrational temperatures have been deduced. The results of best fitting between experimental and simulated spectra for OH emission in the active zone of the plasma jet for He and He + 0.1% $O_2$ are shown Similarly the results of best OH spectral fitting in the afterglow region of the plasma jet for He and He + 0.1% $O_2$ are shown Based on the fitting method, the OH rotational temperatures in the active zone region of the plasma jet was measured to be 310 ± 25 K for helium only and 340 ± 25 K for helium with 0.1% oxygen gas mixture.

Whereas the measured rotational temperature in the afterglow region at 5 mm away from the capillary edge has increased to 320 ± 25 K for helium only and 360 ± 25 K for helium with 0.1% oxygen gas mixture. In addition, the vibrational temperatures of the plasma jet was measured to be 2200 ± 100 K for helium only and 2500 ± 100 K for helium with 0.1% oxygen gas mixture. Our results show that the OH rotational temperatures of the afterglow region of the plasma jet are slightly higher than the active zone region. The non-equilibrium characteristic of the plasma is resulting from the significant difference in the vibrational and rotational temperatures. Based on the results, the higher vibrational temperatures compared to rotational temperature ($T_{vib} > T_{rot}$) demonstrate that, the plasma jet produced is in a non-equilibrium condition.[6] In atmospheric pressure plasmas the gas temperature is equal to the rotational temperature due to the higher collisional rates, demonstrating the very low gas temperature of the plasma jet and its suitability for biomedical applications and surface treatment of bio-polymers. The plasma jet was tested on heat sensitive polymer films used in biomedical applications such as polyethylene terephthalate (PET) and poly-L-lactide (PLLA) continuously for several minutes without causing any physical or thermal damage on the film surfaces.

Optical emission spectroscopy diagnosis was successfully employed for characterizing the atmospheric pressure non-thermal helium plasma jet and the effects of addition of small fractions of oxygen at 0.1 - 0.5% on the characteristics of the plasma jet were investigated. The addition of oxygen resulted in a decrease in plasma plume length due to the electronegativity property of oxygen. The voltage-current characteristics of the plasma discharge were analyzed and the average plasma power was measured to be around 18 W. The reactive species produced by the plasma jet which are critical to a range of biomedical applications. Using optical emission spectroscopy diagnostics the identification of radicals and excited species produced in the active zone and

afterglow region of the plasma jet have been carried out. It was observed that, the most intensive spectral lines belong to the OH emission lines transition $A^2\Sigma^+(\nu = 0,1) \rightarrow X^2\Pi(\Delta\nu = 0)$ at 308 nm and $A^2\Sigma^+(\nu = 0,1) \rightarrow X^2\Pi(\Delta\nu = 1)$ at 287 nm, the spectral lines of the helium atoms including He I transition $3p^3P^0 \rightarrow 2s^3S$ at 388.8 nm, He I transition $3p^1P^0 \rightarrow 2s^1S$ at 501.6 nm, He I transition $3d^3D \rightarrow 2p^3P^0$ at 587.6 nm, He I transition $3d^1D \rightarrow 2p^1P^0$ at 667.8 nm, He I transition $3s^3S^1 \rightarrow 2p^3P^0$ at 706.5 nm, He I transition $3s^1S^0 \rightarrow 2p^1P^0$ at 728.1 nm, and $H_\alpha$ transition 2p-3d at 656.3 nm, O I transition $3p^5P \rightarrow 3s^5S^0$ at 777.41 nm and O I transition $3p^3P \rightarrow 3s^3S^0$ at 844.6 nm. Additionally, in the afterglow region of the plasma jets strong emission of the molecular nitrogen $N_2$(C-B) second positive system (SPS) with electronic transition $C^3\Pi_u \rightarrow B^3\Pi_g$ in the range of 300-450 nm and $N_2^+$(B-X), first negative system (FNS) spectral band with electronic transition $B^2\Sigma_u^+ \rightarrow X^2\Sigma_g^+(\Delta\nu = 0)$ at 391.4 nm were observed. Also, the spectra produced in the active zone and afterglow region in the atmospheric air, showed a significant variation in the emission spectra and spectral line intensities. The active zone emission spectra were dominated by OH and helium line intensities whereas the afterglow region emission spectra were dominated by a range of $N_2$ lines intensities. A high resolution OES was applied to determine the rotational and vibrational temperature of OH radicals transition $A^2\Sigma^+(\nu = 0) \rightarrow X^2\Pi(\Delta\nu = 0)$ in the range of 306-312 nm. The OH rotational temperature equivalent to plasma gas temperature was measured to be 310 ± 25 K and 340 ± 25 K in the active region and it increased to 320 ± 25 K and 360 ± 25 K in the afterglow region in the atmospheric air for pure helium and helium/oxygen (0.1%) mixture, respectively. The vibrational temperatures of the OH radicals estimated to be 2200 ± 100 K and 2500 ± 100 K, for pure helium and helium/oxygen (0.1%) mixture, respectively. The difference between the vibrational and rotational temperature represents the non-equilibrium level of the discharge. The results indicate that the OH rotational temperatures of the afterglow region of the plasma jet are slightly higher

than the active zone region, yet the temperatures are very low and suitable for treating heat sensitive materials such as bio-polymers. The plasma jet was tested on heat sensitive polymer films that are used in biomedical applications such as polyethylene terephthalate (PET) and poly-L-lactide (PLLA) films continuously for several minutes without causing any physical or thermal damage on the film surfaces. In conclusion, the OES technique was used to characterize an atmospheric pressure plasma jet in helium and helium/oxygen discharge. The plasma jet generates the significant reactive species at low gas temperatures which promises its great potential for a wide range of biomedical applications.

## III. Characterization of a non-thermal helium and helium/oxygen gas mixture plasma jet.

In this project period, we have also applied optical emission spectroscopy diagnostics to investigate the characteristics of a non-thermal atmospheric pressure helium and helium/oxygen gas mixture plasma jet. In this work, an atmospheric pressure low temperature plasma pencil generated in helium and helium/oxygen gas mixtures was characterized in detail for its discharge characteristics, plasma power, reactive plasma species produced, plasma density and plasma temperatures using electrical and optical emission spectroscopy (OES) diagnostics. A visible plasma plume length of approximately 33 mm was generated using a 60 kHz AC HV power supply. The OES results showed the most intensive plasma emission lines of OH transition $A^2\Sigma^+(\nu = 0,1) \rightarrow X^2\Pi(\Delta\nu = 0)$ at 308 nm and OH transition $A^2\Sigma^+(\nu = 0,1) \rightarrow X^2\Pi(\Delta\nu = 1)$ at 287 nm, O I transition $3p^5P \rightarrow 3s^5S^0$ at 777.41 nm, O I transition $3p^3P \rightarrow 3s^3S^0$ at 844.6 nm and $N_2$(C-B) second positive system (SPS) with electronic transition $C^3\Pi_u \rightarrow B^3\Pi_g$ in the range of 300-450 nm. The effects of controlled oxygen content on the plasma pencil and on various helium plasma emissions and electrical properties are studied. A spatial distribution of reactive plasma species produced by the

plasma pencil is presented. The electron density of plasma jet was estimated to be in the order of $2.1 \times 10^{14}$ $cm^{-3}$ using Stark broadening line profile of the hydrogen alpha emission. The temperatures of afterglow plasma pencil were evaluated using OH rotational temperatures and the results demonstrate temperatures of 316 K and 362 K for pure He and $He/O_2$ gas mixtures (0.1% $O_2$), respectively. Preliminary results on inactivation of *S. pneumoniae* on a solid surface and in liquid suspension were carried out using the plasma pencil for biomedical applications.

Atmospheric pressure non-thermal plasma sources operating over a range of power levels has been used for industrial and materials processing applications,[1-4] and increasingly applied in biomedical applications.[2, 3, 5, 6] Several atmospheric pressure plasma sources have been developed recently, including the plasma pencil that produces stable plasma at room temperatures applied for bacterial inactivation,[7] non-destructive sub-mm radio frequency plasma needle applied for surface treatment of biomaterials,[8] one atmosphere uniform glow discharge plasma,[9] dielectric barrier discharge based atmospheric pressure plasma jet,[10] resistive barrier plasma discharge,[11-13] and microwave powered atmospheric pressure plasma jets.[14] In general, the majority of the plasma sources operate with a flow of noble gasses like helium, argon and/or their mixtures with other gases such as air, nitrogen, oxygen and water vapor.[14] Depending on the specific application requirements, a plasma source has to be developed and the characteristics of the plasma need to be diagnosed. In this work, we have constructed an atmospheric pressure plasma pencil in our laboratory based on kHz driven dielectric barrier discharge suitable for biomedical applications. A similar plasma source was investigated previously by the author,[15] however it was carried out in argon and argon/water vapor mixture as a source for polymer surface treatment application. The main goal of this current work was to produce a low-temperature atmospheric pressure plasma generating higher concentration

of selective reactive plasma species required for biomedical applications, e.g. OH radicals, singlet oxygen, RNS and ROS.

In this work, we describe the characteristics of an atmospheric pressure plasma pencil in helium and helium/oxygen mixture propagating in to open air. The plasma pencil is capable of working in different gas mixtures, e.g. argon, helium and their mixture with oxygen and water vapors. The different modes of operation and its low gas temperatures along with its efficient production of active species will potentially allow for a wide range of applications. The electrical characterization was performed based on voltage-current characterization of the plasma pencil operated in helium and $He/O_2$ gas mixtures. The plasma power was estimated from voltage-current waveforms and the input power was kept constant while varying the applied voltage. Subsequently, optical emission spectroscopy was utilized for investigation of reactive species in plasma and determination of OH radical rotational temperature.

The size and preciseness of the plasma pencil would allow it for a range of biomedical applications that involves localized treatments. One such area of interest is pediatric otorhinolaryngology, specifically the treatment of middle ear and paranasal infections in infants and children. *Streptococcus pneumoniae* (the pneumococcus) is one the primary bacteria that causes such infections in the different locations of the respiratory tract of humans, including acute otitis media (middle ear infection), sinusitis (paranasal infection), bronchitis and pneumonia (lung infections).[16] Of the infections caused by the pneumococcus, otitis media (OM) is one of the highest prevalent pediatric diseases worldwide.[17] OM is the most frequently diagnosed illnesses in children under 15 years of age and is the primary reason for frequent physician visits.[18] Traditional treatment of pneumococcal infections in the middle ear and sinuses has consisted of a series of antibiotics; in fact, OM infections are considered the major reason for antibiotic use in children in

developed countries.[19] Due to the rise in acquired bacterial resistance to antibiotics, there is a pressing need for alternative treatments to both reduce the antibiotic use in children and to combat bacterial infections from already resistant bacteria. To identify the usefulness of the plasma pencil for biomedical applications, we assessed plasma pencil treatment on pneumococcal cultures grown on solid blood agar plates and within liquid media.

**A. Plasma pencil and diagnostics**

In this investigation an atmospheric pressure plasma pencil has been developed. The plasma was generated in a quartz capillary with inside and outside diameters of 1.3 and 3.0 mm, respectively. We demonstrated a schematic of our atmospheric pressure plasma pencil system and diagnostics.

The plasma pencil consists of two electrodes, separated by air gap and a dielectric quartz capillary tube. The high voltage electrode is a 0.5 mm diameter tungsten rod placed inside the quartz capillary connected to a 25 kV, 60 kHz in-house constructed high voltage power supply. The ground electrode is a copper ring of 10 mm long placed around the capillary tube and axially positioned at 40 mm away from the high voltage electrode tip. The gas flow was monitored by a two channel power supply/readout (model: MKSPR400) and controlled by two mass flow meters (Model: MKS 1179A).

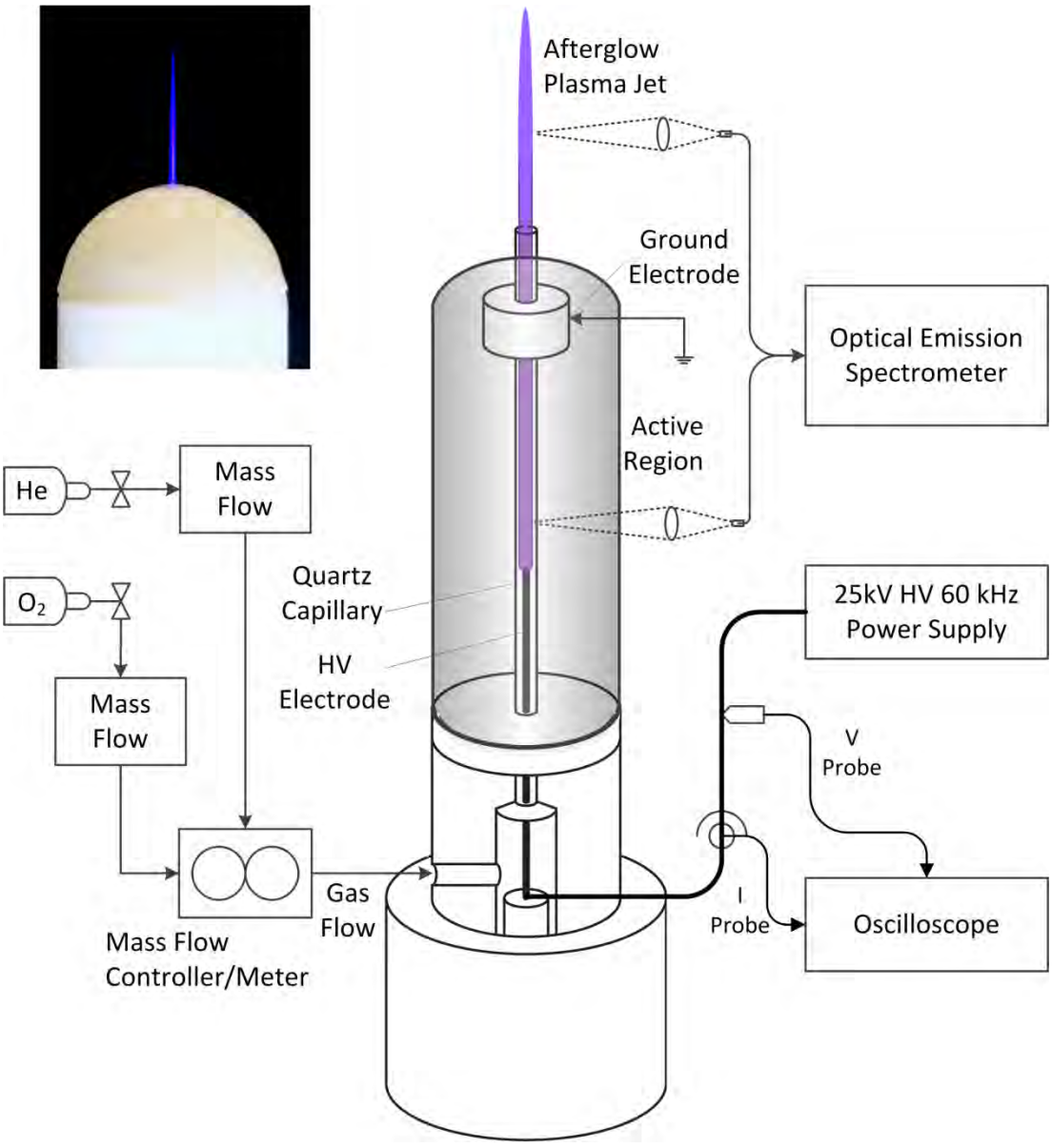


Schematic of our atmospheric pressure plasma pencil system and diagnostics.

Plasma is generated inside the quartz capillary and in between the electrodes excited by a 60 kHz sinusoidal wave voltage. The applied voltage was varied from 4 kV to 8 kV peak to peak. The applied voltage waveforms were monitored using a high voltage probe (Tektronix P6015A) and the current waveforms were monitored by a current probe (Tektronix TCP202). The current and voltage signals were recorded using a digital oscilloscope (Tektronix TDS 3034C). High purity He

with main impurity of $H_2O$ present in the helium cylinder at a range of 0.5 ppm were used for generating plasma at flow rates ranging from 1 slm to 7 slm (slm: standard liters per minute). In our experiments, admixtures of oxygen at varied percentages from 0.1 to 1% of the primary He operating gas were employed by changing of the gas flow rates. Two types of optical diagnostics were used for characterization of the plasma pencil. The time and space resolved spectroscopy measurements of the plasma emission was carried out using a broadband spectrometer (Ocean Optics HR2000+ES) in the range of 200-900 nm with 0.83 nm resolution. The emission of OH radicals in the range of 300-350 nm (transition $A^2\Sigma^+(v=0) \rightarrow X^2\Pi(v=0)$) was recorded with 500 $\mu$s integration time using a 0.08 nm resolution spectrometer system made up of a monochromator (Princeton Instruments Acton SP2750) and a CCD (ACTON IStar). The plasma emissions were collected in a direction perpendicular to the plasma pencil axis and at 1 mm increments in axial direction using a collimating lens. The plasma emission was transmitted to the spectrometer via optical fiber. The spectrometer was equipped with double grating turrets, one with 1200 grooves $mm^{-1}$ grating and the other 600 grooves $mm^{-1}$ grating.

**B. Bacterial sample preparation and plasma treatment procedure**

*S. pneumoniae* strain TIGR4 was grown in Todd-Hewitt broth with 0.3% yeast extract and cells were collected during logarithmic growth $OD_{620nm} = 0.5$ for solid surface cultures and $OD_{620nm} = 0.4$ for liquid media cultures. The bacterial concentration for $OD_{620} = 0.5$ was $10^7 – 10^8$ CFU $ml^{-1}$ (CFU = colony forming units) and for $OD_{620} = 0.4$ was $10^6$-$10^7$ CFU $ml^{-1}$. For treatments of solid surfaces, 100µl ($4 \times 10^6$ CFU) of bacterial samples were inoculated onto the center of a 50 mm diameter Petri dish (plate). A disposable 35 mm wide Drigalski spatula was placed with one end at the inner edge of the Petri dish and the other end over the inoculated sample. The plate was

rotated at least 10 times to allow for spread of bacterial sample over the entire agar surface, allowing a pneumococcal density of approximately $2.04 \times 10^3$ CFU $mm^{-2}$ on the blood agar plate. For treatment of bacteria on the agar surface, the plasma pencil was fixed at distance of 10 mm between the plasma-pencil nozzle and agar surface. The cultures were exposed to 60s and 120s of either He or He/0.5% $O_2$. After treatment with plasma, the cultures were grown overnight at 37°C in 5% $CO_2$. The treated area was assessed in comparison to the untreated surrounding agar surface for zones of inactivation. The areas of the zones of inactivation were measured to quantify the amount of pneumococcal inactivation.

For treatment of the pneumococcus in liquid cultures, the bacteria suspension was prepared as described above to $OD_{620} = 0.4$. From the prepared bacterial suspension, 200 µl was transferred to a 96 well micro-well plate. The plasma pencil was fixed at distance of 3 mm between the plasma-pencil nozzle and the liquid media surface. The pneumococcal suspensions were exposed to 60s, 120s, and 300s of either He or He/0.5% $O_2$. After treatment, serial dilutions were performed and 10 µl of sample was placed onto a blood agar plate to grow overnight at 37 °C in 5% $CO_2$. After overnight growth, the efficacy of the inactivation was determined by taking CFU counts of the untreated and treated samples.

**C. Electrical characterization**

The electrical characterization experiments were performed on the atmospheric pressure plasma pencil with helium and oxygen admixtures. Initially, the helium gas was injected into the quartz capillary at a flow rate of 1 slm and the breakdown discharge occurred between the two electrodes and inside the quartz capillary occurred at a minimum input voltage of 3.5 $kV_{p-p}$. However, the discharge was unstable inside the quartz capillary at this minimum input voltage of 3.5 $kV_{p-p}$ and therefore plasma did not exit from the capillary in to surrounding air resulting an absence of a

prominent afterglow region. By increasing the input voltage to 4 $kV_{p-p}$, the plasma pencil successfully produced an afterglow plasma in to the open air and a long plasma plume length was formed. In order to diagnose the electrical properties of the plasma pencil, the voltage and current waveforms were measured during the discharges at 4, 4.5, 5, 5.5 and 6 $kV_{p-p}$ and the effects of gas flow rates and oxygen admixture percentages in the plasma discharge were investigated. We demonstrated the voltage and current waveforms for the plasma pencil for pure helium and helium-oxygen mixture (0.5% $O_2$ in the discharge) at a total gas flow rate of 4 slm.

The plasma pencil generates a very uniform discharge in pure helium gas and only two small current peaks exist on the current waveform during each half period of the applied voltage. Both peaks are smooth, the maximum current is 10.2 mA, and the duration of the current peaks are approximately 1 $\mu$s. A clear change in the voltage-current waveform was observed when oxygen was added to the plasma pencil. Addition of the oxygen to the plasma pencil results in a small increase of the current peak intensity to 10.8 mA and decrease of the current peaks duration to 0.8 $\mu$s. The results indicate that the voltage slightly decreases with increase of the current peaks.

Using the voltage-current waveforms, the average power (W) of the discharge was calculated according to the following equation, where T is the period of the discharge:[20, 21]

$$W = \frac{1}{T}\int_{T}^{T+t} I(t)V(t)\,dt. \qquad (1)$$

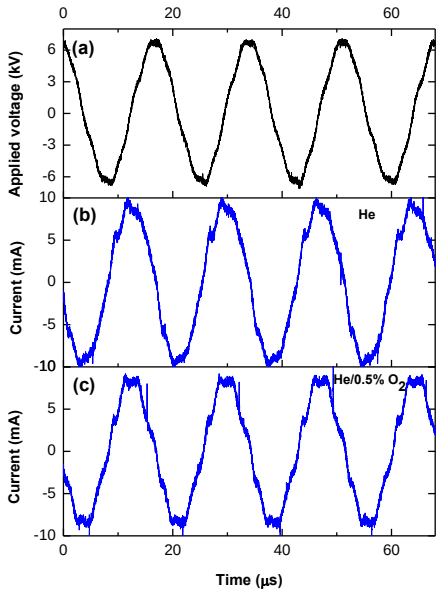


FIG 2. Voltage and current waveforms as a function of time for (a) Applied voltage waveform (b) Current waveform for pure He and (c) Current waveform for $He/O_2$ mixture (0.5%), applied voltage is 6 $kV_{p-p}$ and the total gas flow rate is 4 slm.

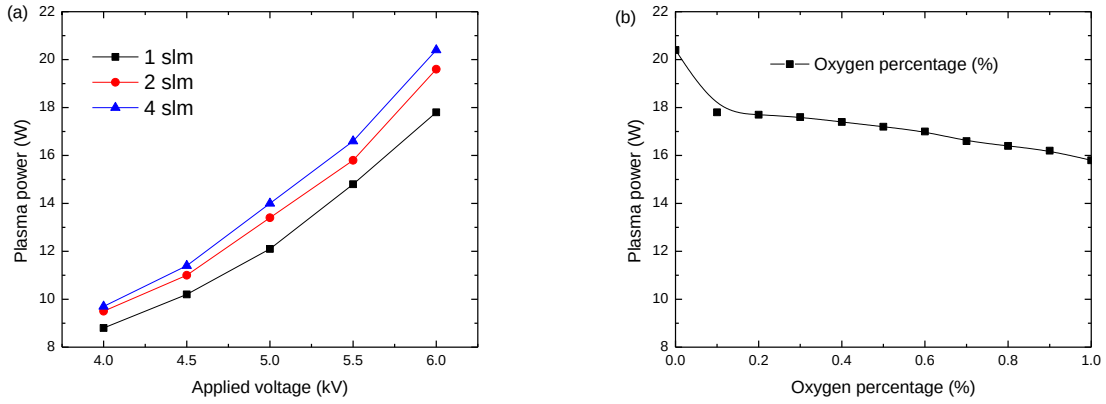


FIG 3. Plasma powers as a function of applied voltage and oxygen percentage. (a) Effect of gas flow rate and applied voltage on plasma power (b) effect of oxygen percentage in the discharge on plasma power, at a total gas flow rate of 4 slm.

power dissipated in the discharge is presented as a function of the applied voltage for different operating gas flow rates used. The minimum power of the plasma pencil is observed to be about 8.8 W for pure Helium plasma at an applied voltage (peak-to-peak) of 4 kV and a gas flow rate of 1 slm. The applied voltage was increased up to 6 kV, which is the breakdown point of the quartz capillary, resulting in an increase of power up to 20.4 W for discharge in pure helium at a gas flow rate of 4 slm. The plasma power as a function of oxygen percentage in the plasma pencil is presented Basically, the power dissipation in pure helium discharge is higher, which is explained by broader current peaks. It is necessary to mention that the addition of oxygen to gas flow results in a decrease of the input power from 20.4 W (in case of pure helium) to 17.8 W and 15.8 W for discharges containing 0.1% and 1% of oxygen, respectively. The decrease in plasma power with addition of oxygen is due to contraction of the current peaks at higher amounts of oxygen in gas mixture that results in decrease of the integral determining power dissipation in the discharge.

**D. Visualization of the plasma pencil in helium and helium/oxygen admixtures**

The plasma pencil can be successfully launched in pure helium discharge with application of voltage at values higher than 3 kV (peak to peak). Addition of oxygen admixture to the feed gases required higher threshold voltages of up to 5 kV, especially at a higher concentration of oxygen (1% oxygen). The plasma pencil generated from a complete breakdown of entire inter-electrode gap (active zone) with formation of a long bright afterglow propagating in to open air and its plume length depends on the composition of the feed gas, applied voltage and flow rates of the operating gas. We demonstrated displays color photographs of the plasma pencil (without Teflon cover) generated at 6 kV and in pure helium for different flow rates in the range of 1-7 slm and FIG 4.b displays the images of the plasma pencil in $He/O_2$ gas mixture from 0.1-1% of Oxygen in discharge.

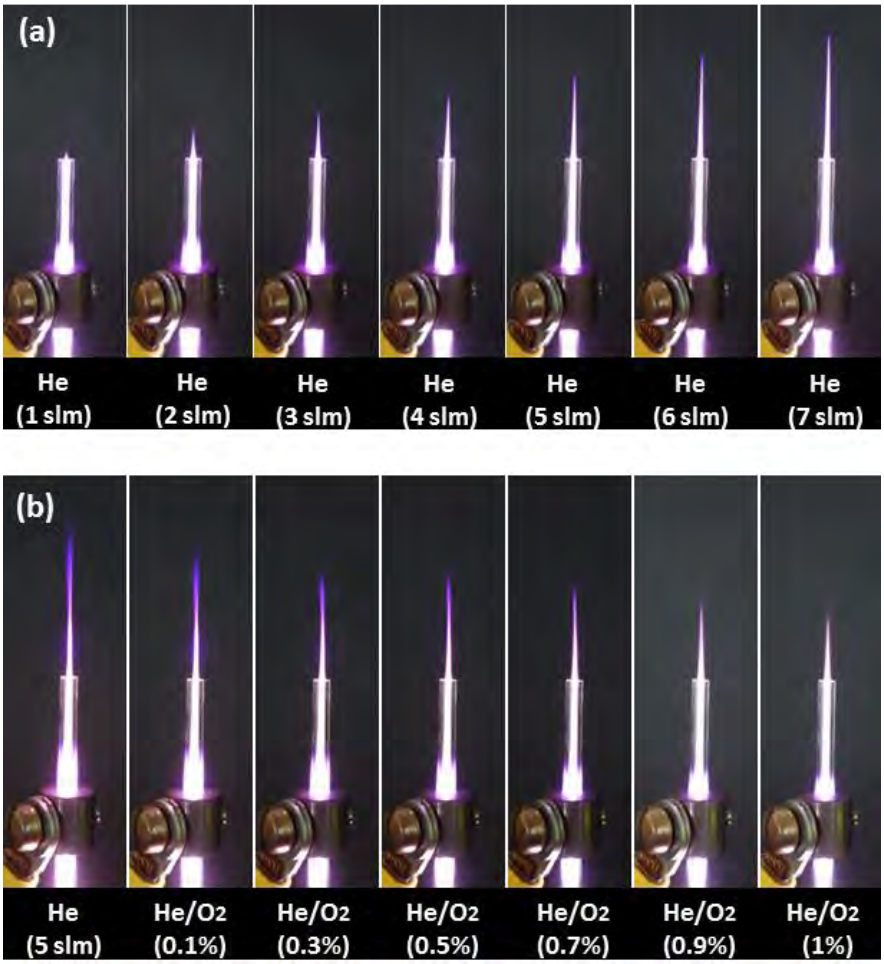


FIG 4. (color) Photographs of the plasma pencil. (a) Images of plasma pencil in pure He as a function of gas flow rate. (b) Images of plasma pencil in $He/O_2$ mixtures for different oxygen percentage in discharge. Plasma power is fixed at 18 Watt.

In addition, we observed that the plasma pencil's plume length greatly depends on the gas flow rate and it shows very small noticeable dependence with changes in applied voltage. Next, the plasma plume length was measured using the plasma pencil images. We demonstrated the plasma plume lengths as a function of helium gas flow rates and oxygen percentages in the discharge, respectively. As can be seen for discharges in pure helium the plume length at lowest flow rate of

0.5 slm is about 10 mm and sharply increases to the maximum value of 33 mm at a flow rate of 5 slm. The plasma pencil's plume length at gas flow rate of 7 slm is about 26 mm. the addition of the oxygen to the plasma pencil results in a sharp decrease of the pencil's plume length. Plasma pencil's plume length in pure helium discharge at 4 slm is 29.8 mm, while the plume length decreases with addition of oxygen to 20.12 mm and 5.1 mm, at discharges contain 0.1% and 1% of oxygen, respectively. The reason for decrease of the plume length is that oxygen is an electronegative molecular gas. The addition of oxygen to the plasma pencil results in electron attachment reactions with oxygen molecules; thus, the electron density in the discharge, and consequently the helium metastable concentrations in the discharge decreases resulting in a decrease of the plasma pencil's plume length.

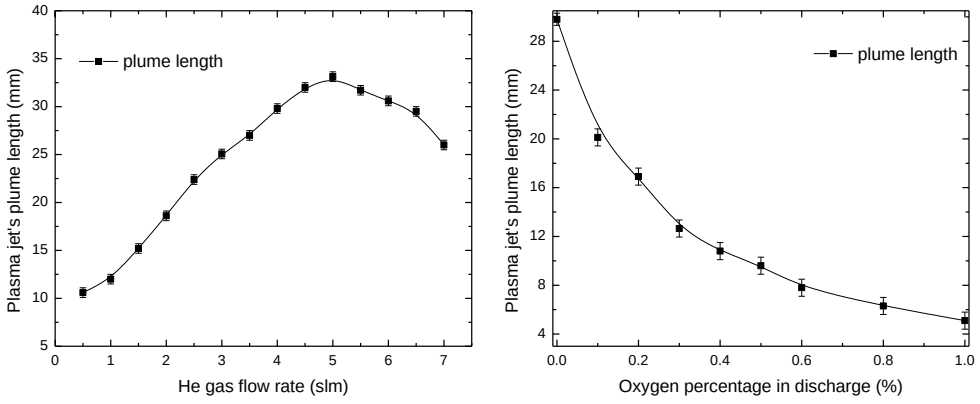


(a) (b)

FIG 5. Plasma pencil's plume length as a function of (a) He gas flow rate ranges from 0.5-7 slm and (b) Oxygen percentage in discharge from 0.1-1% with a fixed total gas flow rate of 4 slm.

**E. Optical emission spectroscopy and plasma pencil species identification**

Optical emission spectroscopy is considered to be a suitable tool in characterizing the plasma properties in terms of the identification of the reactive plasma species, plasma gas temperature evaluation and the relative emission intensities of the various species in different conditions.[22-26] In the non-thermal plasma pencil at atmospheric pressure, the mean electron energy is significantly higher than the energy of neutral plasma species.[27] The reaction between high energy electrons with helium, water vapor, nitrogen and oxygen at atmospheric pressure will induce the molecules to be dissociated, excited and ionized for production of different radicals and active species. In this section, the optical emission spectroscopy was used to study the plasma pencil in He and He/$O_2$ gas mixture and the reactive plasma species were identified. The axial and space resolved emission spectra in the range of 200-900 nm were recorded and analyzed. Axial emission spectrum of the plasma pencil allowed determination of the main reactive plasma species produced in the plasma pencil. the results of spectroscopic measurements with 0.83 nm resolution of the plasma discharge in He and He/$O_2$ mixtures (0.5%) are presented. The emission spectra were recorded in the middle of the active zone region (the distance between the HV and ground electrode) of the plasma pencil. The emission spectra were recorded at 5 mm from the edge of the capillary (afterglow region).

The emission spectra are mainly composed of the spectral line of the He atoms. The most intensive emission lines correspond to He I transition $3p^3P^0 \rightarrow 2s^3S$ at 388.8 nm, He I transition $3p^1P^0 \rightarrow 2s^1S$ at 501.6 nm, He I transition $3d^3D \rightarrow 2p^3P^0$ at 587.6 nm, He I transition $3d^1D \rightarrow 2p^1P^0$ at 667.8 nm, He I transition $3s^3S^1 \rightarrow 2p^3P^0$ at 706.5 nm, and He I transition $3s^1S^0 \rightarrow 2p^1P^0$ at 728.1 nm.

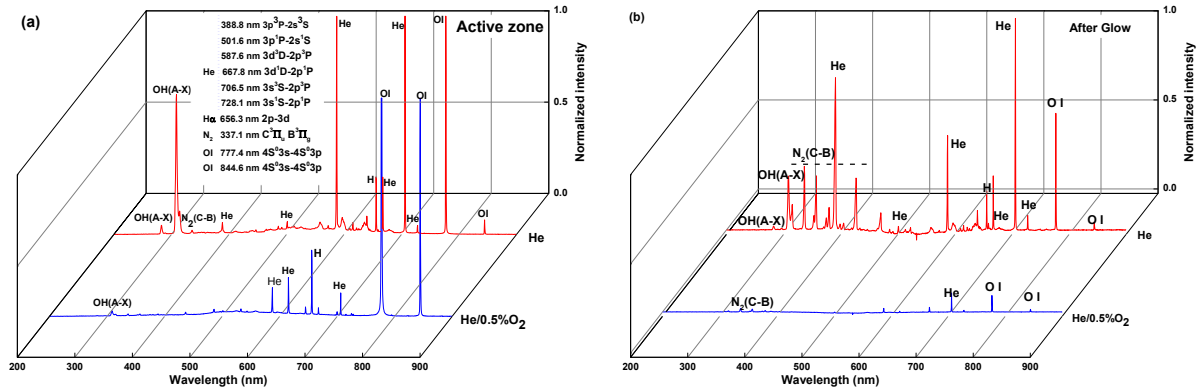


FIG 6. Axial spectrums of the plasma pencil in He and He/$O_2$ mixtures (0.5%), (a) emission spectra of the active zone region and (b) emission spectra of the afterglow region of the discharge measured at 5 mm from the edge of capillary. The total gas flow rate is 4 slm and plasma power is fixed at 18 W.

In addition to He lines, the other identified reactive plasma species include intensive emission lines belonging to OH transition $A^2\Sigma^+ \rightarrow X^2\Pi,\ \Delta v = 0$, at 308 nm, and OH transition $A^2\Sigma^+ \rightarrow X^2\Pi,\ \Delta v = 1$, at 287 nm, the spectral band of the $N_2$ transition $C^3\prod_u - B^3\prod_g,\ \Delta v = 0$, at 337.1 nm, $H_\alpha$ transition 2p-3d at 656.3 nm, O I transition $3p^5P \rightarrow 3s^5S^0$ at 777.41 nm and O I transition $3p^3P \rightarrow 3s^3S^0$ at 844.6 nm. The OH radicals in the active zone region of the plasma are formed from water vapor impurities present in the helium gas cylinder.[28] The corresponding emission lines are identified based on the NIST atomic spectra database[29] and Lofthus et. al.[30]

In order to investigate the effect of $O_2$ on the emission intensities of the reactive plasma species, different concentrations of the $O_2$ were added to the plasma pencil. Next, the emission spectra of the plasma with different $O_2$% in the discharge were collected and the emission lines of OH at 308 nm (transition $A^2\Sigma^+ \rightarrow X^2\Pi,\ \Delta v = 0$), $N_2$ at 337 nm (transition $C^3\prod_u - B^3\prod_g$), $H_\alpha$ at 656 nm

(transition $2p - 3d$), He at 706 nm (transition $1s3s\ ^3S - 1s2p\ ^3P^0$) and O I at 777 nm (transition $2s^2 2p^3(^4S^0)3s - 2s^2 2p^3(^4S^0)3p$) were chosen for space resolved analysis of the emission spectroscopy. The results of spatial distribution of the active species intensities show that the emission spectrum of $He/O_2$ (0.5 %) mixture is very similar to pure helium discharge when comparing identified species. Moreover, it is clearly recognizable that the addition of oxygen to the plasma pencil results in a decrease of the emission lines intensities. The possible reasons for decrease of the emission line intensities are decreases of the plasma power with addition of the oxygen in the discharge and quenching of OH radicals by water vapor present within the helium gas cylinder or in open air.[15, 31] Similar observation has been reported previously by others on plasma containing oxygen or other electronegative molecular gases.[15, 21, 32]

the discharge in pure helium shows a higher intensity of OH radicals compared to the plasma pencil that contains $O_2$ gas mixture for both cases (the active zone and afterglow region) of the plasma pencil. In the active zone of the plasma, the most intensive emission line belongs to O I at 777 nm, while in the afterglow region of the plasma pencil, $N_2$ emission line at 337 nm is the most intensive emission line in the emission spectra. Furthermore, addition of higher amount of oxygen to the plasma results in a decrease of these emission lines in the discharge.

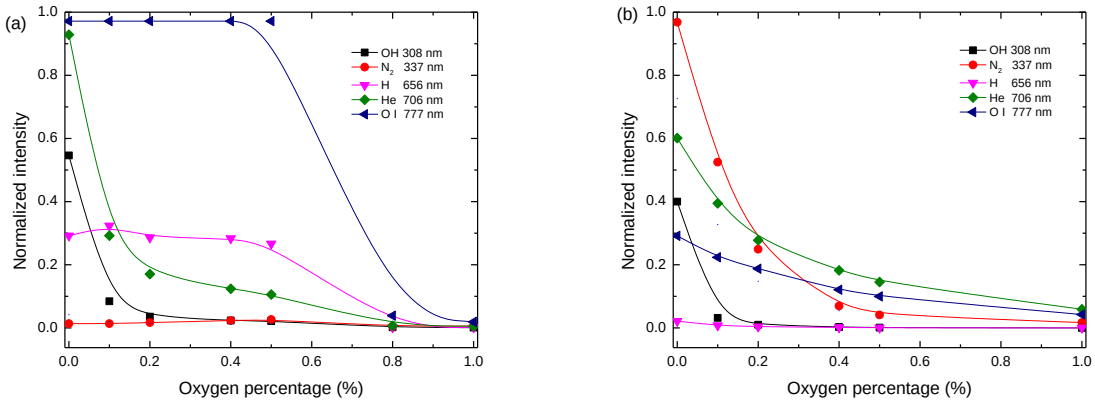


Normalized intensity of the selected reactive species as a function of the oxygen concentration in the discharge with a total gas flow rate of 4 slm. (a) in the active zone region of the plasma pencil and (b) in the afterglow region of the plasma pencil at 3 mm after the edge of capillary.

Oxygen is an electronegative gas, hence, when oxygen is added to the plasma pencil, the added oxygen captures significant free electrons and produces $O^-$ and $O^{2-}$ ions. Thus, the electron attachment by oxygen results in a decrease of the electron density and electron mean energy.[33-35] The OH radicals are mainly produced by electron-water vapor collision process according to the following reaction, and therefore the decrease of the electron density leads to decrease of the intensities of OH and other atomic emission lines at a constant power.[28, 33, 34]

$$e + H_2O \rightarrow e + H + OH \quad (2)$$

The reason for increase of O I intensity in the active zone region of the plasma pencil is that when oxygen is added to the pure helium plasma pencil, the added oxygen can be dissociated according to the following reactions and results in a formation of singlet oxygen (O) and O ($^1$D).

$$e + O_2 \rightarrow O^- + O \quad (3)$$

$$e + O_2 \rightarrow e + O + O(^1D) \quad (4)$$

$$e + O_2 \rightarrow 2e + O^+ + O \quad (5)$$

In addition, in the afterglow region of the discharge when plasma pencil propagates in the open air, the OH radicals can be produced by the interaction of O ($^1$D) and $H_2O$ according to the following reaction:[35]

$$O\ (^1D) + H_2O \rightarrow 2\ OH \quad (6)$$

On the other hand, the singlet oxygen and ozone molecules generated in the discharge react with the produced OH radicals according to the following reactions and thus, the OH radicals intensity in the plasma pencil decreases with addition of oxygen percentage to the pure helium plasma pencil.[35]

$$OH + O \rightarrow H + O_2 \quad (7)$$

$$OH + O_3 \rightarrow HO_2 + O_2 \quad (8)$$

**F. Space resolved optical emission spectroscopy of the plasma pencil**

The spatial distribution characteristics of chemically active species are very important in developing the plasma pencil kinetic model and understanding the mechanism of biomedical applications of the plasma pencil. Here, we present the spatially resolved spectra of the afterglow region of the plasma pencil.

The spatially resolved optical emission spectra of the afterglow region were collected for pure helium and helium/oxygen mixture (0.5%), with resolution of 2.5 mm. Next, the intensities of the intensive reactive plasma species were chosen for deeper analysis of the space resolved emission spectroscopy.

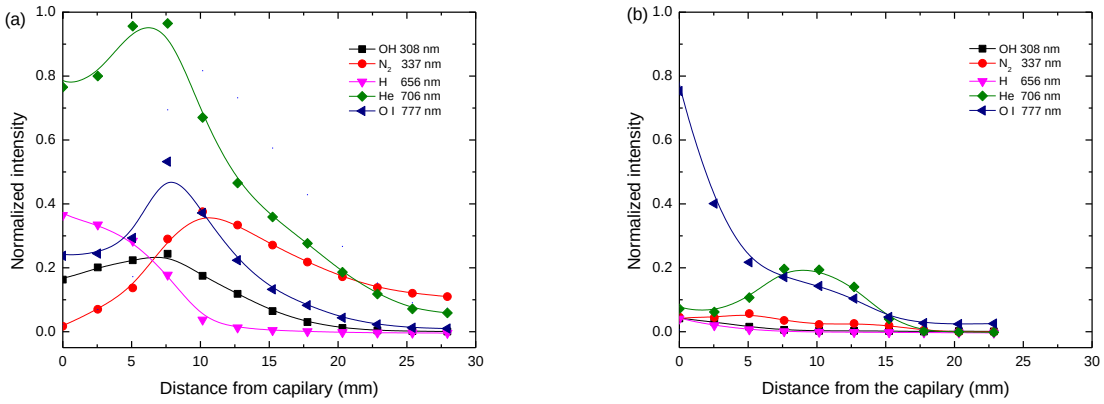


The spatial distribution of the reactive species emission intensities as a function of the distance from the edge of capillary. (a) Pure He (b) He/$O_2$ (0.5%)

the emission intensity of the OH radicals ( $A^2\Sigma^+ \rightarrow X^2\Pi, \quad \Delta v = 0$ ) and $N_2$ ( $C^3\prod_u - B^3\prod_g$ ), $H_\alpha$ and O I and helium vary with distance from the edge of quartz capillary. the emission intensity of helium, O I and $N_2$ ( $C^3\prod_u - B^3\prod_g$ ) rises initially up to 7 mm from the edge of capillary and then decreases, while the emission intensity of the OH ( $A^2\Sigma^+ \rightarrow X^2\Pi, \quad \Delta v = 0$ ) and $H_\alpha$ decreases with increase of distance from the capillary. The emission intensity of $N_2$ at 10 mm is almost 8-10 times larger than the intensity at the edge of the capillary. Moreover, the emission intensity of $N_2$ reaches a maximum value after OH radicals. The maximum intensity of $N_2$ is located at 10 mm while the OH radicals' maximum intensity is located at 7 mm. This behavior can be explained by the fact that $H_2O$ dissociation is initiated by electron induced processes inside the discharge and in the short distance after the edge of capillary, where the electron exhibit required the energy.[15] In the case of the plasma pencil in helium/oxygen mixture (0.5%), the intensity decay of the helium in the plasma plume has an exponential decay, initially increasing up to 10 mm from the edge of capillary and after that again decreasing (FIG 8.b). The most intensive emission line belong to O

I, which is located inside the quartz capillary. The $N_2$ emission intensity reaches to its maximum outside the capillary and at 5 mm distance from the edge of capillary. The identified excited nitrogen molecules are produced from electron impact reactions in the plasma plume as it propagates into the ambient air.[28] The main reason for the decrease of the emission intensities of the reactive plasma species with the distance from the edge of capillary is the decrease of the high energy electron density and mean energy.[32] Outside the capillary the increase of the $N_2$ (SPS) emission could be a result of energy transfer from metastables and decreasing of the OH emission by increasing $N_2$ in the plasma pencil and lower $H_2O$ density in the surrounding air compared to nitrogen.

The identified reactive plasma species such as the singlet oxygen, hydroxyl radicals, and neutral nitrogen molecules detected in the plasma pencil can play a significant role in biomedical applications especially operating at the atmospheric pressure.[36, 37] Similar significant generation of reactive oxygen species such as singlet oxygen (O) and $O_3$ were observed with $He/O_2$ gas mixture used in a plasma pencil which can result in enhanced efficacy of bacterial inactivation.[26, 38] It is believed that the oxygen species in the discharge contributes to the sterilization process due to its strong oxidative effect on the outer structure of the cells,[36, 37] while the OH radicals generated by the plasma plays a significant role through chemically attacking the outer structure of the cells and the production of the nitrogen containing group adds to the lethality of the process.[39]

## G. OH rotational temperature determination using Boltzmann plot method

The plasma gas temperature has been derived from OH rotational temperatures. The OH rotational temperature is usually considered to be equal to the plasma gas temperature considering the low rotational level of the OH radicals OH (A-X) and small rotational quantum numbers $J$.[15, 40-42] The Boltzmann plot of the rotational population of the OH radicals has been widely used for this purpose.[15, 40, 43, 44] We demonstrated the high resolution emission spectra of the OH radicals in pure helium and helium oxygen (0.5%), respectively. Using the OH emission spectra and assuming that the OH rotational states are Boltzmann distributed according to the following equation

$$I_{J'J''} \approx h\nu_{J'J''}(2J+1)A_{J'J''}\exp\left(-\frac{B_\nu hcJ(J+1)}{k_B T_{rot}}\right), \qquad (9)$$

where $\nu_{J'J''}$ is the frequency of transition from rotational level $J'$ to $J''$, $A_{J'J''}$ is the corresponding transition probability, $B_\nu$ is the rotational constant, $k_B$ is the Boltzmann constant and $h$ is the Planck constant. The rotational energy $E(cm^{-1})$ equals to $B_\nu J(J+1)$. The energy and probability data of OH transitions were taken from literature.[45, 46] The corresponding OH rotational temperature is equal with gas temperature when the rotational population distribution is in equilibrium with heavy species translational temperature in the discharge. In atmospheric pressure plasma, this assumption is valid on atmospheric pressure plasmas when high collisional reactions occur. A detailed description of the used method can be found in Sarani. et, al. 2010.[15]

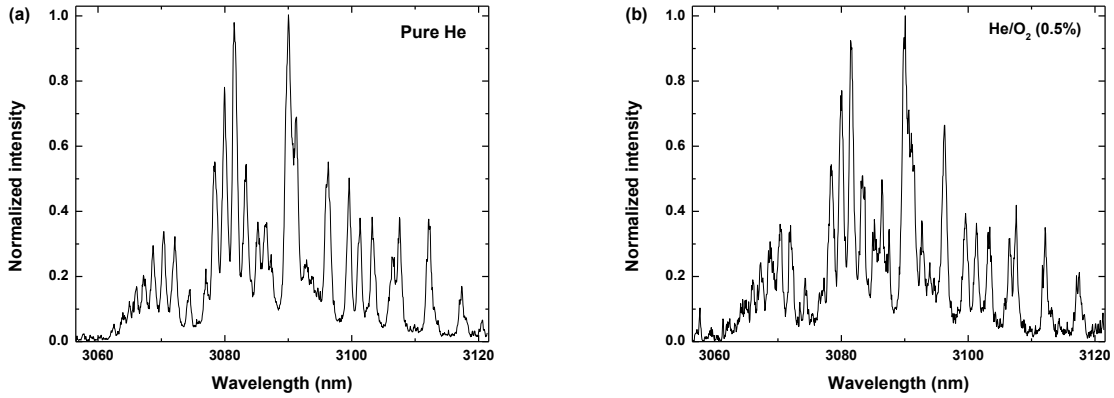


High resolution OH emission spectra. (a) Pure He. (b) $He/O_2$ (0.5%). Plasma power is 18 W and total gas flow rate is 4 slm.

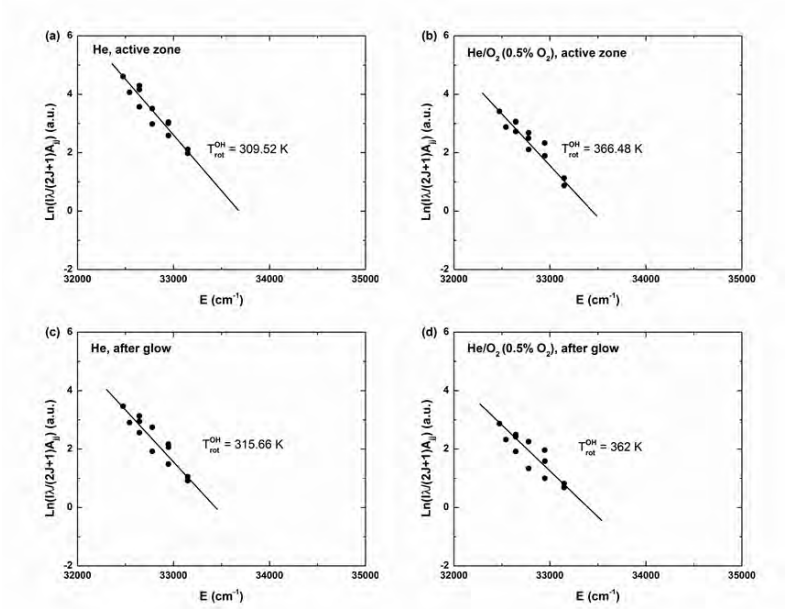


Boltzmann plot of the OH $(A^2\Sigma - X^2\Pi)$ transition in plasma of (a) Discharge in pure He and in active zone region (between HV and ground electrodes). (b) Discharge in $He/O_2$ mixture (0.5%) and in active zone region (between HV and ground electrodes). (c) Discharge in pure He and in the afterglow region. (d) Discharge in $He/O_2$ mixture (0.5%) and in the afterglow region. Plasma power was fixed at 18 W.

we presented $\ln(I\lambda/(2J+1)A_{JJ})$ for transition $OH(A^2\Sigma - X^2\Pi)$ as a function of levels energy for *J<13*. This plot describing distribution of $OH(A^2\Sigma)$ radicals among rotational levels for pure helium and helium/oxygen mixture (0.5%) at discharge generated at fixed power of 18 W. Based on the Boltzmann plot method, the OH rotational temperature in the active zone region of the plasma pencil was measured to be 309.52 K and 366.48 K, for pure helium and helium/oxygen gas mixture (0.5% oxygen), respectively. Whereas the measured rotational temperature in the afterglow region at 5 mm away from the capillary edge was increased to 315.66 K and 362 K, for pure helium and helium/oxygen gas mixture (0.5% oxygen), respectively. As can be seen, the addition of the oxygen to the plasma pencil results in an increase of the OH rotational temperature. The excited OH radicals characterized by low rotational temperature are produced by electron impact excitation of ground state OH according to flowing reaction.[15]

$$OH(X^2\Pi) + e \rightarrow OH(A^2\Sigma)^* + e, \qquad (E_{threshold} = 4\,eV), \tag{10}$$

**H. Electron density calculation**

The analysis of the stark broadened line profiles is a well-established technique for plasma diagnostics. Plasma electron density can be obtained from some of their characteristics such as their full width at half maximum (FWHM).[47-49] One of the most common methods for determination of the electron density is using the hydrogen Balmer full width at half maximum.[47]

At atmospheric pressure, the profile of atomic spectral lines emitted from the plasma can be approximated by a Voigt function. In this work, the line shape of the hydrogen alpha transition is determined by Lorentzian and Gaussian broadening mechanisms that results in a Voigt function.[41] The Lorentzian part of the profile correspond to the contribution of the Stark and Van der Waals collisional broadening that have their origin in the interaction between the emitting particles and

the particles around them. The Gaussian part of the profile corresponds to the contribution of the Doppler and instrumental broadening. The Doppler broadening is due to the thermal movement of the emitted particle and instrumental broadening caused by measurement devices.[41] The broadening due to the natural lifetime is too small and is not taken into account in the present work.

For atmospheric pressure plasmas, low gas temperature condition, and electron densities around $10^{14}$ $cm^3$, the Van der Waals broadening has to be taken into account. The van der Waals broadening is caused by the neutral perturbers and its FWHM can be estimated as[50]

$$\Delta\lambda_{vdW} = 8.18 * 10^{-26}\lambda_0^2(\bar{R}^2)^{\frac{2}{5}}T_{gas}^{\frac{3}{10}}N\sum_i\left(\frac{\alpha_i^{\frac{2}{5}}\chi_i}{\mu_i^{\frac{3}{10}}}\right) \quad (11)$$

where $\lambda_0$ is the wavelength in nm, μ is the reduced mass in atomic mass unit, N is the neutral particle density in $cm^{-3}$ , $i$ is the helium gas and χ is the fraction of the perturber.[50] The value of the polarizability of the α pertuber for helium gas is $2.05\times10^{-25}$ $cm^3$.[51] After considering the fine structure and calculating the value for atomic lines, the FWHM can be estimated as

$$\Delta\lambda_{vdW}(nm) = \frac{C}{T^{\frac{7}{10}}} \quad (12)$$

where C is a constant for Van der Waals broadening and in the case of the hydrogen alpha line in helium gas has the value of 2.42.[51] Using the above equation the Van der Waals broadening was estimated as 0.0393 nm.

The Doppler broadening and Resonance broadening are not taken into account in the present work because their values are negligible due to the low gas temperature and atmospheric pressure conditions. In this work, the instrumental slit function is well approximated by a Gaussian profile due to the fact that mocochromator slits with equal width were used. The shape and the broadening

caused by instrumental were determined by using a Mercury-Argon pen lamp and considering the emission line at 435 nm. The instrumental profile resulted after using our experimental device very well fitted with a Gaussian function with an instrumental width of 0.17 nm. The convolution of the above Lorentzian and Gaussian line shapes results in a so-called Voigt shape with FWHM, $\Delta\lambda_V$ of [52]

$$\Delta\lambda_V \approx \sqrt{\left(\frac{\Delta\lambda_L}{2}\right) + {\Delta\lambda_G}^2} + \frac{\Delta\lambda_L}{2} \tag{13}$$

The Lorentzian full width at half maximum (FWHM) is the sum of the Lorentzian FWHMs, while the Gaussian FWHM is the square root of the sum of the squared Gaussian FWHMs.[41] In order to determine the electron density, the measured line of the $H_\alpha$ is fitted with a Voigt function with FWHM of 0.22 nm. We demonstrated the measured line broadening of $H_\alpha$ line for the helium plasma fitted with a Voigt function along with the instrumental broadening of the line at 435 nm of the Mercury-Argon pen lamp fitted with Gaussian function.

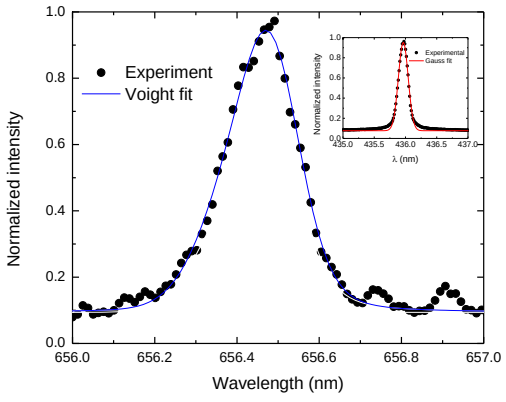


FIG 11. An example of the Voigt fit of the $H_\alpha$ line for pure helium plasma along with the instrumental broadening of the Mercury-Argon pen lamp fitted with Gaussian function.

The Lorentzian part of the FWHM is used to estimate the Stark broadening which results in a $\Delta\lambda_s$ of 0.014 nm. Using Eq. (14) for Stark broadening of the $H_\alpha$,[51] the electron density in the afterglow region of the plasma pencil was estimated as $2.1 \times 10^{14}$ $cm^3$.

$$\Delta\lambda_s = 1.78\left(\frac{n_e}{10^{23}m^{-3}}\right)^{\frac{2}{3}} \quad (14)$$

**I. Plasma pencil treatment of *S. pneumoniae* on blood agar plates and in liquid media**

The plasma treatment of the pneumococcus on the solid blood agar plates caused inactivation within the treated surface area. A time-dependent and input gas-dependent response was observed in the pneumococcal inactivation on the solid blood agar surface. A mean inactivation of $4.0 \times 10^4$ CFU and $1.3 \times 10^5$ CFU was observed after treatment for 60s with He plasma and He/0.1% $O_2$, respectively. By increasing the treatment time to 120s, a mean inactivation of $5.2 \times 10^5$ CFU and $1.0 \times 10^6$ CFU was identified for He and He/0.1% $O_2$ plasma, respectively. It was interesting that a mere 0.1% addition of oxygen gas was able to double the inactivation rate of the plasma treatment. In a similar study using *Streptococcus mutans*, a close relative to the pneumococcus, investigators identified an increase in the inactivation by injection of $O_2$ into the He plasma.[53] It has been known for some time now that oxygen radicals play a role in bactericidal activity.[54] This has further been demonstrated with several other plasma systems.[7, 55, 56] Another aspect of this research identified that doubling of the treatment time allowed for the formation of widespread inactivation zones. The respiratory tract is covered with a mucous membrane that secretes mucous to lubricate and protect the membrane.[57]

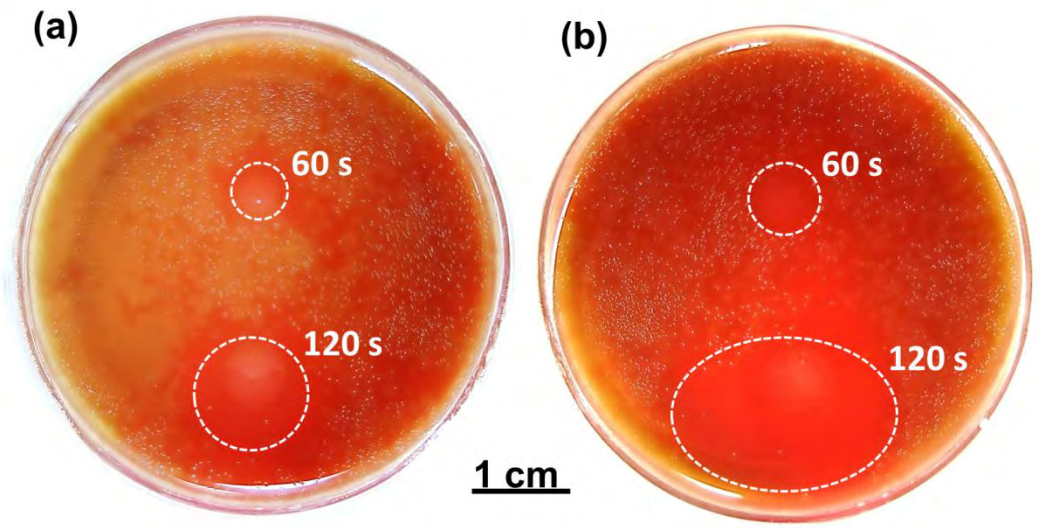


FIG 12. Plasma treated area (indicated by white circles) on agar plate inoculated with *S. pneumoniae.* (a) discharge in pure He and (b) discharge in $He/O_2$ (0.1%).

During pneumococcal infection, fluid buildup occurs around the mucous membranes due to increased swelling.[58] To identify the effectives of the plasma pencil for inactivation of *S. pneumoniae* in liquid, we treated pneumococcal suspensions in liquid media. As was identified with treatment of solid surfaces, we observed a time-dependent and input gas dependent response to plasma treatment. Pneumococcal suspensions in liquid media treated with He plasma for 60s, 120s, and 300s did not show a significant inactivation as compared to untreated samples. However, the addition of 0.1% $O_2$ to the admixture allowed for a 40% inactivation from $1.8 \times 10^7$ CFU $ml^{-1}$ to $7.1 \times 10^6$ CFU $ml^{-1}$ ± SEM $2.9 \times 10^6$ of the pneumococcal suspension after 300s of treatment. We have designed, constructed and investigated a low temperature plasma pencil driven by a kHz AC power supply. The electrical and optical characteristics of the plasma pencil in helium and helium/oxygen gas mixture have been investigated using electrical characterization and optical emission spectroscopy diagnostic techniques. The effects of oxygen at various concentrations on the helium plasma pencil were investigated. The plasma power was estimated to be in the range of

8-20 W for different applied voltages and gas mixtures. Identification of the different radicals and excited species produced in the active zone and afterglow region of the plasma pencil have been carried out. The emission spectroscopy analysis revealed that the most intensive emission lines belong to OH transition $A^2\Sigma^+(v = 0,1) \rightarrow X^2\Pi(\Delta v = 0)$ at 308 nm and OH transition $A^2\Sigma^+(v = 0,1) \rightarrow X^2\Pi(\Delta v = 1)$ at 287 nm, O I transition $3p^5P \rightarrow 3s^5S^0$ at 777.41 nm, O I transition $3p^3P \rightarrow 3s^3S^0$ at 844.6 nm and $N_2$(C-B) second positive system (SPS) with electronic transition $C^3\Pi_u \rightarrow B^3\Pi_g$ in the range of 300-450 nm. Also, different atomic emission lines include He I transition 3p3 P0→2s3S at 388.8 nm, He I transition $3p^1P^0 \rightarrow 2s^1S$ at 501.6 nm, He I transition $3d^3D \rightarrow 2p^3P^0$ at 587.6 nm, He I transition $3d^1D \rightarrow 2p^1P^0$ at 667.8 nm, He I transition $3s^3S^1 \rightarrow 2p^3P^0$ at 706.5 nm, He I transition $3s^1S^0 \rightarrow 2p^1P^0$ at 728.1 nm and $H_\alpha$ transition 2p-3d at 656.3 nm have been identified. The effect of adding oxygen on electrical and spectral properties of the plasma pencil has been investigated. Addition of oxygen to the plasma pencil resulted in a decrease in plasma power and therefore decreased the electron density and also the intensity of emission lines. Plasma density has been estimated from Stark broadening of the hydrogen line at 656 nm and is in order of $2.1\times10^{14}$ $cm^{-3}$. The plasma gas temperature was evaluated using OH rotational temperature. The OH rotational temperature for pure He plasma is 315.66 K and is 362 K for pure helium and helium/oxygen gas mixture (0.5% oxygen), respectively. The plasma pencil generates significant amounts of reactive species at low gas temperatures which promises its great potential for a range of biomedical applications. The preliminary work with inactivation of *S. pneumoniae* on solid surface and liquid suspension using the plasma pencil suggests this as a potential tool for biomedical applications. Further studies on the biological side such as the effects on inactivation on mucosal tissue need to be assessed.

Atmospheric pressure non-thermal plasma sources operating over a range of power levels has been used for industrial and materials processing applications,[1-4] and increasingly applied in biomedical applications.[2, 3, 5, 6] Several atmospheric pressure plasma sources have been developed recently, including the plasma pencil that produces stable plasma at room temperatures applied for bacterial inactivation,[7] non-destructive sub-mm radio frequency plasma needle applied for surface treatment of biomaterials,[8] one atmosphere uniform glow discharge plasma,[9] dielectric barrier discharge based atmospheric pressure plasma jet,[10] resistive barrier plasma discharge,[11-13] and microwave powered atmospheric pressure plasma jets.[14] In general, the majority of the plasma sources operate with a flow of noble gasses like helium, argon and/or their mixtures with other gases such as air, nitrogen, oxygen and water vapor.[14] Depending on the specific application requirements, a plasma source has to be developed and the characteristics of the plasma need to be diagnosed. In this work, we have constructed an atmospheric pressure plasma pencil in our laboratory based on kHz driven dielectric barrier discharge suitable for biomedical applications.

In this work, we describe the characteristics of an atmospheric pressure plasma pencil in helium and helium/oxygen mixture propagating in to open air. The plasma pencil is capable of working in different gas mixtures, e.g. argon, helium and their mixture with oxygen and water vapors. The different modes of operation and its low gas temperatures along with its efficient production of active species will potentially allow for a wide range of applications. The electrical characterization was performed based on voltage-current characterization of the plasma pencil operated in helium and $He/O_2$ gas mixtures. The plasma power was estimated from voltage-current waveforms and the input power was kept constant while varying the applied voltage. Subsequently,

optical emission spectroscopy was utilized for investigation of reactive species in plasma and determination of OH radical rotational temperature.

The size and preciseness of the plasma pencil would allow it for a range of biomedical applications that involves localized treatments. One such area of interest is pediatric otorhinolaryngology, specifically the treatment of middle ear and paranasal infections in infants and children. *Streptococcus pneumoniae* (the pneumococcus) is one the primary bacteria that causes such infections in the different locations of the respiratory tract of humans, including acute otitis media (middle ear infection), sinusitis (paranasal infection), bronchitis and pneumonia (lung infections).[16] Of the infections caused by the pneumococcus, otitis media (OM) is one of the highest prevalent pediatric diseases worldwide.[17] OM is the most frequently diagnosed illnesses in children under 15 years of age and is the primary reason for frequent physician visits.[18] Traditional treatment of pneumococcal infections in the middle ear and sinuses has consisted of a series of antibiotics; in fact, OM infections are considered the major reason for antibiotic use in children in developed countries.[19] Due to the rise in acquired bacterial resistance to antibiotics, there is a pressing need for alternative treatments to both reduce the antibiotic use in children and to combat bacterial infections from already resistant bacteria. To identify the usefulness of the plasma pencil for biomedical applications, we assessed plasma pencil treatment on pneumococcal cultures grown on solid blood agar plates and within liquid media.

## EXPERIMENTAL SET UP

### Plasma pencil and diagnostics

In this investigation an atmospheric pressure plasma pencil has been developed. The plasma was generated in a quartz capillary with inside and outside diameters of 1.3 and 3.0 mm, respectively. We demonstrated a schematic of our atmospheric pressure plasma pencil system and diagnostics. The plasma pencil consists of two electrodes, separated by air gap and a dielectric quartz capillary tube. The high voltage electrode is a 0.5 mm diameter tungsten rod placed inside the quartz capillary connected to a 25 kV, 60 kHz in-house constructed high voltage power supply. The electrical circuit of the power supply has been purchased from Piezomechanik GmbH, Germany. The ground electrode is a copper ring of 10 mm long placed around the capillary tube and axially positioned at 40 mm away from the high voltage electrode tip. The gas flow was monitored by a two channel power supply/readout (model: MKSPR400) and controlled by two mass flow meters (Model: MKS 1179A).

Plasma is generated inside the quartz capillary and in between the electrodes excited by a 60 kHz sinusoidal wave voltage. The applied voltage was varied from 8 $kV_{pk-pk}$ to 16 $kV_{pk-pk}$. The applied voltage waveforms were monitored using a high voltage probe (Tektronix P6015A) and the current waveforms were monitored by a current probe (Tektronix TCP202). The current and voltage signals were recorded using a digital oscilloscope (Tektronix TDS 3034C). High purity helium (99.99%) was purchased from MATHESON, TX for generating plasma at flow rates ranging from 1 slm to 7 slm (slm: standard liters per minute). A very low concentration of the water vapor present in the helium cylinder at a range of 0.5 ppm. In our experiments, admixtures of oxygen at varied percentages from 0.1 to 1% of the primary He operating gas were employed by changing of the gas flow rates. Two types of optical diagnostics were used for characterization

of the plasma pencil. The time and space resolved spectroscopy measurements of the plasma emission was carried out using a broadband spectrometer (Ocean Optics HR2000+ES) in the range of 200-900 nm with 0.83 nm resolution. The emission of OH radicals in the range of 300-350 nm (transition $A^2\Sigma^+(v=0) \rightarrow X^2\Pi(v=0)$) was recorded with 500 $\mu$s integration time using a 0.08 nm resolution spectrometer system made up of a monochromator (Princeton Instruments Acton SP2750) and a CCD (ACTON IStar). The plasma emissions were collected in a direction perpendicular to the plasma pencil axis and at 1 mm increments in axial direction using a collimating lens. The plasma emission was transmitted to the spectrometer via optical fiber. The spectrometer was equipped with double grating turrets, one with 1200 grooves $mm^{-1}$ grating and the other 2400 grooves $mm^{-1}$ grating. The grating with 2400 $g.mm^{-1}$ and holographic blaze is selected to record OH (A-X) band at 306-312 nm for determination of the gas temperature using Boltzmann plot of the rotational population of the OH radicals. The second grating of 1200 $g.mm^{-1}$ and blaze wavelength of 500 nm, is selected to record $H_\alpha$ (656.4 nm) and Ar 435 nm for plasma electron density measurements using Stark broadening method.

**Bacterial sample preparation and plasma treatment procedure**

*S. pneumoniae* strain TIGR4 was grown in Todd-Hewitt broth with 0.3% yeast extract and cells were collected during logarithmic growth $OD_{620nm} = 0.5$ for solid surface cultures and $OD_{620nm} = 0.4$ for liquid media cultures. The bacterial concentration for $OD_{620} = 0.5$ was $10^7 – 10^8$ CFU $ml^{-1}$ (CFU = colony forming units) and for $OD_{620} = 0.4$ was $10^6$-$10^7$ CFU $ml^{-1}$. For treatments of solid surfaces, 100µl ($4 \times 10^6$ CFU) of bacterial samples were inoculated onto the center of a 50 mm diameter Petri dish (plate). A disposable 35 mm wide Drigalski spatula was placed with one end at the inner edge of the Petri dish and the other end over the inoculated sample. The plate was rotated at least 10 times to allow for spread of bacterial sample over the entire agar surface,

allowing a pneumococcal density of approximately $2.04 \times 10^3$ CFU $mm^{-2}$ on the blood agar plate. All treated samples were insulated from ground. For treatment of bacteria on the agar surface, the plasma pencil was fixed at distance of 10 mm between the plasma-pencil nozzle and agar surface. The cultures were exposed to 60s and 120s of either He or He/0.5% $O_2$. After treatment with plasma, the cultures were grown overnight at 37°C in 5% $CO_2$. The treated area was assessed in comparison to the untreated surrounding agar surface for zones of inactivation. The areas of the zones of inactivation were measured to quantify the amount of pneumococcal inactivation.

For treatment of the pneumococcus in liquid cultures, the bacteria suspension was prepared as described above to $OD_{620} = 0.4$. From the prepared bacterial suspension, 200 µl was transferred to a 96 well micro-well plate. The plasma pencil was fixed at distance of 3 mm between the plasma-pencil nozzle and the liquid media surface. The pneumococcal suspensions were exposed to 60s, 120s, and 300s of either He or He/0.5% $O_2$. After treatment, serial dilutions were performed and 10 µl of sample was placed onto a blood agar plate to grow overnight at 37 °C in 5% $CO_2$. After overnight growth, the efficacy of the inactivation was determined by taking CFU counts of the untreated and treated samples.

**Electrical characterization**

The electrical characterization experiments were performed on the atmospheric pressure plasma pencil with helium and oxygen admixtures. Initially, the helium gas was injected into the quartz capillary at a flow rate of 1 slm and the breakdown discharge occurred between the two electrodes and inside the quartz capillary occurred at a minimum input voltage of 7 $kV_{pk-pk}$. However, the discharge was unstable inside the quartz capillary at this minimum input voltage of 7 $kV_{pk-pk}$ and therefore plasma did not exit from the capillary in to surrounding air resulting an absence of a prominent afterglow region. By increasing the input voltage to 8 $kV_{pk-pk}$, the plasma pencil

successfully produced an afterglow plasma in to the open air and a long plasma plume length was formed. In order to diagnose the electrical properties of the plasma pencil, the voltage and current waveforms were measured during the discharges at 8, 9, 10, 11 and 12 $kV_{pk-pk}$ and the effects of gas flow rates and oxygen admixture percentages in the plasma discharge were investigated. We demonstrated the voltage and current waveforms for the plasma pencil for pure helium and helium-oxygen mixture (0.5% $O_2$ in the discharge) at a total gas flow rate of 4 slm.

The plasma pencil generates a very uniform discharge in pure helium gas and only small current peaks exist on the current waveform during each half period of the applied voltage. The maximum current is 10.2 mA. A clear change in the voltage-current waveform was observed when oxygen was added to the plasma pencil. Addition of the oxygen to the plasma pencil results in a small increase of the current peak intensity to 10.8 mA. The results indicate that the voltage slightly decreases with increase of the current peaks.

Using the voltage-current waveforms, the average power (W) of the discharge was calculated according to the following equation, where T is the period of the discharge:[20, 21]

$$W = \frac{1}{T}\int_{T}^{T+t} I(t)V(t)\,dt. \tag{1}$$

power dissipated in the discharge is presented as a function of the applied voltage for different operating gas flow rates used. The minimum power of the plasma pencil is observed to be about 8.8 W for pure Helium plasma at an applied voltage (peak-to-peak) of 8 $kV_{pk-pk}$ and a gas flow rate of 1 slm. The applied voltage was increased up to 12 $kV_{pk-pk}$, which is the breakdown point of the quartz capillary, resulting in an increase of power up to 20.4 W for discharge in pure helium at a gas flow rate of 4 slm. The plasma power as a function of oxygen percentage in the plasma pencil. Basically, the power dissipation in pure helium discharge is higher, which is explained by broader current peaks. It is necessary to mention that the addition of oxygen to gas flow results in

a decrease of the input power from 20.4 W (in case of pure helium) to 17.8 W and 15.8 W for discharges containing 0.1% and 1% of oxygen, respectively. The decrease in plasma power with addition of oxygen is due to contraction of the current peaks at higher amounts of oxygen in gas mixture that results in decrease of the integral determining power dissipation in the discharge.

**Visualization of the plasma pencil in helium and helium/oxygen admixtures**

The plasma pencil can be successfully launched in pure helium discharge with application of voltage at values higher than 6 $kV_{pk-pk}$ . Addition of oxygen admixture to the feed gases required higher threshold voltages of up to 10 $kV_{pk-pk}$ , especially at a higher concentration of oxygen (1% oxygen). The plasma pencil generated from a complete breakdown of entire inter-electrode gap (active zone) with formation of a long bright afterglow propagating in to open air and its plume length depends on the composition of the feed gas, applied voltage and flow rates of the operating gas. We demonstrated color photographs of the plasma pencil (without Teflon cover) generated at 12 $kV_{pk-pk}$ and in pure helium for different flow rates in the range of 1-7 slm and FIG 4.b displays the images of the plasma pencil in $He/O_2$ gas mixture from 0-1% of Oxygen in discharge.

In addition, we observed that the plasma pencil's plume length is greatly depends on the gas flow rate and it shows very small noticeable dependence with changes in applied voltage. Next, the plasma plume length has been measured using the plasma pencil images. We demonstrated the plasma plume lengths as a function of helium gas flow rates and oxygen percentages in the discharge, respectively. As can be seen for discharges in pure helium the plume length at lowest flow rate of 1 slm is about 10 mm and sharply increases to the maximum value of 27 mm at a flow rate of 7 slm. Increase of the gas flow rates to a value higher than 7 slm, results in a decrease in the plasma pencil plume length due to change of the gas dynamic from laminar to turbulent flow.

the addition of the oxygen to the plasma pencil results in a sharp decrease of the pencil's plume length. Plasma pencil's plume length in pure helium discharge at 5 slm is 18 mm, while the plume length decreases with addition of oxygen to 15 mm and 10 mm, at discharges contain 0.1% and 1% of oxygen, respectively. The reason for decrease of the plume length is that oxygen is an electronegative molecular gas, therefore, the addition of the oxygen to the plasma pencil results to electron attachment reactions with oxygen molecules and therefore, the electron density in the discharge and consequently the helium metastable concentrations in the discharge decreases which results in a decrease of the plasma pencil's plume length.

**Optical emission spectroscopy and plasma pencil species identification**

Optical emission spectroscopy is considered to be a suitable tool in characterizing the plasma properties in terms of the identification of the reactive plasma species, plasma gas temperature evaluation and the relative emission intensities of the various species in different conditions.[22-26] In the non-thermal plasma pencil at atmospheric pressure, the mean electron energy is significantly higher than the energy of neutral plasma species.[27] The reaction between high energy electrons with helium, water vapor, nitrogen and oxygen at atmospheric pressure will induce the molecules to be dissociated, excited and ionized for production of different radicals and active species. In this section, the optical emission spectroscopy was used to study the plasma pencil in He and $He/O_2$ gas mixture and the reactive plasma species were identified. The axial and space resolved emission spectra in the range of 200-900 nm were recorded and analyzed. Axial emission spectrum of the plasma pencil allowed determination of the main reactive plasma species

produced in the plasma pencil. the results of spectroscopic measurements with 0.83 nm resolution of the plasma discharge in He and He/$O_2$ mixtures (0.5%) are presented. The emission spectra were recorded in the middle of the active zone region (the region between the HV and ground electrode) of the plasma pencil. The emission spectra shown were recorded at 5 mm from the edge of the capillary (afterglow region). The emission spectra are mainly composed of the spectral line of the He atoms. The most intensive emission lines correspond to He I transition $3p^3P^0 \rightarrow 2s^3S$ at 388.8 nm, He I transition $3p^1P^0 \rightarrow 2s^1S$ at 501.6 nm, He I transition $3d^3D \rightarrow 2p^3P^0$ at 587.6 nm, He I transition $3d^1D \rightarrow 2p^1P^0$ at 667.8 nm, He I transition $3s^3S^1 \rightarrow 2p^3P^0$ at 706.5 nm, and He I transition $3s^1S^0 \rightarrow 2p^1P^0$ at 728.1 nm. In addition to He lines, the other identified reactive plasma species include intensive emission lines belonging to OH transition $A^2\Sigma^+ \rightarrow X^2\Pi, \quad \Delta v = 0$, at 308 nm, and OH transition $A^2\Sigma^+ \rightarrow X^2\Pi, \quad \Delta v = 1$, at 287 nm, the spectral band of the $N_2$ transition $C^3\prod_u - B^3\prod_g, \quad \Delta v = 0$, at 337.1 nm, $H_\alpha$ transition 2p-3d at 656.3 nm, O I transition $3p^5P \rightarrow 3s^5S^0$ at 777.41 nm and O I transition $3p^3P \rightarrow 3s^3S^0$ at 844.6 nm. The OH radicals in the active zone region of the plasma are formed from water vapor present in the helium gas cylinder.[28] Another investigation by Sarani et al. [15] has been shown that the OH radicals concentration can be precisely controlled by using bubbling system and controlling the water vapor content in the feed stream. The corresponding emission lines are identified based on the NIST atomic spectra database[29] and Lofthus et. al.[30]

In order to investigate the effect of $O_2$ on the emission intensities of the reactive plasma species, different concentrations of the $O_2$ were added to the plasma pencil. Next, the emission spectra of the plasma with different $O_2$% in the discharge were collected and the emission lines of OH at 308 nm (transition $A^2\Sigma^+ \rightarrow X^2\Pi, \quad \Delta v = 0$), $N_2$ at 337 nm (transition $C^3\prod_u - B^3\prod_g$), $H_\alpha$ at 656 nm

(transition $2p - 3d$), He at 706 nm (transition $1s3s\ ^3S - 1s2p\ ^3P^0$) and O I at 777 nm (transition $2s^2 2p^3(^4S^0)3s - 2s^2 2p^3(^4S^0)3p$) were chosen for space resolved analysis of the emission spectroscopy. The results of spatial distribution of the active species intensities show that the emission spectrum of $He/O_2$ (0.5 %) mixture is very similar to pure helium discharge when comparing identified species. Moreover, it is clearly recognizable that the addition of oxygen to the plasma pencil results in a decrease of the emission lines intensities. The main reason for decrease of the emission line intensities is the decreases of the plasma power with addition of the oxygen in the discharge..[15, 31] Similar observation has been reported previously by others on plasma containing oxygen or other electronegative molecular gases.[15, 21, 32]

As can be seen the discharge in pure helium shows a higher intensity of OH radicals compared to the plasma pencil that contains $O_2$ gas mixture for both cases (the active zone and afterglow region) of the plasma pencil. In the active zone of the plasma, the most intensive emission line belongs to O I at 777 nm, while in the afterglow region of the plasma pencil, $N_2$ emission line at 337 nm is the most intensive emission line in the emission spectra. Furthermore, addition of higher amount of oxygen to the plasma results in a decrease of these emission lines in the discharge. Oxygen is an electronegative gas, hence, when oxygen is added to the plasma pencil, the added oxygen captures significant free electrons and produces $O^-$ and $O^{2-}$ ions. Thus, the electron attachment by oxygen results in a decrease of the electron density and electron mean energy.[33-35] The OH radicals are mainly produced by electron-water vapor collision process according to the following reaction, and therefore the decrease of the electron density leads to decrease of the intensities of OH and other atomic emission lines at a constant power.[28, 33, 34]

$$e + H_2O \rightarrow e + H + OH \quad (2)$$

The reason for increase of O I intensity in the active zone region of the plasma pencil is that when oxygen is added to the pure helium plasma pencil, the added oxygen can be dissociated according to the following reactions and results in a formation of singlet oxygen (O) and O ($^1$D).

$$e + O_2 \rightarrow O^- + O \quad (3)$$

$$e + O_2 \rightarrow e + O + O(^1D) \quad (4)$$

$$e + O_2 \rightarrow 2e + O^+ + O \quad (5)$$

In addition, in the afterglow region of the discharge when plasma pencil propagates in the open air, the OH radicals can be produced by the interaction of O ($^1$D) and $H_2O$ according to the following reaction:[35]

$$O(^1D) + H_2O \rightarrow 2\,OH \quad (6)$$

On the other hand, the singlet oxygen and ozone molecules generated in the discharge react with the produced OH radicals according to the following reactions and thus, the OH radicals intensity in the plasma pencil decreases with addition of oxygen percentage to the pure helium plasma pencil.[35]

$$OH + O \rightarrow H + O_2 \quad (7)$$

$$OH + O_3 \rightarrow HO_2 + O_2 \quad (8)$$

**Space resolved optical emission spectroscopy of the plasma pencil**

The spatial distribution characteristics of chemically active species are very important in developing the plasma pencil kinetic model and understanding the mechanism of biomedical applications of the plasma pencil. Here, we present the spatially resolved spectra of the afterglow region of the plasma pencil.

The spatially resolved optical emission spectra of the afterglow region were collected for pure helium and helium/oxygen mixture (0.5%), with resolution of 2.5 mm. Next, the intensities of the

intensive reactive plasma species were chosen for deeper analysis of the space resolved emission spectroscopy. As can be seen the emission intensity of the OH radicals ( $A^2\Sigma^+ \rightarrow X^2\Pi, \quad \Delta v = 0$ ) and $N_2$ ( $C^3\prod_u - B^3\prod_g$ ), $H_\alpha$ and O I and helium vary with distance from the edge of quartz capillary. It can be seen that the emission intensity of helium, O I and $N_2$ ( $C^3\prod_u - B^3\prod_g$ ) rises initially up to 7 mm from the edge of capillary and then decreases, while the emission intensity of the OH ( $A^2\Sigma^+ \rightarrow X^2\Pi, \quad \Delta v = 0$ ) and $H_\alpha$ decreases with increase of distance from the capillary. The emission intensity of $N_2$ at 10 mm is almost 8-10 times larger than the intensity at the edge of the capillary. Moreover, the emission intensity of $N_2$ reaches a maximum value after OH radicals. The maximum intensity of $N_2$ is located at 10 mm while the OH radicals' maximum intensity is located at 7 mm. This behavior can be explained by the fact that $H_2O$ dissociation is initiated by electron induced processes inside the discharge and in the short distance after the edge of capillary, where the electron exhibit required the energy.[15] In the case of the plasma pencil in helium/oxygen mixture (0.5%), the intensity decay of the helium in the plasma plume has an exponential decay, initially increasing up to 10 mm from the edge of capillary and after that again decreasing (FIG 8.b). The most intensive emission line belong to O I, which is located inside the quartz capillary. The $N_2$ emission intensity reaches to its maximum outside the capillary and at 5 mm distance from the edge of capillary. The identified excited nitrogen molecules are produced from electron impact reactions in the plasma plume as it propagates into the ambient air.[28] The main reason for the decrease of the emission intensities of the reactive plasma species with the distance from the edge of capillary is the decrease of the high energy electron density and mean energy.[32] Outside the capillary the increase of the $N_2$ (SPS) emission could be a result of energy transfer from metastables and decreasing of the OH emission by increasing $N_2$ in the plasma pencil and lower $H_2O$ density in the surrounding air compared to nitrogen.

The identified reactive plasma species such as the singlet oxygen, hydroxyl radicals, and neutral nitrogen molecules detected in the plasma pencil can play a significant role in biomedical applications especially operating at the atmospheric pressure.[36, 37] Similar significant generation of reactive oxygen species such as singlet oxygen (O) and $O_3$ were observed with $He/O_2$ gas mixture used in a plasma pencil which can result in enhanced efficacy of bacterial inactivation.[26, 38] It is believed that the oxygen species in the discharge contributes to the sterilization process due to its strong oxidative effect on the outer structure of the cells,[36, 37] while the OH radicals generated by the plasma plays a significant role through chemically attacking the outer structure of the cells and the production of the nitrogen containing group adds to the lethality of the process.[39]

**OH rotational temperature determination using Boltzmann plot method**

The plasma gas temperature has been derived from OH rotational temperatures. The OH rotational temperature is usually considered to be equal to the plasma gas temperature considering the low rotational level of the OH radicals OH (A-X) and small rotational quantum numbers *J*.[15, 40-42] The Boltzmann plot of the rotational population of the OH radicals has been widely used for this purpose.[15, 40, 43, 44] We demonstrated the high resolution emission spectra of the OH radicals in pure helium and helium oxygen (0.5%), respectively. Using the OH emission spectra and assuming that the OH rotational states are Boltzmann distributed according to the following equation

$$I_{J'J''} \approx h\nu_{J'J''}(2J+1)A_{J'J''}\exp\left(-\frac{B_v hcJ(J+1)}{k_B T_{rot}}\right), \qquad (9)$$

where $\nu_{J'J''}$ is the frequency of transition from rotational level $J'$ to $J''$, $A_{J'J''}$ is the corresponding transition probability, $B_v$ is the rotational constant, $k_B$ is the Boltzmann constant and $h$ is the Planck constant. The rotational energy $E(cm^{-1})$ equals to $B_v J(J+1)$. The energy and probability data of OH transitions were taken from literature.[45, 46] The corresponding OH rotational temperature is equal with gas temperature when the rotational population distribution is in equilibrium with heavy species translational temperature in the discharge. In atmospheric pressure plasma, this assumption is valid on atmospheric pressure plasmas when high collisional reactions occur. A detailed description of the used method can be found in Sarani. et, al. 2010.[15]

We presented $\ln(I\lambda/(2J+1)A_{JJ})$ for transition $OH(A^2\Sigma - X^2\Pi)$ as a function of levels energy for *J<13*. This plot describing distribution of $OH(A^2\Sigma)$ radicals among rotational levels for pure helium and helium/oxygen mixture (0.5%) at discharge generated at fixed power of 18 W. Based on the Boltzmann plot method, the OH rotational temperature in the active zone region of the plasma pencil was measured to be 309.52 K and 366.48 K, for pure helium and helium/oxygen gas mixture (0.5% oxygen), respectively. Whereas the measured rotational temperature in the afterglow region at 5 mm away from the capillary edge was increased to 315.66 K and 362 K, for pure helium and helium/oxygen gas mixture (0.5% oxygen), respectively. As can be seen, the addition of the oxygen to the plasma pencil results in an increase of the OH rotational temperature. The excited OH radicals characterized by low rotational temperature are produced by electron impact excitation of ground state OH according to flowing reaction.[15]

$$OH(X^2\Pi) + e \rightarrow OH(A^2\Sigma)^* + e, \qquad (E_{threshold} = 4\,eV), \tag{10}$$

The results of the OH rotational temperature obtained in this work by using Boltzmann plot method are in a good agreement with those data obtained by fitting of the OH spectra using LIFBASE

software in our previous publication [47]. The OH rotational temperatures for active zone of the pure helium plasmas are 309.52 ± 25 K and 310 ± 25 K by using Boltzmann plot method and fitting of the OH rotational spectra by LIFBASE software [47], respectively.

**Electron density determination using line broadening**

The analysis of the stark broadened line profiles is a well-established technique for plasma diagnostics. Plasma electron density can be obtained from the full width at half maximum (FWHM) of the stark broadened profile of the hydrogen lines.[48-50] One of the most common methods for determination of the electron density is using the hydrogen Balmer full width at half maximum.[48]

At atmospheric pressure, the profile of atomic spectral lines emitted from the plasma can be approximated by a Voigt function. In this work, the line shape of the hydrogen alpha transition is determined by Lorentzian and Gaussian broadening mechanisms that results in a Voigt function.[41] The Lorentzian part of the profile correspond to the contribution of the Stark and Van der Waals collisional broadening that have their origin in the interaction between the emitting particles and the particles around them. The Gaussian part of the profile corresponds to the contribution of the Doppler and instrumental broadening. The Doppler broadening is due to the thermal speed of the emitting particle and instrumental broadening caused by measurement devices.[41] The broadening due to the natural lifetime is too small and is not taken into account in the present work.

For atmospheric pressure plasmas, low gas temperature condition, and electron densities around $10^{14}$ $cm^3$, the Van der Waals broadening has to be taken into account. The van der Waals broadening is caused by the neutral perturbers and its FWHM can be estimated as[51]

$$\Delta\lambda_{vdW} = 8.18 * 10^{-26}\lambda_0^2(\bar{R}^2)^{\frac{2}{5}}T_{gas}^{\frac{3}{10}}N\sum_i\left(\frac{\alpha_i^{\frac{2}{5}}\chi_i}{\mu_i^{\frac{3}{10}}}\right) \quad (11)$$

where $\lambda_0$ is the wavelength in nm, μ is the reduced mass in atomic mass unit, N is the neutral particle density in $cm^{-3}$ , $i$ is the helium gas and χ is the fraction of the perturber.[51] The value of the polarizability of the α pertuber for helium gas is $2.05\times10^{-25}$ $cm^3$.[52] After considering the fine structure and calculating the value for atomic lines, the FWHM can be estimated as

$$\Delta\lambda_{vdW}(nm) = \frac{C}{T^{\frac{7}{10}}} \quad (12)$$

where C is equal to 2.42, the Van der Waals broadening constant for hydrogen alpha line in helium plasma.[52] Using the above equation the Van der Waals broadening was estimated as 0.0393 nm.

The Doppler broadening and Resonance broadening are not taken into account in the present work because their values are negligible due to the low gas temperature and atmospheric pressure conditions. In this work, the instrumental slit function is well approximated by a Gaussian profile due to the fact that monochromator slits with equal width were used. The shape and the broadening caused by instrumental were determined by using a Mercury-Argon pen lamp and considering the emission line at 435 nm. The instrumental profile resulted after using our experimental device very well fitted with a Gaussian function with an instrumental width of 0.17 nm. The convolution of the above Lorentzian and Gaussian line shapes results in a Voigt profile with FWHM, $\Delta\lambda_V$ of [53]

$$\Delta\lambda_V \approx \sqrt{\left(\frac{\Delta\lambda_L}{2}\right) + {\Delta\lambda_G}^2} + \frac{\Delta\lambda_L}{2} \quad (13)$$

The Lorentzian full width at half maximum (FWHM) is the sum of the Lorentzian FWHMs, while the Gaussian FWHM is the square root of the sum of the squared Gaussian FWHMs.[41] In order to determine the electron density, the measured line of the $H_\alpha$ is fitted with a Voigt function with FWHM of 0.22 nm. We demonstrated the measured line broadening of $H_\alpha$ line for the helium plasma fitted with a Voigt function along with the instrumental broadening of the line at 435 nm of the Mercury-Argon pen lamp fitted with Gaussian function. The Lorentzian part of the FWHM is used to estimate the Stark broadening which results in a $\Delta\lambda_s$ of 0.014 nm. Using Eq. (14) for Stark broadening of the $H_\alpha$,[52] the electron density in the afterglow region of the plasma pencil was estimated as $2.1 \times 10^{14}$ $cm^3$.

$$\Delta\lambda_s = 1.78\left(\frac{n_e}{10^{23}m^{-3}}\right)^{\frac{2}{3}} \quad (14)$$

**Plasma pencil treatment of *S. pneumoniae* on blood agar and in liquid media**

The plasma treatment of the pneumococcus on the solid blood agar plates caused inactivation within the treated surface area. A time-dependent and input gas-dependent response was observed in the pneumococcal inactivation on the solid blood agar surface. A mean inactivation of $4.0 \times 10^4$ CFU and $1.3 \times 10^5$ CFU was observed after treatment for 60s with He plasma and He/0.1% $O_2$, respectively. By increasing the treatment time to 120s, a mean inactivation of $5.2 \times 10^5$ CFU and $1.0 \times 10^6$ CFU was identified for He and He/0.1% $O_2$ plasma, respectively. It was interesting that a mere 0.1% addition of oxygen gas was able to double the inactivation rate of the plasma treatment. In a similar study using *Streptococcus mutans*, a close relative to the pneumococcus, investigators identified an increase in the inactivation by injection of $O_2$ into the He plasma.[54]

It has been known for some time now that oxygen radicals play a role in bactericidal activity.[55] This has further been demonstrated with several other plasma systems.[7, 56, 57] Another aspect of this research identified that doubling of the treatment time allowed for the formation of widespread inactivation zones. The respiratory tract is covered with a mucous membrane that secretes mucous to lubricate and protect the membrane.[58] During pneumococcal infection, fluid buildup occurs around the mucous membranes due to increased swelling.[59] To identify the effectives of the plasma pencil for inactivation of *S. pneumoniae* in liquid, we treated pneumococcal suspensions in liquid media. As was identified with treatment of solid surfaces, we observed a time-dependent and input gas dependent response to plasma treatment. Pneumococcal suspensions in liquid media treated with He plasma for 60s, 120s, and 300s did not show a significant inactivation as compared to untreated samples. However, the addition of 0.1% $O_2$ to the admixture allowed for a 40% inactivation from $1.8 \times 10^7$ CFU $ml^{-1}$ to $7.1 \times 10^6$ CFU $ml^{-1}$ ± SEM $2.9 \times 10^6$ of the pneumococcal suspension after 300s of treatment.

We have designed, constructed and investigated a low temperature plasma pencil driven by a kHz AC power supply. The electrical and optical characteristics of the plasma pencil in helium and helium/oxygen gas mixture have been investigated using electrical characterization and optical emission spectroscopy diagnostic techniques. The effects of oxygen at various concentrations on the helium plasma pencil were investigated. The plasma power was estimated to be in the range of 8-20 W for different applied voltages and gas mixtures. Identification of the different radicals and excited species produced in the active zone and afterglow region of the plasma pencil have been carried out. The emission spectroscopy analysis revealed that the most intensive emission lines belong to OH transition $A^2\Sigma^+(\nu = 0,1) \rightarrow X^2\Pi(\Delta\nu = 0)$ at 308 nm and OH transition $A^2\Sigma^+(\nu = 0,1) \rightarrow X^2\Pi(\Delta\nu = 1)$ at 287 nm, O I transition $3p^5P \rightarrow 3s^5S^0$ at 777.41 nm, O I transition $3p^3P \rightarrow 3s^3S^0$ at

844.6 nm and $N_2$(C-B) second positive system (SPS) with electronic transition $C^3\Pi_u \rightarrow B^3\Pi_g$ in the range of 300-450 nm. Also, different atomic emission lines include He I transition 3p3 P0→2s3S at 388.8 nm, He I transition $3p^1P^0 \rightarrow 2s^1S$ at 501.6 nm, He I transition $3d^3D \rightarrow 2p^3P^0$ at 587.6 nm, He I transition $3d^1D \rightarrow 2p^1P^0$ at 667.8 nm, He I transition $3s^3S^1 \rightarrow 2p^3P^0$ at 706.5 nm, He I transition $3s^1S^0 \rightarrow 2p^1P^0$ at 728.1 nm and $H_\alpha$ transition 2p-3d at 656.3 nm have been identified. The effect of adding oxygen on electrical and spectral properties of the plasma pencil has been investigated. Addition of oxygen to the plasma pencil resulted in a decrease in plasma power and therefore decreased the electron density and also the intensity of emission lines. Plasma density has been estimated from Stark broadening of the hydrogen line at 656 nm and is in order of $2.1\times10^{14}$ $cm^{-3}$. The plasma gas temperature was evaluated using OH rotational temperature. The OH rotational temperature for pure He plasma is 315.66 K and is 362 K for pure helium and helium/oxygen gas mixture (0.5% oxygen), respectively. The plasma pencil generates significant amounts of reactive species at low gas temperatures which promises its great potential for a range of biomedical applications. The preliminary work with inactivation of *S. pneumoniae* on solid surface and liquid suspension using the plasma pencil suggests this as a potential tool for biomedical applications. Further studies on the biological side such as the effects on inactivation on mucosal tissue need to be assessed.

# KEY RESEARCH ACCOMPLISHMENTS

**Table . Status and remarks of the project milestones**

| Task | Proposed Milestones | Base Line Plan Date | Status/Remark |
|---|---|---|---|
| **I. Objective 1: Establish Plasma Engineering Research Lab** | | | |
| 1 | Setup a direct current - atmospheric - resistive barrier cold plasma system | 26 OCT 2011 | Completed |
| 2 | Setup a 13.56 MHz radio frequency dielectric barrier plasma system | 26 OCT 2011 | Completed |
| 3 | Setup a 900 MHz/2.45 GHz wave plasma system | 26 OCT 2011 | Completed |
| 4 | Setup a laser induced breakdown plasma experimental system | 26 OCT 2011 | Completed |
| 5 | Implement plasma shadowgraphy diagnostics Setup | 26 OCT 2011 | Completed |
| 6 | Implement a two color laser interferomtery diagnostics setup | 26 OCT 2011 | Completed |
| 7 | Implement a optical emission spectroscopy diagnostics setup | 26 OCT 2011 | Completed |
| **II. Objective 2: Develop Portable Plasma Source** | | | |
| 8 | Design phase: Design an optimized portable plasma source system | 26 OCT 2012 | Completed |
| 9 | Construction phase: Construct the portable plasma source based on the design analysis and utilizing the existing resources and knowledge gained from objective 1. | 26 OCT 2012 | Completed |
| 10 | Testing and characterization phase: Portable plasma source will be tested and characterized for its operating parameters and plasma parameters. | 26 OCT 2014 | Completed |
| 11 | Biological testing: In-vitro biological testing. | 26 OCT 2015 | Completed |

# REPORTABLE OUTCOMES

## MENTORING

**The PI is dedicated to mentor students of diversity and underrepresented minority groups.**

The PI has mentored the following scientists in the research

Dr. Zhen Ma

Dr. Kenneth Williamson

Dr. Abdollah Sarani

Dr. Cosmina Nicula

Xavier Gonzales

The PI has mentored the following Graduate Students

Heather Anderson

Anudeep Reddy Kandi

Jennifer Chancellor

The PI has mentored the following Undergraduate Students

Eduardo Valdez

Francisco Rodriguez

Bokang Yang

Thurman Walling

James Shames

Isaac Colmenero

Kim Pham

Megan Norfolk

Jennifer Anderson

Amanda Whitmill

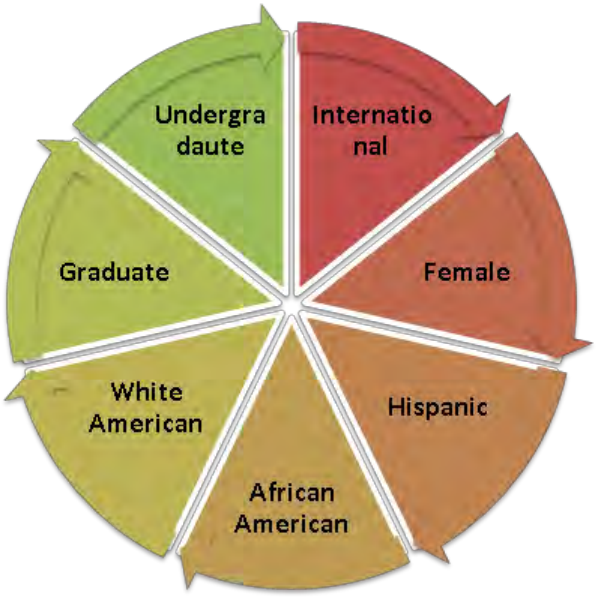

**i. Peer-Reviewed Books**

1. Magesh Thiyagarajan. "Laser Induced Plasmas & Optical Diagnostics: Infrared & Ultraviolet Laser Breakdown Plasmas & Shadowgraphy, Interferometry, Optical Emission Spectroscopy Diagnostics." (LAP LAMBERT, 2011). ©. 268 pages, (2011). (ISBN: 978-3846548745).
2. Magesh Thiyagarajan. "Experimental Investigation of 193 nm Excimer Laser Induced Plasma in Air" (ProQuest, 2011). ©. 120 pages, (2011). (ISBN: 978-1243508751).

**ii. Peer-Reviewed & Indexed Book Chapter Series**

*[$]Postdoc, [#]Graduate Student, *Undergraduate Student*

3. Magesh Thiyagarajan, Xavier F. Gonzales[$], Heather Anderson[#]. "Regulated Cellular Exposure to Non-Thermal Plasma Allows Preferentially Directed Apoptosis in Acute Monocytic Leukemia Cells." Studies in Health Technology and Informatics, IOS Press, vol. 184, 436 – 442. (2013) (ISBN: 978-1-61499-208-0). (DOI 10.3233/978-1-61499-209-7-436). (PubMed 23400198).
4. Magesh Thiyagarajan, Abdollah Sarani[$], Xavier F. Gonzales[$]. "Characterization of an Atmospheric Pressure Plasma Jet and its Applications for Disinfection and Cancer Treatment" Studies in Health Technology and Informatics, IOS Press, vol. 184, 443 – 449. (2013) (ISBN: 978-1-61499-208-0). (DOI 10.3233/978-1-61499-209-7-443). (PubMed 23400199).
5. Magesh Thiyagarajan, Lillian Waldbeser and Amanda Whitmill*. "THP-1 leukemia cancer treatment using a portable plasma device." Studies in Health Technology and Informatics, IOS Press, vol. 173, 515 – 517. (2012) (ISBN: 978-1-61499-021-5). (DOI 10.3233/978-1-61499-022-2-515). (PubMed 22357047).
6. Magesh Thiyagarajan and Lillian Waldbeser. "Portable plasma medical device for infection treatment." Studies in Health Technology and Informatics, IOS Press, vol. 173, 518 – 520. (2012) (ISBN: 978-1-61499-021-5). (DOI 10.3233/978-1-61499-022-2-518). (PubMed 22357048).

**iii. Peer-Reviewed Journal Publications (ISI Journals)**

*$Postdoc, #Graduate Student, *Undergraduate Student*

7. Abdollah Sarani[$], and Cosmina Nicula[$], Xavier F. Gonzales[$], Magesh Thiyagarajan. "Characterization of Kilohertz-Ignited Non-thermal He and He/O2 Plasma Pencil for Biomedical Applications." *IEEE Transactions on Plasma Science - Special Issue on Pulsed Power Science and Technology*, (2014). vol. 42, no. 10, (2014).
8. Magesh Thiyagarajan, Heather Anderson[#], Xavier F. Gonzales[$]. "Induction of apoptosis in human myeloid leukemia cells by remote exposure of resistive barrier cold plasma." *Biotechnology and Bioengineering,* 2014.
9. Magesh Thiyagarajan, Abdollah Sarani[$], and Cosmina Nicula[$]. "Optical emission spectroscopic diagnostics of a non-thermal atmospheric pressure helium-oxygen plasma jet for biomedical applications." *Journal of Applied Physics*, (2013). vol. 113, p. 233302, (2013). DOI: 10.1063/1.4811339.
10. Magesh Thiyagarajan. "A Portable Atmospheric Air Plasma Device for Biomedical Treatment Applications." *ASME Journal of Medical Devices.* vol. 7, Issue 1, p. 011007, (2013). DOI: 10.1115/ 1.4023498.
11. Magesh Thiyagarajan, Abdollah Sarani[$], and Xavier Gonzales[$]. "Atmospheric pressure resistive barrier air plasma jet induced bacterial inactivation in aqueous environment." *Journal of Applied Physics*, vol. 113, p. 093302, (2013). DOI: 10.1063/1.4794333.
12. Magesh Thiyagarajan, Abdollah Sarani[$], and Xavier Gonzales[$]. "Characterization of Portable Resistive Barrier Plasma Jet and Its Direct and Indirect Treatment for Antibiotic Resistant Bacteria and THP-1 Leukemia Cancer Cells." *IEEE Transactions on Plasma Science. (Special Topics on Atmospheric Pressure Plasma Jets).* 40, no. 12, p. 3533 – 3545 (2012). DOI: 10.1109/TPS.2012.2222391.

13. Magesh Thiyagarajan, Kenneth Williamson[$], and Anudeep Reddy Kandi[#]. "Experimental Investigation of 1064-nm IR Laser-Induced Air Plasma Using Optical Laser Shadowgraphy Diagnostics." *IEEE Transactions on Plasma Science (Special Topics on Pulsed Power Technology)* 40, no. 10, p. 2491 – 2500 (2012). DOI: 10.1109/TPS.2012.2206406.
14. Magesh Thiyagarajan and Shane Thompson. "Optical breakdown threshold investigation of 1064 nm laser induced air plasmas" *Journal of Applied Physics*, vol. 111, p. 073302, (2012). DOI: 10.1063/1.3699368.

## CONFERENCE PUBLICATIONS

117. Magesh Thiyagarajan. Diagnostics of laser Induced Plasmas in Different Phases and at phase boundaries using Laser Shadowgraphy, Two-wavelength Laser Interferometry, Schlieren Imaging and Optical Emission Spectroscopy. (Washington, DC: 41st IEEE International Conference on Plasma Science (ICOPS/BEAMS), 2014).

116. Magesh Thiyagarajan, Cosmina Nicula, Abdollah Sarani. Characterization of Non-Thermal Atmospheric Pressure Plasma Jet in Helium, Argon and Oxygen Gas Mixtures. (Washington, DC: 41st IEEE International Conference on Plasma Science (ICOPS/BEAMS), 2014).

115. Magesh Thiyagarajan and Xavier Gonzales. Atmospheric Pressure Resistive Barrier Low Temperature Plasma Treatment for Food Industry. (Washington, DC: 41st IEEE International Conference on Plasma Science (ICOPS/BEAMS), 2014).

114. Magesh Thiyagarajan, Heather Anderson, Xavier Gonzales. Induction of Apoptosis in Human Myeloid Leukemia Cells by Remote Exposure of Resistive Barrier Cold Plasma. (Washington, DC: 41st IEEE International Conference on Plasma Science (ICOPS/BEAMS), 2014).

113. Magesh Thiyagarajan. An Emerging Cold Plasma Technology for Bioengineering - Apoptotic Activation in Leukemia Cancer Cells by Novel Cold Plasma Technology. (Urbana-Champaign, Illinois: Frontiers in Bioengineering, University of Illinois at Urbana-Champaign, Illinois, 2014).

112. Magesh Thiyagarajan, Kenneth Williamson. Experimental Investigation of 1064 nm IR Laser Induced Plasmas in Gases and in Liquids. (San Francisco, California: 40th IEEE International Conference on Plasma Science (ICOPS), 2013).

111. Magesh Thiyagarajan. Scalable Nanoparticle Synthesis in Liquids Using Laser Induced Plasmas at Phase Boundaries. (San Francisco, California: 40th IEEE International Conference on Plasma Science (ICOPS), 2013).

110. Heather Anderson, Xavier Gonzales, Samantha Valdez, Magesh Thiyagarajan. Activation of Apoptotic Cell Death in Human Myeloid Leukemia Cells by RNS: A Novel Antitumor Approach Using Resistive Barrier Plasma. (San Francisco, California: 40th IEEE International Conference on Plasma Science (ICOPS), 2013).

109. Xavier Gonzales, Guadalupe Vidal-Martínez, Jennifer Ausland, Kim Hoang Pham, Magesh Thiyagarajan. Air Plasma Jet Induced Bacterial Inactivation in Dry, Aqueous and Food Environments. (San Francisco, California: 40th IEEE International Conference on Plasma Science (ICOPS), 2013).

108. Magesh Thiyagarajan, Kenneth Williamson. Laser Shadowgraphy, Two-Wavelength Laser Interferometry, Schlieren Imaging and Optical Emission Spectroscopy Diagnostics of Laser Induced Plasmas in Different Phases and at Phase Boundaries. (San Francisco, California: 40th IEEE International Conference on Plasma Science (ICOPS), 2013).

107. Abdollah Sarani, Cosmina Nicula, Magesh Thiyagarajan. Characterization of Non-Thermal Atmospheric Pressure Helium Plasma Jet for Biomedical Applications. (San Francisco, California: 40th IEEE International Conference on Plasma Science (ICOPS), 2013).

106. Abdollah Sarani, Magesh Thiyagarajan, Edy Valdez, Valerie Ferdin. Surface Modification of Polyethylene Terephthalate and Polylactic Acid by Atmospheric Pressure Cold Plasma Jet. (San Francisco, California: 40th IEEE International Conference on Plasma Science (ICOPS), 2013).

105. Valerie Ferdin, Abdollah Sarani and Magesh Thiyagarajan. *Surface Modification of Polyethylene Terephthalate by Atmospheric Pressure Non-thermal Plasma Jet*. (College Station, TX: 9th Annual LSAMP Conference (**Best Paper Award**), 2013).

104. Eduardo Valdes, Abdollah Sarani and Magesh Thiyagarajan. *Surface modification of Polyurethane sheets using an atmospheric pressure RF plasma jet in helium/oxygen gas mixture*. (College Station, TX: 9th Annual LSAMP Conference (**Best Paper Award**), 2013).

103. Valerie Ferdin, Abdollah Sarani and Magesh Thiyagarajan. *Surface Modification of Polyethylene Terephthalate by Atmospheric Pressure Non-thermal Plasma Jet*. (Corpus Christi, TX: Sigma Xi 12th Annual Undergraduate Research Symposium (**Best Paper Award**), 2013).

102. Eduardo Valdes, Abdollah Sarani and Magesh Thiyagarajan. *Surface modification of Polyurethane sheets using an atmospheric pressure RF plasma jet in helium/oxygen gas mixture*. (Corpus Christi, TX: Sigma Xi 12th Annual Undergraduate Research Symposium, 2013).

101. Jennifer Ausland, Guadalupe Vidal, Kim Pham, Magesh Thiyagarajan. *Effective deactivation of Bacillus cereus and Salmonella Typhimurium in chicken poultry, eggs, tomato and papaya using non-thermal plasma.* (Corpus Christi, TX: Sigma Xi 12th Annual Undergraduate Research Symposium, 2013).

100. Samantha Valdez, Heather Anderson, Xavier Gonzales, Magesh Thiyagarajan. *Application of Non-thermal Plasma on Acute Myeloid Leukemia Cells to Induce Apoptosis.* (Corpus Christi, TX: Sigma Xi 12th Annual Undergraduate Research Symposium, 2013).

99. Daniel Cantu, Jennifer Chancellor, Xavier Gonzales, Magesh Thiyagarajan. *Cold Plasma Stimulated Anti-infection Accelerated Wound Healing*. (Corpus Christi, TX: Sigma Xi 12th Annual Undergraduate Research Symposium, 2013).

98. Cody Torno, Abdollah Sarani, Cosmina Nicula, Magesh Thiyagarajan. *Non-Thermal Plasma Jets for Biomedical Applications – Research and Review*. (Corpus Christi, TX: Sigma Xi 12th Annual Undergraduate Research Symposium, 2013).

97. Jennifer Ausland, Guadalupe Vidal, Kim Pham, Magesh Thiyagarajan. *Effective deactivation of Bacillus cereus and Salmonella Typhimurium in chicken poultry, eggs, tomato and papaya using non-thermal plasma.* (College Station, TX: 9th Annual LSAMP Conference 2013).

96. Samantha Valdez, Heather Anderson, Xavier Gonzales, Magesh Thiyagarajan. *Application of Non-thermal Plasma on Acute Myeloid Leukemia Cells to Induce Apoptosis.* (College Station, TX: 9th Annual LSAMP Conference 2013).

95. Daniel Cantu, Jennifer Chancellor, Xavier Gonzales, Magesh Thiyagarajan. *Cold Plasma Stimulated Anti-infection Accelerated Wound Healing*. (College Station, TX: 9th Annual LSAMP Conference 2013).

94. Magesh Thiyagarajan, Abdollah Sarani, Xavier F. Gonzales. Characterization of an Atmospheric Pressure Plasma Jet and its Applications for Disinfection and Cancer Treatment. (San Diego, CA: Annual MMVR20/NextMed Conference, 2013)

93. Magesh Thiyagarajan, Xavier F. Gonzales, Heather Anderson. Regulated Cellular Exposure to Non-Thermal Plasma Allows Preferentially Directed Apoptosis in Acute Monocytic Leukemia Cells. (San Diego, CA: Annual MMVR20/NextMed Conference, 2013)

**Conclusion**

The project entitled - Lightweight Portable Plasma Medical Device – Plasma Engineering Research Laboratory has been completed and it made a significant advancement in the plasma engineering research area as well as met the proposed objectives and tasks. The project had two objectives, in which the objective 1 is to develop a plasma research facility and establish a range of experimental plasma systems and diagnostics. The tasks under objective 1 were completed. The project's second objective is to develop a prototype of a portable plasma source for biomedical applications such as sterilization, infection treatment and cancer treatment. We have developed a portable plasma source and tested on a range of bacteria and cancer cells and results were obtained. We have redesigned, reconstructed and optimized the portable non-thermal atmospheric pressure plasma jet that was developed earlier based on a dielectric barrier discharge configuration. The plasma and biological testing and characterization of the optimized plasma jet are completed. The PI has mentored over 25 undergraduate students and 2 graduate students to perform various research projects. Several of these students have presented their work at various conferences and symposiums and few of those presentations has received best paper awards. The PI has mentored a visiting scientist and 5 postdoctoral research associates. The PI and the research team have published over 10 journal articles and over 50 conference proceedings and over 50 symposiums and meetings. The PERL has received a great visibility in the university campus as well as in the nation and around the world.

## REFERENCES


[1] A. Schutze, J. Y. Jeong, S. E. Babayan, J. Park, G. S. Selwyn, and R. F. Hicks, "The atmospheric-pressure plasma jet: A review and comparison to other plasma sources," *Ieee Transactions on Plasma Science,* vol. 26, pp. 1685-1694, Dec 1998.

[2] K. D. Weltmann, R. Brandenburg, T. von Woedtke, J. Ehlbeck, R. Foest, M. Stieber, and E. Kindel, "Antimicrobial treatment of heat sensitive products by miniaturized atmospheric pressure plasma jets (APPJs)," *Journal of Physics D-Applied Physics,* vol. 41, Oct 7 2008.

[3] K. D. Weltmann, E. Kindel, R. Brandenburg, C. Meyer, R. Bussiahn, C. Wilke, and T. von Woedtke, "Atmospheric Pressure Plasma Jet for Medical Therapy: Plasma Parameters and Risk Estimation," *Contributions to Plasma Physics,* vol. 49, pp. 631-640, Oct 2009.

[4] W.-C. Zhu, Q. Li, X.-M. Zhu, and Y.-K. Pu, "Characteristics of atmospheric pressure plasma jets emerging into ambient air and helium," *Journal of Physics D: Applied Physics,* vol. 42, p. 202002, 2009.

[5] J. Park, I. Henins, H. W. Herrmann, G. S. Selwyn, and R. F. Hicks, "Discharge phenomena of an atmospheric pressure radio-frequency capacitive plasma source," *Journal of Applied Physics,* vol. 89, pp. 20-28, Jan 1 2001.

[6] J. Park, I. Henins, H. W. Herrmann, and G. S. Selwyn, "Gas breakdown in an atmospheric pressure radio-frequency capacitive plasma source," *Journal of Applied Physics,* vol. 89, pp. 15-19, Jan 1 2001.

[7] M. Laroussi, C. Tendero, X. Lu, S. Alla, and W. L. Hynes, "Inactivation of bacteria by the plasma pencil," *Plasma Processes and Polymers,* vol. 3, pp. 470-473, Aug 2006.

[8] E. Stoffels, A. J. Flikweert, W. W. Stoffels, and G. M. W. Kroesen, "Plasma needle: a non-destructive atmospheric plasma source for fine surface treatment of (bio)materials," *Plasma Sources Science & Technology,* vol. 11, pp. 383-388, Nov 2002.

[9] R. Ben Gadri, J. R. Roth, T. C. Montie, K. Kelly-Wintenberg, P. P. Y. Tsai, D. J. Helfritch, P. Feldman, D. M. Sherman, F. Karakaya, Z. Y. Chen, and U. P. S. Team, "Sterilization and plasma processing of room temperature surfaces with a one atmosphere uniform glow discharge plasma (OAUGDP)," *Surface & Coatings Technology,* vol. 131, pp. 528-542, Sep 1 2000.

[10] M. Teschke, J. Kedzierski, E. G. Finantu-Dinu, D. Korzec, and J. Engemann, "High-speed photographs of a dielectric barrier atmospheric pressure plasma jet," *Ieee Transactions on Plasma Science,* vol. 33, pp. 310-311, Apr 2005.

[11] M. Thiyagarajan, A. Sarani, and X. Gonzales, "Characterization of Portable Resistive Barrier Plasma Jet and Its Direct and Indirect Treatment for Antibiotic Resistant Bacteria and THP-1 Leukemia Cancer Cells," *Ieee Transactions on Plasma Science,* vol. 40, pp. 3533-3545, Dec 2012.

[12] I. Alexeff, A. Balasundaram, E. P. Pradeep, N. Karnam, and N. R. Pulasani, "Biological decontamination using an atmospheric pressure resistive barrier plasma discharge," in *NATO Science for Peace and Security Series A-Chemistry and Biology*, S. Guceri and A. Fridman, Eds., ed: Springer, Po Box 17, 3300 Aa Dordrecht, Netherlands, 2008, pp. 3-19.

[13] M. Thiyagarajan and I. Alexeff, "A Dual Mode – Steady State Atmospheric Pressure Nonthermal Resistive Barrier Plasma Discharge," in *Gaseous Electronics Conference, American Physical Society*, San Francisco, California, 2003.

[14] J. Ehlbeck, U. Schnabel, M. Polak, J. Winter, T. von Woedtke, R. Brandenburg, T. von dem Hagen, and K. D. Weltmann, "Low temperature atmospheric pressure plasma sources for microbial decontamination," *Journal of Physics D-Applied Physics,* vol. 44, Jan 2011.

[15] A. Sarani, A. Y. Nikiforov, and C. Leys, "Atmospheric pressure plasma jet in Ar and Ar/H(2)O mixtures: Optical emission spectroscopy and temperature measurements," *Physics of Plasmas,* vol. 17, Jun 2010.

[16] E. I. Tuomanen, R. Austrian, and H. R. Masure, "Pathogenesis of pneumococcal infection," *N Engl J Med,* vol. 332, pp. 1280-4, May 11 1995.

[17] G. L. Rodgers, A. Arguedas, R. Cohen, and R. Dagan, "Global serotype distribution among Streptococcus pneumoniae isolates causing otitis media in children: Potential implications for pneumococcal conjugate vaccines," *Vaccine,* vol. 27, pp. 3802-3810, Jun 12 2009.

[18] K. T. Vakharia, N. L. Shapiro, and N. Bhattacharyya, "Demographic Disparities Among Children With Frequent Ear Infections in the United States," *Laryngoscope,* vol. 120, pp. 1667-1670, Aug 2010.

[19] A. Vergison, R. Dagan, A. Arguedas, J. Bonhoeffer, R. Cohen, I. Dhooge, A. Hoberman, J. Liese, P. Marchisio, A. A. Palmu, G. T. Ray, E. A. Sanders, E. A. Simoes, M. Uhari, J. van Eldere, and S. I. Pelton, "Otitis media and its consequences: beyond the earache," *Lancet Infect Dis,* vol. 10, pp. 195-203, Mar 2010.

[20] F. Massines and G. Gouda, "A comparison of polypropylene-surface treatment by filamentary, homogeneous and glow discharges in helium at atmospheric pressure," *Journal of Physics D-Applied Physics,* vol. 31, pp. 3411-3420, Dec 21 1998.

[21] A. Sarani, N. De Geyter, A. Y. Nikiforov, R. Morent, C. Leys, J. Hubert, and F. Reniers, "Surface modification of PTFE using an atmospheric pressure plasma jet in argon and argon + CO2," *Surface & Coatings Technology,* vol. 206, pp. 2226-2232, Jan 15 2012.

[22] J. P. Lim, H. S. Uhm, and S. Z. Li, "Influence of oxygen in atmospheric-pressure argon plasma jet on sterilization of Bacillus atrophaeous spores," *Physics of Plasmas,* vol. 14, Sep 2007.

[23] Z. Machala, M. Janda, K. Hensel, I. Jedlovský, L. Leštinská, V. Foltin, V. Martišovitš, and M. Morvová, "Emission spectroscopy of atmospheric pressure plasmas for bio-medical and environmental applications," *Journal of Molecular Spectroscopy,* vol. 243, pp. 194-201, 2007.

[24] N. Bai, P. Sun, H. X. Zhou, H. Y. Wu, R. X. Wang, F. X. Liu, W. D. Zhu, J. L. Lopez, J. Zhang, and J. Fang, "Inactivation of Staphylococcus aureus in Water by a Cold, He/O-2 Atmospheric Pressure Plasma Microjet," *Plasma Processes and Polymers,* vol. 8, pp. 424-431, May 20 2011.

[25] S. Z. Li, Q. Wu, W. Yan, D. Z. Wang, and H. S. Uhm, "Influence of oxygen traces on an atmospheric-pressure radio-frequency capacitive argon plasma discharge," *Physics of Plasmas,* vol. 18, Oct 2011.

[26] Z. Xiong, X. P. Lu, A. Feng, Y. Pan, and K. Ostrikov, "Highly effective fungal inactivation in He+O-2 atmospheric-pressure nonequilibrium plasmas," *Physics of Plasmas,* vol. 17, Dec 2010.

[27] D. Z. Pai, K. Ostrikov, S. Kumar, D. A. Lacoste, I. Levchenko, and C. O. Laux, "Energy efficiency in nanoscale synthesis using nanosecond plasmas," *Scientific Reports,* vol. 3, Feb 5 2013.

[28] Z. Machala, M. Janda, K. Hensel, I. Jedlovsky, L. Lestinska, V. Foltin, V. Martisovits, and M. Morvova, "Emission spectroscopy of atmospheric pressure plasmas for bio-medical and environmental applications," *Journal of Molecular Spectroscopy,* vol. 243, pp. 194-201, Jun 2007.

[29] A. Kramida, Ralchenko, Yu., Reader, J., and NIST ASD Team, "NIST Atomic Spectra Database (ver. 5.0), [Online]. Available: http://physics.nist.gov/asd [2012, November 15]. National Institute of Standards and Technology, Gaithersburg, MD.," 2012.

[30] A. Lofthus and P. H. Krupenie, "Spectrum of Molecular Nitrogen," *Journal of Physical and Chemical Reference Data,* vol. 6, pp. 113-307, 1977.

[31] A. Yanguas-Gil, J. Cotrino, and A. R. Gonzalez-Elipe, "Global model of a low pressure ECR microwave plasma applied to the PECVD of SiO2 thin films," *Journal of Physics D-Applied Physics,* vol. 40, pp. 3411-3422, Jun 7 2007.

[32] F. Liu, W. Wang, W. Zheng, and Y. Wang, "Investigation of spatially resolved spectra of OH and N2+ in N2 and H2O mixture wire-plate positive pulsed streamer discharge," *Spectrochimica Acta Part A: Molecular and Biomolecular Spectroscopy,* vol. 69, pp. 776-781, 2008.

[33] F. Liu, W. C. Wang, W. Zheng, and Y. N. Wang, "Optical study of radicals (OH, O, H, N) in a needle-plate negative pulsed streamer corona discharge," *Plasma Chemistry and Plasma Processing,* vol. 26, pp. 469-480, Oct 2006.

[34] F. Liu, W. Wanga, W. Zheng, and Y. Wang, "Optical study of radicals (OH, O, H, N) in a needle-plate bi-directional pulsed corona discharge," *European Physical Journal D,* vol. 38, pp. 515-522, Jun 2006.

[35] W. Wang, S. Wang, F. Liu, W. Zheng, and D. Wang, "Optical study of OH radical in a wire-plate pulsed corona discharge," *Spectrochimica Acta Part A: Molecular and Biomolecular Spectroscopy,* vol. 63, pp. 477-482, 2006.

[36] M. Laroussi, "Nonthermal decontamination of biological media by atmospheric-pressure plasmas: Review, analysis, and prospects," *Ieee Transactions on Plasma Science,* vol. 30, pp. 1409-1415, Aug 2002.

[37] G. Fridman, G. Friedman, A. Gutsol, A. B. Shekhter, V. N. Vasilets, and A. Fridman, "Applied plasma medicine," *Plasma Processes and Polymers,* vol. 5, pp. 503-533, 2008.

[38] M. Laroussi and F. Leipold, "Evaluation of the roles of reactive species, heat, and UV radiation in the inactivation of bacterial cells by air plasmas at atmospheric pressure," *International Journal of Mass Spectrometry,* vol. 233, pp. 81-86, Apr 15 2004.

[39] A. I. Kuzmichev, Soloshenko, I. A., Tsiolko, V. V., Kryzhanovsky, V. I., Bazhenov, V. Y., Mikhno, I. L. & Khomich, V. A. Year. , "Feature of sterilization by different type of atmopsheric pressure discharges.," in *7th International Symposium on High Pressure Low Temperature Plasma Chemistry- Hakone VII, 2001* 2000 Greifswald (Germany). , 2001, pp. 402-406

[40] Z. S. Chang, G. J. Zhang, X. J. Shao, and Z. H. Zhang, "Diagnosis of gas temperature, electron temperature, and electron density in helium atmospheric pressure plasma jet," *Physics of Plasmas,* vol. 19, Jul 2012.

[41] C. O. Laux, T. G. Spence, C. H. Kruger, and R. N. Zare, "Optical diagnostics of atmospheric pressure air plasmas," *Plasma Sources Science & Technology,* vol. 12, pp. 125-138, May 2003.

[42] J. L. Walsh and M. G. Kong, "Room-temperature atmospheric argon plasma jet sustained with submicrosecond high-voltage pulses," *Applied Physics Letters,* vol. 91, Nov 26 2007.

[43] B. A. Cruden and M. Meyyappan, "Characterization of a radio frequency carbon nanotube growth plasma by ultraviolet absorption and optical emission spectroscopy," *Journal of Applied Physics,* vol. 97, Apr 15 2005.

[44] R. K. Garg, T. N. Anderson, R. P. Lucht, T. S. Fisher, and J. P. Gore, "Gas temperature measurements in a microwave plasma by optical emission spectroscopy under single-wall carbon nanotube growth conditions," *Journal of Physics D-Applied Physics,* vol. 41, May 7 2008.

[45] I. L. Chidsey and D. R. Crosley, "Calculated Rotational Transition-Probabilities for the a-X System of Oh," *Journal of Quantitative Spectroscopy & Radiative Transfer,* vol. 23, pp. 187-199, 1980.

[46] G. H. Dieke and H. M. Crosswhite, "The Ultraviolet Bands of Oh - Fundamental Data," *Journal of Quantitative Spectroscopy & Radiative Transfer,* vol. 2, pp. 97-&, 1962.

[47] A. S. Magesh Thiyagarajan, and Cosmina Nicula "Optical emission spectroscopic diagnostics of a non-thermal atmospheric pressure helium-oxygen plasma jet for biomedical applications " *Journal of Applied Physics,* vol. 113, p. 233302, 2013 2013.

[48] M. A. Gonzalez and M. A. Gigosos, "Analysis of Stark line profiles for non-equilibrium plasma diagnosis," *Plasma Sources Science & Technology,* vol. 18, Aug 2009.

[49] A. Ionascut-Nedelcescu, C. Carlone, U. Kogelschatz, D. V. Gravelle, and M. I. Boulos, "Calculation of the gas temperature in a throughflow atmospheric pressure dielectric barrier discharge torch by spectral line shape analysis," *Journal of Applied Physics,* vol. 103, Mar 15 2008.

[50] C. Yubero, M. C. Garcia, and M. D. Calzada, "On the use of the H alpha spectral line to determine the electron density in a microwave (2.45GHz) plasma torch at atmospheric pressure," *Spectrochimica Acta Part B-Atomic Spectroscopy,* vol. 61, pp. 540-544, May 2006.

[51] C. Yubero, M. S. Dimitrijevic, M. C. Garcia, and M. D. Calzada, "Using the van der Waals broadening of the spectral atomic lines to measure the gas temperature of an argon microwave plasma at atmospheric pressure," *Spectrochimica Acta Part B-Atomic Spectroscopy,* vol. 62, pp. 169-176, Feb 2007.

[52] S. Hofmann, A. F. H. van Gessel, T. Verreycken, and P. Bruggeman, "Power dissipation, gas temperatures and electron densities of cold atmospheric pressure helium and argon RF plasma jets," *Plasma Sources Science & Technology,* vol. 20, Dec 2011.

[53] E. E. Whiting, "AN EMPIRICAL APPROXIMATION TO VOIGT PROFILE," *Journal of Quantitative Spectroscopy & Radiative Transfer,* vol. 8, pp. 1379-&, 1968.

[54] X. H. Zhang, J. Huang, X. D. Liu, L. Peng, L. H. Guo, G. H. Lv, W. Chen, K. C. Feng, and S. Z. Yang, "Treatment of Streptococcus mutans bacteria by a plasma needle," *Journal of Applied Physics,* vol. 105, Mar 15 2009.

[55] B. Halliwell and J. M. C. Gutteridge, "Oxygen-Toxicity, Oxygen Radicals, Transition-Metals and Disease," *Biochemical Journal,* vol. 219, pp. 1-14, 1984.

[56] G. Fridman, A. D. Brooks, M. Balasubramanian, A. Fridman, A. Gutsol, V. N. Vasilets, H. Ayan, and G. Friedman, "Comparison of direct and indirect effects of non-thermal atmospheric-pressure plasma on bacteria," *Plasma Processes and Polymers,* vol. 4, pp. 370-375, May 23 2007.

[57] W. Chen, J. Huang, N. Du, X.-D. Liu, X.-Q. Wang, G.-H. Lv, G.-P. Zhang, L.-H. Guo, and S.-Z. Yang, "Treatment of enterococcus faecalis bacteria by a helium atmospheric cold plasma brush with oxygen addition," *Journal of Applied Physics,* vol. 112, Jul 1 2012.

[58] C. M. Evans and J. S. Koo, "Airway mucus: the good, the bad, the sticky," *Pharmacol Ther,* vol. 121, pp. 332-48, Mar 2009.